Study of the fingerprint of Essential Tremor in motor control and its links on cerebellar-cortical connectivity

Flo Blondiaux

Thesis submitted in partial fulfillment
of the requirements for the degree of

Doctor in Engineering Sciences

May 2024

Thesis committee

Prof. Frédéric Crevecoeur (Advisor), UCLouvain, Belgium
Prof. Bernard Hanseeuw (co-Advisor), UCLouvain, Belgium
Prof. Philippe Lefèvre (Chair), UCLouvain, Belgium
Dr. Laurence Dricot, UCLouvain, Belgium
Prof. Gilles Vannuscorps, UCLouvain, Belgium
Prof. Juan Alvaro Gallego, Imperial College London, UK
Prof. Tarkeshwar Singh, The Pennsylvania State University, USA

Acknowledgements

Cette thèse représente l'aboutissement de quatre années de travail, un travail qui n'aurait pas été possible sans l'aide précieuse de nombreuses personnes, de près ou de loin, tout au long de ce parcours.

Tout d'abord, je tiens à remercier mes promoteurs pour leur encadrement. Merci à Fred pour ta confiance, ton optimisme, et tes commentaires précieux sur les publications et posters, qui m'ont permis de progresser au fil des années. Bernard, merci pour ton suivi des projets de recherche et pour nos discussions sur la suite de ma carrière.

Un merci spécial à Laurence pour tes précieux conseils et les nombreux enseignements sur la partie imagerie de mon projet, mais merci également pour nos discussions et pour ton écoute.

Merci également à Gilles et Philippe d'avoir accepté de faire partie de mon comité d'accompagnement, et aux membres externes, Tarkeshwar Singh et Juan Alvaro Gallego, d'avoir accepté de faire partie de mon jury. Je tiens à remercier toutes ces personnes pour le temps consacré à la lecture de ma thèse et pour vos précieux commentaires, qui ne peuvent l'avoir rendue que meilleure.

Merci à Konstantina Kilteni et son équipe, Xavier, Noa et Lili, pour les échanges en conférences et pour l'accueil lors de mon séjour au Karolinska Institutet. Cet échange aura permis de lancer la suite de ce projet.

Un grand merci aux travailleureuses de l'ombre dont le support est crucial dans le travail des chercheureuses. Merci à Marie-Christine, Pascale et Cathy pour leur aide sur les aspects administratifs de cette thèse. Merci à CATL, CREDEM et KINARM pour leur aide technique dans l'utilisation, la création et la réparation des setups. Merci à Gaetan Duchêne pour l'élaboration et l'optimisation des séquences d'IRM.

Merci aux collègues du labo, anciens comme actuels, pour les moments partagés en conférence, lors des retraites de labo, pour les discussions de recherche, les analyses de données, et la formation à l'utilisation des setups. Votre rôle a été précieux dans cette thèse.

Merci également aux collègues des pôles Inma et Neur, pour les moments passés ensemble, les afterworks, et pour avoir facilité mon intégration dans ces instituts malgré le confinement.

Je tiens à remercier le pôle Neur de m'avoir adopté.e en fin de thèse, pour les repas partagés à 12:01 précises, pour le support et de m'avoir permis de travailler dans une bonne ambiance et d'évoluer dans un environnement stimulant grâce à la diversité de nos projets de recherche.

Un merci particulier à Lise et Louisien pour leurs contributions dans mes projets de recherche, pour leur aide lors des évaluations cliniques, et leurs précieux retours sur les papiers. Merci également à Anne qui m'a accompagné.e tout au long de mon mémoire et de ma thèse. Merci pour tous les partages, le support, les relectures et les discussions. Avoir quelqu'un à suivre dans cette thèse a été précieux et motivant.

Un tout grand merci également à ma famille et mes ami.e.s pour leur support tout au long de ma thèse. Même si vous n'avez peut-être pas toujours compris ce que je faisais, votre présence m'a permis de garder un cap, particulièrement dans les derniers mois de thèse.

Merci au FNRS pour le financement accordé à ce projet, leur confiance a été déterminante pour l'accomplissement de ces recherches.

Enfin, cette thèse n'aurait pas été possible sans le support précieux de l'ASBL Tremblement Essentiel Belgique. Un grand merci pour leur aide dans le recrutement des participants, le relais de nos communications, et l'accueil dans la communauté. Un grand merci aux 102 volontaires pour leur participation enthousiaste sans laquelle de nombreux résultats ne seraient pas possible. Je tiens à remercier particulièrement les personnes atteintes de tremblement avec qui j'ai pu partager de très sincères discussions enrichissantes. Ces interactions donnent un sens concret à cette recherche. En espérant que les résultats de ces travaux permettront à terme de clarifier les causes de cette pathologie et que les futures recherches amélioreront la qualité de vie des personnes atteintes de Tremblement Essentiel.

Contents

Chapter 1

General introduction

On a daily basis, our interactions with our environment often involve movement, from simple tasks like grasping objects to more complex actions such as writing or playing a musical instrument. However, for some individuals, these interactions are complicated by a persistent tremor. Essential Tremor (ET) manifests predominantly as a tremor during voluntary movements, significantly impacting routine tasks like inserting a key into a door lock, preparing meals, or buttoning clothes. Despite the considerable advancements in understanding neurological disorders made in the last few years, ET origin remains poorly understood. This thesis aims to contribute to this understanding by exploring potential mechanisms underlying tremor genesis in ET.

In this introductory chapter, we will first provide an overview of Essential Tremor, its clinical manifestations and prevalent hypothesis regarding its pathophysiology. We will then discuss cerebellar deficits, circuits and functions considering the pivotal role of cerebellum in motor control and its implication in ET pathology. Subsequently, we will explore computational models of motor control, examining how theoretical frameworks can inform our understanding of tremor generation in ET. Finally, we will outline the goals of this thesis and provide a presentation of the subsequent chapters.

1.1 What is Essential Tremor ?

Essential Tremor (ET) is among the most common movement disorder in adults. It is a neurological disease with as main hallmark an action

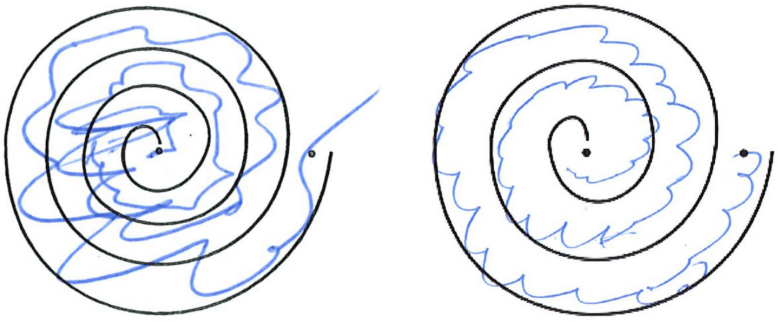

FIGURE 1.1: Spiral drawn by two exemplar ET participants as part of the Fahn-Tolosa-Marin Tremor Rating Scale assessment (Fahn et al., 1993).

tremor of the upper limbs. The tremor being mainly present during movements as illustrated on Figure 1.1

1.1.1 Clinical manifestations

Essential Tremor is one of the most frequent neurological disorders, affecting around 0.9% of the general population (Louis & Ferreira, 2010). The prevalence increases with age, affecting 4.8% of adults above 65 years old (Benito-León et al., 2003) and more than 20% of people above 95 years old (Louis & Ferreira, 2010). In 50% of the cases, these patients had a familial history of ET (Shanker, 2019). The onset of the disease has a bimodal distribution and can be divided into young onset vs. old onset. The young onset cases are usually observed in patients with a familial history of ET while old onset is usually associated with a faster disease progression (Pan & Kuo, 2022)

The main motor manifestation of ET is upper limb tremor with a frequency usually ranging from 4 to 12 Hz (Clark & Louis, 2018). The tremor commonly manifests as a postural tremor, occurring when sustaining a posture against gravity, and as an action tremor, with the tremor worsening during movement or during highly skilled tasks like writing (Gruol et al., 2016). The amplitude of the action tremor is often more important than postural tremor (Shanker, 2019). This tremor

evolves usually symmetrically affecting both hands similarly. With disease progression, the tremor tends to spread beyond the arms affecting the head, the tongue, the voice, the trunk or even lower limbs (Clark & Louis, 2018).

In opposition with physiological tremor, which has a peripheral origin, ET frequency is independent of loading (Elble, 2003; Elble et al., 1994). This property suggests that ET does not originate from peripheral origin but would rather originate from the central nervous system (Pan & Kuo, 2022). Tremor frequency tends to decrease with age, with a frequency of 0.12 Hz/Year, having the consequence to increase oscillations amplitude due to the low pass filtering properties of muscles and limbs (Hellwig et al., 2009).

ET symptoms are not limited to motor symptoms even if those are the most frequently studied and documented. Studies reported mild cognitive disorders (Louis et al., 2019), impairments in executive functions - responsible for controlling and sequencing multiple cognitive operations - (Bermejo-Pareja & Puertas-Martín, 2012) as well as increased levels of anxiety and depression in this population (Clark & Louis, 2018). These non-motor symptoms lead to the definition of ET plus, for patients having a tremor with the characteristics of ET coupled with additional neurological symptoms (Shanker, 2019). Due to the reported presence of etiological, clinical and pathological heterogeneity, there is a growing support for the notion of ET being a family of disorders (Louis, 2021).

The first-line treatments for tremor reduction in ET are β-Blockers (propranolol) and anticonvulsants (primidone) (Gruol et al., 2016). However, their efficacy is limited: only half of the patients have a significant reduction of the tremor, the treatment is therefore often discontinued (Shanker, 2019). Surgical interventions also exist for the most heavily affected patients with a pharmacologically refractory tremor. These interventions include deep brain stimulation (DBS) of the VIM or lesional surgeries such as radiofrequency or gamma-knife thalamotomy (Sharma & Pandey, 2020). If these surgeries can be efficient to alleviate tremor for these patients, a subset experience "habituation" with a gradual return of the tremor in the years following the surgery (Pan & Kuo, 2022).

1.1.2 Pathophysiology

The pathophysiology of essential tremor remains only partially understood. Numerous clinical studies pointed towards cerebellum and the cerebellar system as a seat of the disease. The cerebellar origin is supported by numerous imaging studies (Holtbernd & Shah, 2021), as well as clinical observations and electrophysiological (EMG, EEG, TMS) experiments (Cerasa & Quattrone, 2016; Pan & Kuo, 2022). These aspects will be discussed in more detail in the future chapters with a specific focus on imaging studies in Chapter 4.

Postmortem studies reported alterations of Purkinje cells: modest loss of Purkinje cells, swelling of their axons (torpedoes) and displacement of the Purkinje cells bodies away from the Purkinje cell layer (Cerasa & Quattrone, 2016; Louis et al., 2007). These changes are typically associated to cerebellar damages. In addition, surrounding neuronal populations also presented alterations: basket cells developed denser and more elongated plexus around Purkinje cells and abnormal synaptic connections with the Purkinje cells were made by the climbing fibers in the parallel fiber synaptic layer. In addition, climbing fibers formed lateral crossing which innervated multiple Purkinje cells. These climbing fiber extensions appears to be a change specific to ET as it is not reported in other cerebellar disorders. Because climbing fibers originates from the inferior olive, and because of the intrinsic oscillatory activity of the inferior olive, this modification might influence the activity of the Purkinje cells leading to tremor.

In their review Pan and Kuo described the 4 potential non-mutually exclusive hypotheses for ET origin: β-carboline alkaloid exposures, cerebellar GABA deficiency, GluRδ2-dependent climbing fiber synaptic pathology and extra-cerebellar oscillatory activity (Pan & Kuo, 2022). These hypotheses are represented in Figure 1.2.

β-carboline alkaoid exposures and related tremor

Essential Tremor might be caused by several environmental factors. One of them is the exposition to β-carboline alkaloid, found in high concentrations in meat. Higher levels of Harmane, one of the β-carboline alkaloid, was found in ET patients blood as well as in ET cerebellum in postmortem studies. Harmaline, another β-carboline alkaloid, is

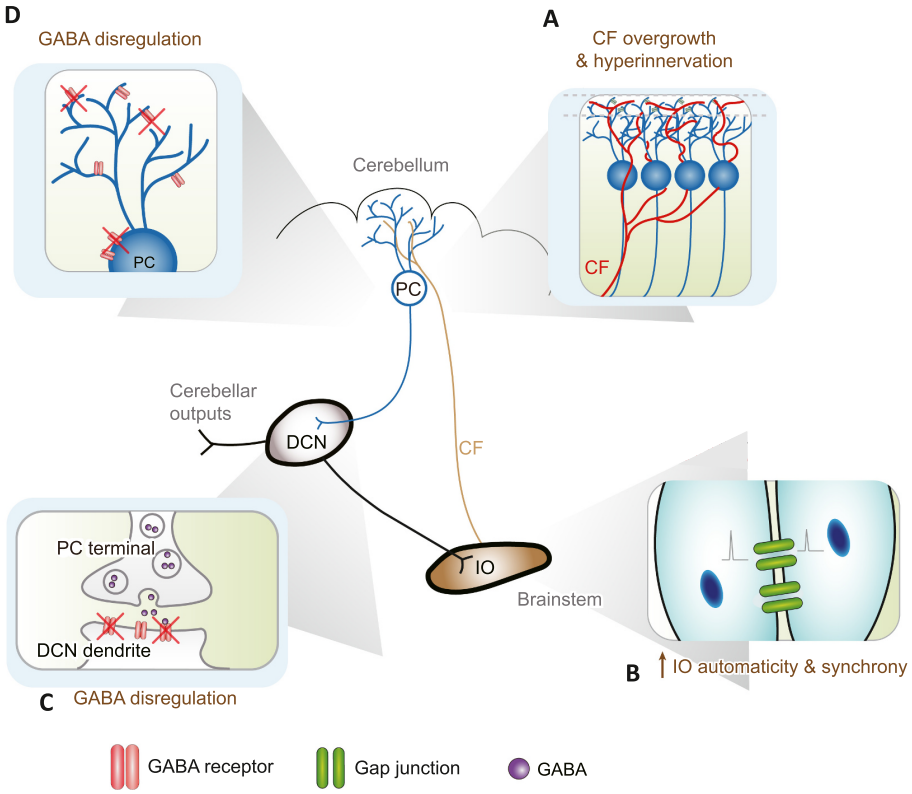

FIGURE 1.2: Summary of ET pathophysiology hypotheses. (A) Climbing fiber overgrowth and hyperinnervation. Reduction of GluRδ2 protein in the Purkinje cells causes climbing fiber synaptic pruning deficits, which lead to hypersynchrony and excessive oscillations in Purkinje cells. (B) Increased inferior olive automaticity and synchrony. β-carboline alkaloids, such as harmaline, lead to increased inferior olive synchrony via gap junctions. (C & D) GABA dysregulation. GABA receptor knockout in Purkinje cells and reduced GABA receptors in the deep cerebellar nucleus can lead to abnormal oscillations in the circuitry. DCN: deep cerebellar nuclei; IO: inferior olive; PC: Purkinje cell. Adapted from (Pan & Kuo, 2022).

known to induce action tremor in animals. Interestingly, the symptoms induced by harmaline can be reduced using propranolol, primidone or alcohol, which is known to reduce tremor in about 50% of ET patients.

The tremor could be explained by the enhancement of the automaticity and synchrony in the inferior olivary neurons caused by the exposition to harmaline. The neurons from the inferior olive projects to cerebellum as climbing fibers innervating Purkinje cells. The activity of these neurons is synchronized by gap junctions, themselves controlled by GABAergic inputs from the deep cerebellar nuclei. Resulting in a closed loop control within the olivo-cerebellar cortex-deep cerebellar nuclei pathway.

Cerebellar GABA deficiency

The therapeutic effects of the GABAergic medication and alcohol intake in ET supported the hypothesis that tremor generation involves GABA-mediated mechanisms. These elements points towards an insufficient GABA neurotransmission in ET. This dysfunction has been suggested to originate from 3 elements within the cerebellar circuit: the deep cerebellar nuclei, the cerebellar cortex and the inferior olive.

- Deep cerebellar nuclei: The reported loss of Purkinje cells associated with their GABAergic function might explain an insufficient GABAergic neurotransmission to the deep cerebellar nuclei. A postmortem study documented reduced levels of $GABA_A$ and $GABA_B$ receptors in the deep cerebellar nuclei, probably predicting less responsiveness to GABAergic agents (Paris-Robidas et al., 2012). A modeling study also showed that a progressive loss of $GABA_A$ $\alpha 1$ receptors leads to the emergence of oscillations (X. Zhang & Santaniello, 2019).

- Cerebellar cortex: Purkinje cells, comprising the cerebellar cortex, have a pacemaking activity. This activity is regulated by GABAergic neurotransmission from different interneurons, including stellate cells and basket cells. The alterations of the basket cells reported from postmortem studies could explain the GABAergic modifications potentially altering the firing pattern.

- Inferior olive: GABAergic activity from the deep cerebellar nuclei regulates the synchronicity of the neural firing in the inferior olive. A dysfunction could affect the spike timing and frequency of the Purkijne cells due to their connections via the climbing fibers.

GluRδ2-dependent climbing fiber synaptic pathology and cerebellar oscillations

One of the most distinguishable patterns observed in postmortem studies is the extension of the climbing fibers into the parallel fiber synaptic territory. The parallel and climbing fibers synapses are organized and regulated by GluRδ2. Reduced levels of this protein was observed in ET and correlated with climbing fibers synaptic pathology. Mutant mice with this pathology developed a progressive and action dependent tremor which is sensitive to ET medication. The tremor could be explained by this overgrowth of the climbing fibers: an hyperinnervation between the climbing fibers and the Purkinje cells synapses leads to an hypersynchronicity and excessive oscillations in the Purkinje cells.

Extra-cerebellar oscillatory activity

All the above hypotheses focused on a cerebellar origin. Other hypotheses suggested oscillators outside of the cerebellum, most often the thalamus or the motor cortex. For example, single neuron recording of the thalamus correlated with tremor or multiple oscillators are suspected to interact creating tremor outside of the cerebellum. So far, no convincing animal model showed evidence that oscillatory activity in these regions can drive a tremor nor postmortem studies supported this hypothesis.

1.2 Cerebellum: deficits, circuits and function

Numerous indicators suggest a potential link between cerebellum and ET. Therefore, gaining insights into the function, structure, connections

and typical disorders associated with cerebellum becomes essential to study the mechanisms underlying ET.

1.2.1 Cerebellar deficits

As summarized by Diedrichsen and Bastian in (Diedrichsen & Bastian, 2014), cerebellar damages are observed in patients with neurological diseases, tumors, strokes and malformations. One of the most obvious deficits associated with cerebellar damage is ataxia, characterized by a loss of motor coordination. These patients often exhibit ataxic reaching movements, movements that are notably more curved and variable from trial to trial compared to neurologically intact individuals. The increased variability may stem from an inability to account for complex limb mechanics as it is often worsened when the movement requires the coordination of several body parts simultaneously (Bastian et al., 1996). Additionally, individuals with cerebellar disorders often experience dysmetria, characterized by an imprecise control over the distance, speed and range of the movements. This can lead to overshooting or undershooting of targets, resulting in observable oscillations during movements. These difficulties may arise from suboptimal use of delayed sensory feedback as oscillations are sometimes reduced when closing eyes. Other symptoms are walking ataxia, irregular gait patterns and balance difficulties. Occulomotor deficits, such as dysmetria of eye movements, nystagmus - involuntary eye movements caused by a slow drift followed by fast resetting phases- as well as abnormal gains of the vestibulo-ocular reflex are also common (Diedrichsen & Bastian, 2014). Additionally, cerebellar deficits can affect speech, leading to dysarthria, as speaking requires coordinated movements of the lips, tongue and palate (Gordon, 1996).

Cerebellum also plays a role in cognition, although these impairments are less thoroughly documented and comprehended. Functional MRI studies have shown that cerebellum is activated during cognitive tasks. In patients with cerebellar disorders, cognitive deficits have been reported in tests involving language, executive functions, emotions and attention. However, there is a considerable variability in the reported non-motor symptoms across studies (Carey, 2024).

Understanding how cerebellar circuits implement these functions and cerebellar connections with the rest of the brain is essential.

1.2.2 Cerebellar circuits

As summarized in the review by Carey, 2024, cerebellum consists of a cortical sheet wrapped around the deep cerebellar nuclei (see Figure 1.3). The main inputs to the cerebellum are conveyed by the mossy fibers, relaying information from the neocortex via the pontine nuclei as well as from the brain stem and the spinal cord. Mossy fibers synapse on granule cells, whose axons form parallel fibers. These parallel fibers provide excitatory synapses onto Purkijne cells and various inhibitory interneurons (stellate, basket and Golgi cells). Purkijne cells, in turn, receive input from tens of thousands individual granule cells. Their action potential trigger in the Purkijne cells traditional single spike action potentials at a rate of 40-70 Hz.

Climbing fibers, originating from the inferior olive, constitute another input to the cerebellum, although less abundant than mossy fibers (with rates of 1-4Hz). Their action potential produce complex responses composed of multiple spikelets. While mossy fibers are believed to convey broad contextual signals encompassing sensory inputs, ongoing movement and motor commands, climbing fibers are believed to specialize in representing highly processed and temporally precise information about unexpected inputs.

Purkijne cells exert inhibitory control on the deep cerebellar nuclei, the primary output of the cerebellum, which comprises three nuclei: the dentate nucleus, the interposed nuclei and the fastigial nucleus. The dentate nucleus receives inputs from the lateral hemispheres of the cerebellar cortex and projects via the thalamus to premotor, prefrontal and parietal neocortical regions. The interposed nucleus receives inputs from the intermediate cerebellar cortex and projects to the spinal cord (via the red nucleus) as well as to the primary motor cortex via the thalamus. Finally, the fastigial nucleus receives inputs from the midline area of the cerebellar cortex (vermis) and projects to neocortical and brainstem targets. These connections are summarized on Figure 1.4.

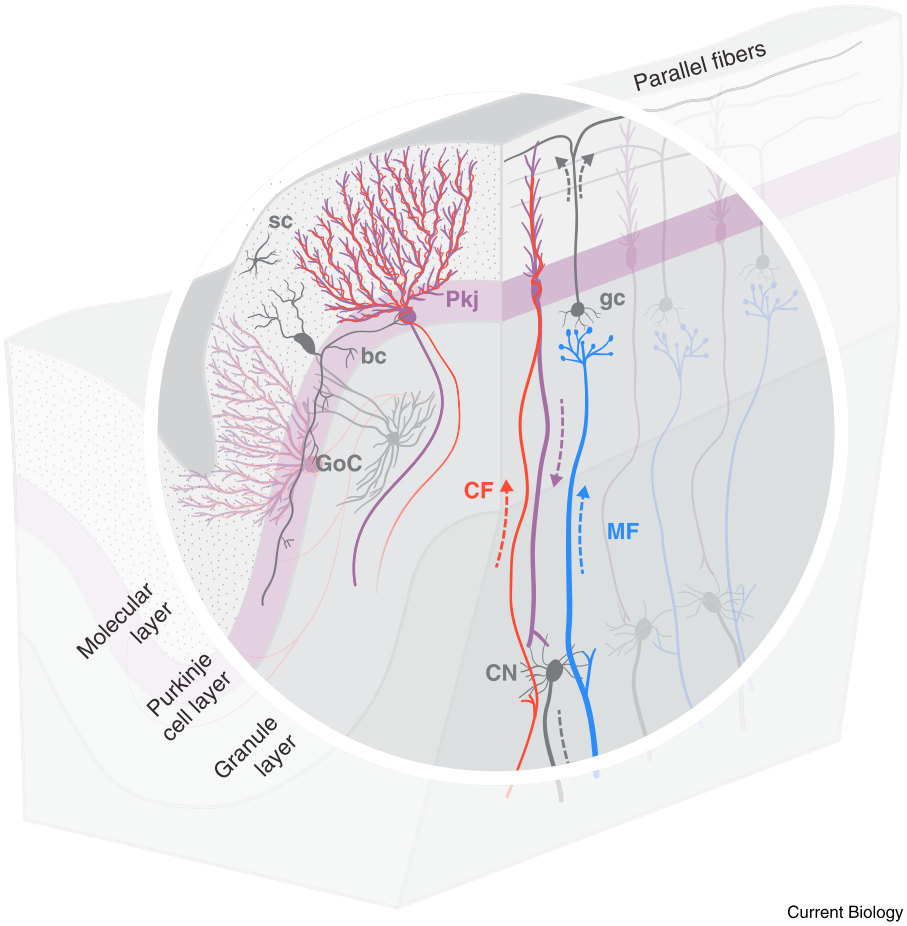

FIGURE 1.3: The canonical cerebellar cortical circuit. Diagram depicting the major layers and cell types of the cerebellum. Excitatory inputs are conveyed by mossy fibers (MF) and climbing fibers (CF), which both project to the cerebellar cortex and send collaterals to the cerebellar nuclei (CN), which represent the major outputs of the cerebellum. More than half the neurons in the vertebrate brain are cerebellar granule cells (gc), which receive MF inputs and in turn project onto Purkinje cells and inhibitory interneurons (stellate cells, sc; basket cells, bc; Golgi cells, GoC) via parallel fiber axons. Purkinje cells have planar dendrites elaborated in the parasagittal plane and are the sole outputs of the cerebellar cortex, projecting to the cerebellar nuclei. (Figure by Gil Costa from Carey, 2024)

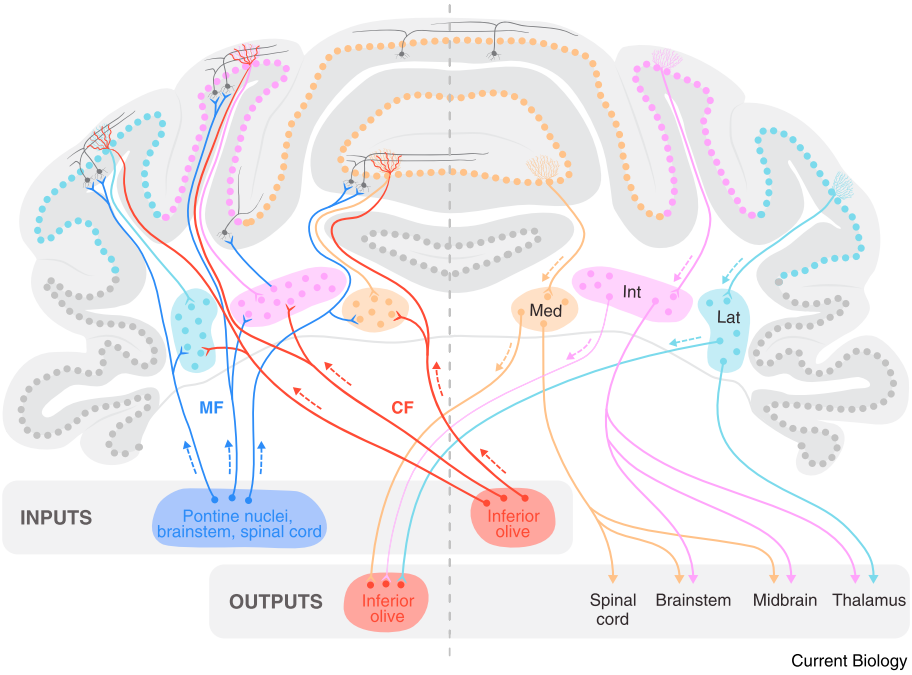

FIGURE 1.4: Modular cerebellar circuitry supports a vast array of inputs and outputs for control of diverse brain functions. A coronal view of the cerebellum and its major input (left) and output (right) pathways. Inputs and outputs are labeled and illustrated on the left and right, respectively. There is a broad medio-lateral functional organization, particularly in terms of outputs, delineated by the distinct projection patterns of the cerebellar nuclei (labeled here as Medial/Fastigial, Med; Interposed, Int; Lateral/Dentate, Lat. Additional output nuclei, including brainstem vestibular nuclei and the parabrachial nucleus, are not shown). (Figure by Rita Félix. From Carey, 2024)

Given its highly homogeneous structure, cerebellum lacks clear parcellation based on cytoarchitectonic organization. In terms of motor control, its representation likely constitutes more of a functional space than body space, as the same body part can be represented multiple times across cerebellum.

The primary efferent pathway is the dentothalamocortical tract, while the main afferent pathway is the corticopontocerebellar tract. Purkijne cells project to the deep cerebellar nuclei, with the dentate nucleus serving as the main output. The dentothalamic tract projects to the contralateral ventral lateral nucleus of the thalamus, which then prjects to the primary motor cortex of the precentral gyrus. From the motor cortex, projections are made to the pontine nuclei via the corticopontine tract, terminating as mossy fibers and completing the loop of this circuit. (Gould et al., 2016)

1.2.3 Cerebellar function in motor control, prediction & learning

One prevalent idea about cerebellum's role in motor control is that it serves as a predictive model (Miall et al., 1993; Wolpert, Miall, & Kawato, 1998). Control theory has demonstrated that internal predictions are crucial for maintaining stability in systems with motor and sensory delays. To illustrate, when we aim to accomplish a task, we generate a set of motor commands to send to the limbs based on an estimate of the state (i.e., position, velocity, ...) as well as sensory feedback. However, delayed-feedback control only cannot explain our ability to make fast and accurate movements. The delay in the sensory feedback makes it challenging to precisely adjust our movements in real time. For instance, we may receive feedback that we are getting close to the target, but due to the delay we would have difficulties to know exactly when to stop to end up in the target. If the endpoint position is not correct (overshoot or undershoot), we would have to correct with another movement, which might also be imprecise, ... This would result in dysmetria and oscillations in the movements (Diedrichsen & Bastian, 2014).

To avoid this limitation, in our closed loop control we can incorporate a predictive mechanism. By using a copy of the motor command

sent to the limbs, we can predict the future state of the limbs. This prediction is then integrated with the delayed sensory feedback, resulting in an optimal estimate of the state. By relying on this estimate rather than the delayed sensory feedback alone, we can mitigate the effects of the delay and achieve smoother and more accurate control over our movements.

Several studies provided evidence supporting the hypothesis of cerebellum as a predictive model. Early support for this idea comes from a study in which researchers cooled the dentate nucleus of monkeys while they were performing a postural perturbation task (Flament et al., 1984). In this task, the monkeys had to maintain a robotic handle still at a target and counteract unexpected perturbations. When a perturbation was applied to the limb, the monkeys initially reacted to the perturbation as pre-cooling. However, they exhibited oscillations around the target due to a lack of precise control over the timing of agonist and antagonist muscle activity, which is essential for stopping the limb at the target. These findings suggest impaired prediction about the consequences of corrective actions.

Predictions also play a crucial role in coordinating movements between multiple limbs or joints. For instance, when we move our elbow, we need to actively stabilize the shoulder to counteract the torques exerted on the shoulder by the elbow motion. Studies on cerebellar patients have shown increased shoulder instabilities during voluntary movements with high interaction torques, indicating their difficulty in coordinating between multiple limbs (Bastian et al., 1996). This coordination between joints is already present in the fast feedback responses, from 50 to 60 ms post perturbation. Cerebellar patients exhibited coordinated feedback responses of a lower magnitude than healthy controls, further highlighting their impairment in coordinating movements across joints (Kurtzer et al., 2013).

Another illustrative task demonstrating the importance of prediction is the waiter task. In this task, participants are required to balance a tray with a load on top and are then instructed to remove the load from the tray. To limit the consequences of load removal, participants reduce their muscular activity in the load-bearing hand approximately 50 ms before the load is actually removed. This anticipatory adjustment

is possible only if predictions are made about the ongoing action. However, if the load is removed by an external agent, participants are unable to form a prediction, resulting in a small upward movement of the tray. Studies involving cerebellar patients have revealed that their anticipatory responses are poorly calibrated in size and timing (Diedrichsen et al., 2005), further supporting the role of cerebellum in forming predictions about the state.

Cerebellum also plays a crucial role in learning. Motor adaptation occurs when repeated errors are observed during movements, leading to gradual adjustments in the motor commands aimed at reducing these errors. Consider a simple example such as throwing darts at a target. If we introduce a visual perturbation using prism glasses, which shifts participant's vision, their initial throws following the introduction of the perturbation will contain large errors, causing them to miss the target (Figure 1.5 a). With trial repetition, movements will gradually adapt to reduce the error. This adaptation process relies on the internal models of body dynamics, which translate observed error into desired changes in motor commands. When the perturbation is removed, an after-effect is observed during which errors are produced because movements were tuned to the perturbation before gradually returning to the original calibration (Diedrichsen & Bastian, 2014).

An early study reported impaired adaptation among cerebellar patients in a task involving throwing clay balls at a target wearing prism glasses. Despite repeated trials, individuals with focal cerebellar lesions failed to adapt to this new environment and upon removing the perturbation, they exhibited no after-effect (Martin et al., 1996). Comparable findings emerged from a study on reaching movements in a force field. Participants experienced a perturbation proportional to their hand velocity through a robotic handle as illustrated on Figure 1.5 c. Cerebellar patients demonstrated impaired adaptation, with reduced after-effects following the removal of the perturbation (Figure 1.5 b, Smith and Shadmehr, 2005). Furthermore, impaired adaptation in these patients extends beyond upper-limb movements, as evidenced by a saccadic adaptation task. Participants experienced repeated jumps of the visual target during the saccade, resulting in an end-point error. As illustrated on Figure 1.5 b, cerebellar patients only partially adapted their motor commands in comparisons with healthy controls

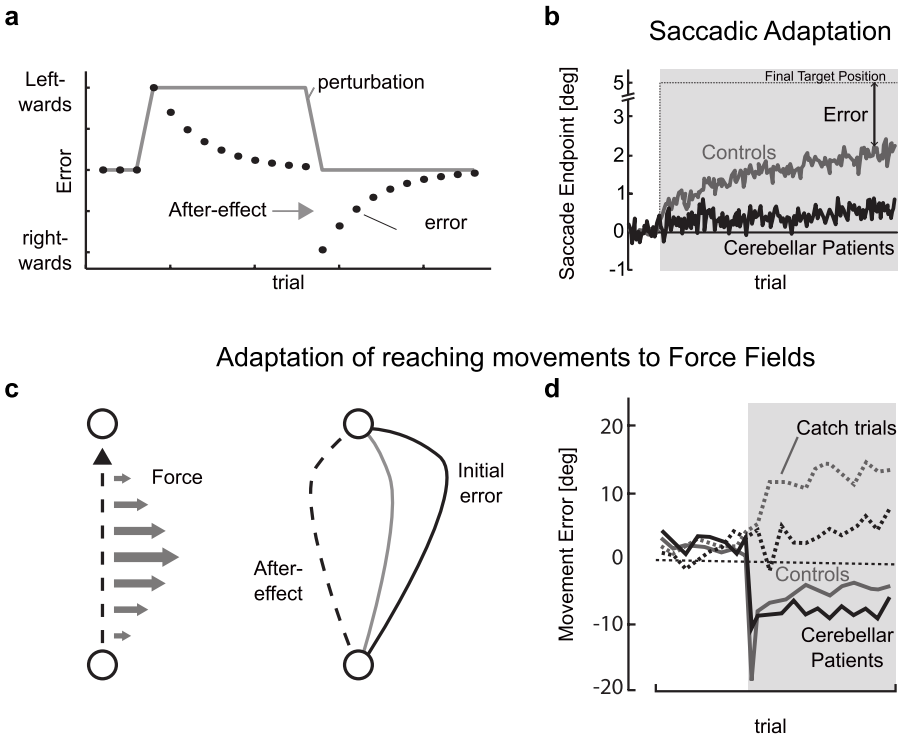

FIGURE 1.5: **a,** Traditional adaptation experiment in which a perturbation suddenly occurs, leading to an exponential learning curve. Upon perturbation removal, an aftereffect is observed. **b,** Deficit of cerebellar patients in adapting to visual target jumps. The target jump (gray box) causes a large endpoint error. Cerebellar patients adaptation is impaired in comparison with the control group. **c,** During a force-field reaching task, a robotic device exerts a force perpendicular to the direction of movement. After an initial error, the movement adapts, resuming a nearly straight trajectory (gray line). When the force is suddenly removed, an aftereffect in the opposite direction occurs. **d,** Deficit of cerebellar patients in adapting to force fields. The force field is switch on (gray box), causing a large initial error. Healthy individuals show increasing after-effects on trials with no force field, but patients with cerebellar degeneration do not. **a,c,** Figures adapted from Diedrichsen and Bastian, 2014. **b,** Figure adapted from Xu-Wilson et al., 2009. **d,** Figure adapted by Diedrichsen and Bastian, 2014 from Smith and Shadmehr, 2005.

(Xu-Wilson et al., 2009).

1.2.4 Links between cellular mechanisms & cerebellar learning

This adaptation mechanism aligns with the structure of cerebellum. In this context, mossy fibers synapsing onto the parallel system could convey information about the motor commands and the current state at a high firing rate. While the climbing fibers could convey the error signal via the complex spikes. These complex spikes in the Purkinje cells trigger an influx of Ca++, inducing a long-term depression. As a result, for the same input in the parallel fibers, we would observe a reduced firing rate of simple spikes, leading to a decreased inhibition of the cerebellar nuclei that might elicit adaptation (Carey, 2024; Diedrichsen & Bastian, 2014).

1.3 Models of movement control

Given the crucial role of cerebellum in movement control, focusing on this topic can provide insights into the mechanisms underlying ET. Models are valuable tools for understanding and predicting outcomes of experiments related to movement control. In this section, we will explore various models proposed for reaching movements, we will briefly discuss some of these models before delving into Optimal Feedback Control, a framework central to this thesis.

1.3.1 Candidate models

As mentioned earlier, prediction and state estimation are essential for skilled and precise movements. In these models, defining a controller is also important as it influences the state of the system by sending control signals to the limbs. In this section, we discuss different candidate models, which state variables are considered and how are the control signals computed.

Inverse models

Similar to forward models, which predicts the sensory consequences from the efferent copy of motor commands, the central nervous system might possess inverse models. These inverse models would convert desired trajectories into motor commands (Kawato, 1999). The resulting motor plan would then be executed in order to reach the desired goal. Motor adaptation supports the hypothesis of an internal representation of the system's dynamics as evidenced by the observed reduction of the initial error and recalibration of motor commands over time following the introduction of a new environment or a perturbation. In this framework, it could be implemented through adjustments of these inverse models. When the perturbation is removed, an aftereffect occurs and would be explained by the time needed by the central nervous system to readapt the inverse model to the initial environment.

How are desired trajectories selected ? One suggestion is to optimize movement smoothness, as proposed by the Minimum Jerk model (Flash & Hogan, 1985). According to this model, trajectories are computed to minimize the derivative of the acceleration of the movement. This model is able to reproduce some classic features of movements, such as bell shape velocity profile or smoothness of the movements. However, this model fails to account for trial-to-trial variability.

An alternate model, the minimum-variance model, was proposed to overcome this limitation (Harris & Wolpert, 1998). In this model, trajectories are selected to minimize the end-point variance. Taking into account a crucial property of the motor system that neural control signals are corrupted by signal dependent noise, meaning that the variance of the noise increases with the control signal. If the noise was independent of the signal, to minimize the noise of our movements and therefore endpoint error, we would produce fastest movement as possible. However in this case, it would require large very high motor commands leading to high noise. In this theory, the trajectory is not only defined based on the kinematics, as in the minimum jerk model, but is also defined based on the dynamics of the system. Trajectories produced by this model are smooth, as rapid changes in the kinematics would necessitate large controls signal, leading to high noise.

A common limitation of these models is their inability to explain

online corrections observed during movements in response to perturbations or changes in the environment. This limitation comes from to the fact that these models assume that the motor plan can be computed a priori from a trajectory and then processed independently, failing to explain the feedback mechanisms observed in response to perturbations.

Impedance control

To address the limitations of previous models, the impedance control model (Gomi & Kawato, 1996, 1997) offers a promising alternative. This model reproduces similar features to those described above and additionally incorporates feedback mechanisms. This theory uses the spring-like properties of the muscles to stabilize the body during motor control by acting on the impedance. The limb impedance is characterized by 3 parameters: joint stiffness, damping, and inertia. Joint stiffness determines how much resistance the limb offers to external forces, damping reflects the limb's ability to absorb energy in response to external forces, and inertia represents the limb's resistance to changes in its motion. In impedance control, the central nervous system would dynamically modulate joint stiffness during movement if the limb deviates from the preplanned trajectory, thereby limiting the effects of perturbations or noise on the limb trajectory.

However, this model has its limitations. It has been demonstrated that impedance can only account for small perturbations, leaving this model unable to explain how the motor system responds to larger perturbations (Crevecoeur & Scott, 2014). Additionally, this theory is based on trajectory control, but experiments have revealed that the motor system behaves differently when having to reach a target versus when explicitly following a constraint trajectory reaching to the same target (Cluff & Scott, 2015), thereby limiting the range of movements that can be effectively modeled within this framework.

1.3.2 Optimal feedback control

Optimal feedback control (OFC), initially developed in the field of control theory, was adapted to human motor control by Emo Todorov

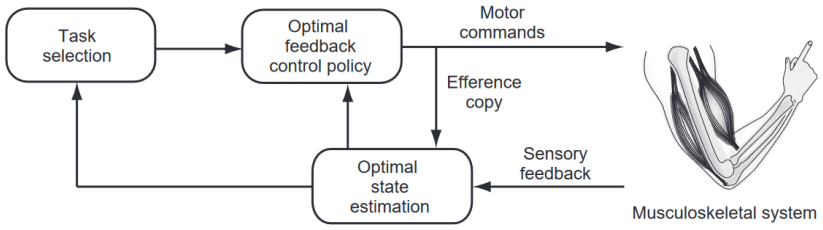

FIGURE 1.6: Illustration of basic processes expected under the OFC framework. The selection of the behavioral task determines the feedback control policy (task selection). The purpose of the feedback control policy is to continuously process and convert sensory data into motor commands that best satisfy the task demand (optimal feedback control policy). Once the sensory feedback is processed, motor commands are sent to the peripheral motor system (biomechanical plant or musculoskeletal system). An efference copy of the descending motor command is used internally to predict the consequences of motor actions. These internal predictions are combined with feedback from sensory receptors to compute the posterior estimate of the state of the body (optimal state estimator). This state estimate is used to adjust the motor commands during the ongoing motor action. Figure from Crevecoeur et al., 2014

(Todorov & Jordan, 2002). In this framework, the controller does not enforce a predetermined trajectory; instead, it intelligently uses feedback to correct deviations that interfere with the task goal. Motor commands are not based on a preplanned trajectory but are rather a linear combination of the state estimate and are optimized to steer the system towards the desired state at each time step.

A schematic block diagram of this model is shown in Figure 1.6. The controller continuously uses the state and the task goal to convert this information into motor commands that best satisfies the task goal. As the system's state is not directly observable due to noises and delays, the model computes an estimate of the state at each time step. The state estimator uses internal models of the system's dynamics and an efferent copy of the motor commands to form a prior estimate of the state at each time step. This prior estimate is then updated using sensory feedback and is used to update the motor commands during the

movements. Unlike the models discussed earlier, which compute an optimal trajectory for control, OFC uses internal models to generate an optimal estimate of the state, which is then used to generate the control signal.

Mathematical derivation of the LQG controller

From a computational point of view, the controller that we used in this work is an LQG controller, a specific case of optimal control. In this framework, the system is assumed to follow a **Linear** dynamic, with a **Quadratic** cost function and a system subject to **Gaussian** noise.

The discrete time system dynamics obtained via Euler integration is defined as:

$$x[t+1] = Ax[t] + Bu[t] + \xi[t], \tag{1.1}$$

where $x \in \mathbb{R}^n$ contains information about the state of the system, $u \in \mathbb{R}^p$ represents the control vector, A and B are real-valued matrices and $\xi[t] \sim \mathcal{N}(0^{n\times 1}, \Sigma_{motor})$ is additive Gaussian white noise with covariance matrix Σ_{motor}.

The cost function is a quadratic function of the state and command defined as follows:

$$J(x,u) = \sum_{i=1}^{N} \{x[i]^T Q[i] x[i] + u[i]^t R u[i]\}, \tag{1.2}$$

where N is the discretized movement time, Q and $R > 0$ which respectively penalize motor error and motor commands at any time step. This cost function allows to translate goals (like reaching a target) to sensorimotor control policies. In the context of reaching movements, Q is usually non-zero only at the end as what matters the most is to reach the goal.

Because the state is not fully observable due to noise and sensory feedback delays, we need to introduce new quantity $y \in \mathbb{R}^m$. The feedback measurement is defined as such:

$$y[t] = Hx[t] + \omega[t], \tag{1.3}$$

where H is the observation matrix (often set to the identity matrix $I^{m\times m}$), and $\xi \sim \mathcal{N}(0^{m\times 1}, \Sigma_{sensory})$ is additive Gaussian white noise with covariance matrix $\Sigma_{sensory}$.

The optimal estimate $\hat{x}[t+1]$ is computed in two steps, first, a prior estimate of the state $x^p[t+1]$ is formed using the efferent copy of the motor commands and internal models about the system dynamics:

$$x^p[t+1] = A\hat{x}[t] + Bu[t]. \tag{1.4}$$

This prior estimate is then corrected with the difference between actual feedback and expected feedback, weighted by the Kalman gain:

$$\hat{x}[t+1] = x^p[t+1] + K[t](y[t] - H\hat{x}[t]), \tag{1.5}$$

$$K[t] = A\Sigma[t]H(H\Sigma[t]H^T + \Sigma_{\text{sensory}})^{-1}, \tag{1.6}$$

$$\Sigma[t+1] = \Sigma_{\text{motor}} + (A - K[t]H)\Sigma[t]A^T. \tag{1.7}$$

The Kalman gains K weights the sensory evidence and the internal prediction in estate estimation and Σ is the covariance matrix of the state estimate $\hat{x}[t]$ at each time step.

In this framework, the optimal motor command is proportional to the estimated state:

$$u = -L\hat{x}. \tag{1.8}$$

The control gains L that minimizes the cost function are computed recursively as follows:

$$L[t] = (R + B^T S[t]B)^{-1}(B^T S[t]A), \tag{1.9}$$

$$S[t-1] = Q[t] + A^T S[t](A - BL[t]), \tag{1.10}$$

$$S[N] = Q_f, \tag{1.11}$$

with Q_f, the cost matrix at the final time step defining the end-point penalty on the motor error, and S a proxy allowing to compute the cost-to-go.

The LQG framework is a good candidate model as it finally links motor costs, expected reward, sensitivity to noise, sensory feedback and internal models into a single framework.

Reaching movements and Optimal Feedback Control

One of the aspects that previous models failed to explain is the reliability of motor systems to reach goals while movements vary from trial

to trial and are rarely reproduced in detail. OFC model addresses this by emphasizing both goal achievement and the richness of motor variability, integrating an important property in its framework: the *minimum intervention principle*. This principle posits that if a disturbance or noise does not interfere with the task, it does not need to be corrected. Correcting such disturbances would require generation of motor commands, implying higher cost as motor commands are penalized by the cost function and the introduction of noise in the system via signal dependent noise. This theory supports the hypothesis that movement execution cannot be dissociated from movement planning.

This principle has been observed in various tasks. In unperturbed reaching tasks, wider endpoints are observed for wider targets (Lowrey et al., 2017; Nashed et al., 2012). Additionally, in tasks where subjects perform movements passing through a series of targets, for the same trajectory, variability is increased for movements with fewer targets as the motor system allows for more or less error depending on the number of targets (Todorov & Jordan, 2002). When mechanical perturbations are present, corrections occurs only if they interfere with the goal. For instance, if a lateral perturbation is applied to the hand during a reaching movement, it would be corrected for a square target, but not for a rectangle target, as it does not interfere with task success (Lowrey et al., 2017). Similar behaviour is observed for movements in an environment with or without obstacles (Nashed et al., 2012). The OFC model is also capable of reproducing behaviours observed in tasks involving target jumps (Liu & Todorov, 2007), bimanual coordination (Diedrichsen, 2007), and reproduces variations in motor responses observed in environments with uncertain targets (Izawa & Shadmehr, 2008).

1.3.3 Neural Basis of Optimal Feedback Control

Although OFC model was developed without specific references to brain structures, it is interesting to map this model to the different brain regions. In their review, Shadmehr and Krakauer identified four key brain regions: the Basal Ganglia which plays a role in the estimation of expected costs and rewards; the Cerebellum, which plays a role in predicting the consequences of our actions; the Parietal Cortex which

plays a role in combining the prior estimate with the sensory feedback; And finally, the Premotor Cortex along with the Primary Motor Cortex are responsible for applying the feedback control policy converting estimated states into motor commands (Shadmehr & Krakauer, 2008). These regions are illustrated on Figure 1.7.

Cerebellum

Cerebellum is believed to play a role in predicting the sensory outcomes of motor commands through the utilization of internal models of the system's dynamics (Kawato, 1999; McNamee & Wolpert, 2019; Wolpert, Miall, & Kawato, 1998). This predictive capacity allows the system to mitigate the impact of noises and delays in the system. By using an efferent copy of the motor commands, cerebellum can construct a prior estimate of the current state. As discussed in the preceding section 1.2, cerebellar deficits are linked with impaired coordination across multiple limbs (Bastian et al., 1996), impaired feedback control responses (Flament et al., 1984; Kurtzer et al., 2013) and reduced motor adaptation (Martin et al., 1996; Smith & Shadmehr, 2005; Tseng et al., 2007; Xu-Wilson et al., 2009). These findings collectively support the role of cerebellum in the formulation of prior estimates of the state.

Parietal cortex

The parietal cortex assumes an important role in optimally combining the prior estimate of the state with the sensory feedback. Lesions of the parietal cortex have been associated with various impairments, including compromised limb state estimation when relying on proprioceptive feedback (Wolpert, Goodbody, & Husain, 1998), impaired reaching movements when dependent on visual or proprioceptive information depending on lesion localization (Rushworth et al., 1997) and impaired online movement corrections when performing movements in an environment with moving targets (Gréa, 2002). Transcranial magnetic stimulation (TMS) applied to this region made participants insensitive to target jumps happening during the movements. Participants continued acting as if the target jump had not occurred, indicating that the prior estimate remained intact (Desmurget et al., 1999).

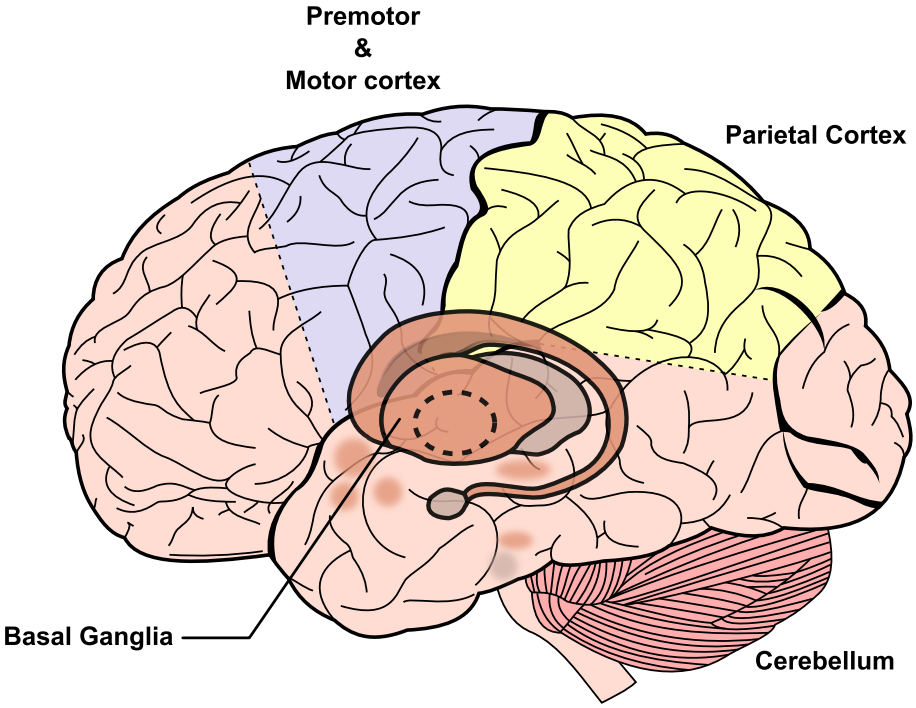

FIGURE 1.7: Schematic representation of the regions implicated in the neural implementation of optimal feedback control in the human brain. Cerebellum computes an internal prediction about the state that is updated with sensory feedback in the parietal cortex creating an estimate of the current state. This estimate combined with expected cost and rewards estimated by the basal ganglia is used by the premotor and motor cortex to generate an optimal motor command in order to meet the current task goal.

Basal ganglia

The basal ganglia, a group of subcortical nuclei, are believed to play a role in integrating the expected task costs and rewards into a cost function (Shadmehr & Krakauer, 2008). This role is supported by studies involving Parkinson's disease (PD) patients, a condition affecting basal ganglia. PD patients typically exhibit bradykinesia, a slowness in movement execution. Mazzoni and colleagues demonstrated that PD patients do not reduce movement speed to enhance movement precision, as movement accuracy remained preserved when compared with data from healthy controls at matched speeds. Instead, their study revealed an increased sensitivity to movement cost in PD patients (Mazzoni et al., 2007). Within the framework of OFC, behavior is explicitly guided by costs and rewards, bradykinesia could be explained by an elevated sensitivity to motor cost (R in Eqn. 1.2) relative to the sensitivity to movement error (Q in Eqn. 1.2), thereby establishing a link between the basal ganglia and the cost function (Shadmehr & Krakauer, 2008).

Premotor and motor cortices

The premotor and motor cortical areas are involved in the continuous implementation of the feedback control policy (Scott, 2012). Using the designated goal and cost function sent by the Basal ganglia, these regions translate the state estimation into motor output (Shadmehr & Krakauer, 2008). Evidence from TMS studies targeting the primary motor cortex indicates that it influences feedback responses counteracting mechanical perturbations as shortly as 50 ms post-perturbation (Pruszynski et al., 2011). Moreover, direct recordings of neurons in the primary motor cortex revealed that their activity is tuned to the task goal (Pruszynski et al., 2014), suggesting the involvement of the primary motor cortex in rapidly selecting new motor actions (Scott, 2016). This reinforces the hypothesis that these regions play a role in feedback control by applying the control policy during both preparation and movement execution.

1.4 Aim of this work

Despite ET being a frequent disorder, the exact source of oscillations remains unidentified. While the cerebellar origin is often suggested, it would be beneficial to identify the mechanisms underlying the generation of oscillations in ET. In this thesis, we delve into the role of cerebellum by focusing on sensorimotor control in specific tasks known to rely on cerebellar integrity: adaptation of upper limb control to force fields, adaptation of saccadic eye movements to sudden changes in the location of a visual stimulus and feedback control.

Our aim was to characterize the impact of ET on limb control and assess whether cerebellar-dependent mechanisms engaged in these tasks could explain the tremor. Additionally, we studied the functional connectivity of the cerebellum and cortex measured during resting-state functional MRI, as well as brain volumes using structural MRI and their correlations with behavioral measurements. The goal of these studies was to better characterize the functional impairments of ET patients and relate these changes with brain volume and functional connectivity.

In Chapter 2, we investigated the fingerprint of ET on two motor adaptation tasks. The first task focused on ET patients' adaptation to force fields. Participants performed upper limb reaching movements with a handle towards targets while the experimental device applied a force to deviate subjects' hand. The second task focused on saccadic adaptation, where we introduced target jumps during the saccades, these jumps are known to induce an adaptation of the saccade end point in order to get closer to the final target position. In both tasks, ET patients' adaptation was impaired in comparison with neurologically intact volunteers. Further decomposition revealed that the impairment stemmed from impaired online control of the movements, as anticipation of the perturbations remained preserved in both tasks. These results suggest that the disorder originate from impaired movement execution.

In Chapter 3, we elaborated on the findings of Chapter 2 by studying a feedback control task specifically. We used a standard postural perturbation protocol, volunteers experienced perturbations of unexpected magnitude and direction and were instructed to counter the

perturbations and steer their hand back to the target. After an initially preserved reaction to the perturbation, we observed perturbation-dependent deficits in the ET group, confirming suspected feedback control deficits and supporting the hypothesis that the tremor is generated by the feedback controller. Our study explored the possibility that oscillations results from an erroneous compensation of sensorimotor delays, as similar oscillations can arise in systems not compensating properly for feedback delays. We showed that errors in delay compensation reproduced the experimental results, supporting the computational hypothesis that ET originates from an erroneous compensation of sensory delays, a function that has been linked with cerebellum.

In Chapter 4, to better understand the role played by cerebellum in ET, we investigated volumetric and functional connectivity changes in ET patients and assessed their relationship with behavioral measurements collected outside of the MRI scanner. Participants underwent a 3 T MRI protocol, including resting-state fMRI and structural imaging. Using seed-based and connectome-based approaches, we observed a reduction of the functional connectivity in the cerebello-thalamo-cortical pathway in ET participants. In addition, these changes were correlated with tremor severity. Using the functional connectivity data, we were able to predict the clinical score as well as the average spectral power density of the tremor in the patient subgroup. Finally, we observed an atrophy of the thalamic sub-nuclei that correlated with tremor severity. Overall, these results support the implication of cerebellum and its projections in the tremor genesis.

Finally, in Chapter 5 we summarized the contributions of Chapters 2-4 and discussed their results. We identified some limitations of these studies and discussed open questions that remain unanswered following the observations made in this work. Finally, we suggested some ideas of experiments that could be conducted in future research.

In conclusion, all elements support the hypothesis that ET could have a cerebellar origin, and that the tremor could originate from an altered estimation of sensory delays. The novelty of this work lies in combining different behavioral, computational, and neuroimaging approaches to shed some light on the functional role of cerebellum in ET. A better understanding of the mechanisms behind the generation of the tremor represents a first step towards improving patients' quality

of life and exploring new perspectives for diagnostic, treatments and rehabilitation.

1.5 Publications and communications

Published

- **Blondiaux F., Lebrun L., Hanseeuw B., Crevecoeur F.** Impairments of saccadic and reaching adaptation in Essential Tremor are linked to movement execution. *J Neurophysiol.* 130(5):1092-1102, 2023
- **Blondiaux F., Colmant L., Lebrun L., Hanseeuw B., Crevecoeur F.** Erroneous compensation for long-latency feedback delays as origin of Essential Tremor. *Journal of Neuroscience*, 44(25):e0069242024, 2024

Proceedings

- **Blondiaux F., Lebrun L., Hanseeuw B., Crevecoeur F.** Essential tremor: a cerebellar disorder ? *Benelux Workshop on Systems and Control 2021*, Rotterdam, Netherlands, 2021 [Talk]
- **Blondiaux F., Lebrun L., Hanseeuw B., Crevecoeur F.** Impact of essential tremor on saccadic adaptation, *30th Annual Meeting of the Neural Control of Movement Society*, Online, 2021 [Poster]
- **Blondiaux F., Lebrun L., Hanseeuw B., Crevecoeur F.** Motor adaptation is impaired with Essential Tremor patients, *50th Annual Meeting of the Society for Neuroscience*, Online, 2021 [Poster]
- **Blondiaux F., Colmant L., Lebrun L., Hanseeuw B., Crevecoeur F.** Long-latency feedback responses preserved in Essential Tremor patients *31st Annual Meeting of the Neural Control of Movement Society*, Dublin, Ireland, 2022 [Poster]
- **Blondiaux F., Colmant L., Lebrun L., Duchêne G., Dricot L., Hanseeuw B., Crevecoeur F.** Long-latency feedback responses preserved in Essential Tremor patients *52nd Annual Meeting of the Society for Neuroscience*, Washington, DC, 2023 [Poster]

Chapter 2

Impairments of saccadic and reaching adaptation in Essential Tremor are linked to movement execution

Published as : Blondiaux F., Lebrun L., Hanseeuw B., and Crevecoeur F., Impairments of saccadic and reaching adaptation in Essential Tremor are linked to movement execution, *Journal of Neurophysiology*, 130 (5), 1092-1102, 2023.

ESSENTIAL tremor (ET) is a neurological disorder characterized by involuntary oscillations of the limbs. Previous studies have hypothesized that ET is a cerebellar disorder and reported impairments in motor adaptation. However, recent advances have highlighted that motor adaptation involves several components linked to anticipation and control, all dependent on cerebellum. We studied the contribution of both components in adaptation to better understand the adaptation impairments observed in ET from a behavioral perspective. To address this question, we investigated behavioral markers of adaptation in ET patients (n = 20) and age-matched neurologically intact volunteers (n = 20) in saccadic and upper limb adaptation tasks, probing compensation for target jumps and for velocity-dependent force fields, respectively. We found that both groups adapted their movements to

the novel contexts; however, ET patients adapted to a lesser extent compared with neurologically intact volunteers. Importantly, components of the movement linked to anticipation were preserved in the ET group, whereas components linked to movement execution appeared responsible for the adaptation deficit in this group. Altogether, our results suggest that execution deficits may be a specific functional consequence of the alteration of neural pathways associated with ET.

New & Noteworthy: We tested Essential Tremor patients' adaptation abilities in classical tasks including saccadic adaptation to target jumps and reaching adaptation to force field disturbances. Patients' adaptation was present but impaired in both tasks. Interestingly, the deficits were mainly present during movement execution, while the anticipatory components of movements were similar to neurologically intact volunteers. These findings reinforce the hypothesis of a cerebellar origin for essential tremor and detail the motor adaptation impairments previously found in this disorder.

2.1 Introduction

Essential tremor (ET) is one of the most common movement disorders provoking involuntary oscillations of patients' limbs (Louis & Ferreira, 2010). Typical clinical features of ET are kinetic and intention tremors of limbs, particularly upper limbs and, to a lesser extent, head and trunk (Bhatia et al., 2018; Clark & Louis, 2018; Shanker, 2019). To date, the pathophysiology of this neurological disorder is not fully understood, but some previous works have suggested a cerebellar origin (Ibrahim et al., 2021). Neuroimaging studies reported abnormalities in the structure and connectivity of cerebellum as well as differences in the cerebello-thalamo-cortical loop (Mavroudis et al., 2021; Muthuraman et al., 2018; Pietracupa, Bologna, Tommasin, Elifani, et al., 2021; Tikoo et al., 2020). Postmortem studies also pointed towards alterations of cerebellar cells (Louis & Faust, 2020a). Characterizing whether specific cerebellar functions are preserved or impaired in this condition is therefore important to better understand this disorder.

Crucial functions of cerebellum include movement control, state-estimation, and adaptation (Diedrichsen & Bastian, 2014; McNamee & Wolpert, 2019; Therrien & Bastian, 2015). The central nervous system cannot exactly access the state of the limbs (position, speed, etc.) due to the intrinsic delays in sensory feedback and to sensorimotor noise. As a result of this uncertainty, the brain must predict the next state that will be used to plan and control fast and accurate movements. The prediction is computed based on the delayed sensory feedback and an efferent copy of the motor command used in conjunction with prior knowledge of body and environmental dynamics. This operation of state estimation, which makes use of internal models, has been associated with cerebellum (Kilteni et al., 2020; Miall et al., 1993; Miall et al., 2007; Wolpert, Miall, & Kawato, 1998).

The ability to adapt motor patterns to novel environments rests on our ability to update the internal models used for estimation and control, thereby allowing for predictive compensation for sustained disturbance. It has been reported that adaptation depends on the integrity of cerebellum. The involvement of cerebellum in motor adaptation has been studied with a variety of movements, with non-human species (Baizer et al., 1999; Ojakangas & Ebner, 1992), as well as with cerebellar patients (Smith & Shadmehr, 2005; Tseng et al., 2007; Xu-Wilson et al., 2009), who have shown deficits of adaptation in response to repeated perturbations. These results possibly reflect inaccurate internal models and a relative inability to update them in a way that counters the disturbance induced by the novel environment (Diedrichsen & Bastian, 2014; Therrien & Bastian, 2015).

Given the involvement of cerebellum in sensorimotor adaptation and its putative link with tremor, we set out to describe motor adaptation impairments in ET across two different tasks. Previous works reported that these patients were able to adapt to perturbations, but to a lesser extent than neurologically intact volunteers in force-field, visuomotor and prism adaptation tasks, as well as eyeblink conditioning (Bindel et al., 2022; Chen et al., 2006; Hanajima et al., 2016; Kronenbuerger et al., 2007). Considering that sensorimotor adaptation may involve multiple components (Mathew & Crevecoeur, 2021), we aimed to expound this adaptation deficit using two tasks probing visual and upper limb motor systems. In particular, we focused on the contributions

of anticipation and movement execution on motor adaptation deficits. To do so, we studied adaptation in saccadic eye movements evoked by peri-saccadic target jumps, and upper limb reaching adaptation to velocity-dependent force fields as well as the correlation of adaptation performances in both tasks. We found that motor adaptation deficits observed in both tasks were due to the time course of movement execution while anticipatory compensation for the perturbation was comparable to the control group.

Our results support the hypothesis of a cerebellar origin for essential tremor but suggest a specific alteration of the pathways linked to the real-time motor execution across both visual and upper limb motor systems.

2.2 Methods

2.2.1 Participants

A total of 22 Essential Tremor (ET) patients and 20 neurologically intact (NI) volunteers participated in this study. All participants provided written informed consent following procedures approved by the Ethics Committee at the host institution (Comité d'Éthique Hospitalo Facultaire, UCLouvain, Belgium). A neurologist performed a clinical evaluation with the Fahn-Tolosa-Marin Tremor Rating Scale (FTM-TRS) (Fahn et al., 1993) on all participants to evaluate the severity of the tremor. ET patients did not interrupt their medication before the assessment. We kept track of current medications and dosages (Supplementary Table 1). All but four ET participants took part in the two experiments. For the reaching experiment, one participant could not perform the task due to the amplitude of their hand tremor, another participant did not complete the task due to pre-existing shoulder condition. For the saccadic adaptation experiment, two other participants were excluded following technical limitations impeding calibration of the eye-tracking system. As a result, each population of ET patients was composed of 20 volunteers. Force sensors were defective for one ET participant, and another ET participant decided to stop the experiment a block earlier.

We kept the data for the analyses and took into account the missing trials and the absence of force recordings. All NI volunteers participated in the two tasks, resulting in a group of 20 NI volunteers.

The FTM tremor rating scale was divided into three sections. Part A quantified the tremor amplitude of the limbs at rest, with posture holding, and during action. Part B quantified the action tremor of the upper limbs, particularly writing, drawing, and pouring liquids. Part C quantified the functional disability, evaluating patients' impairments in daily life activities (eating, drinking, working, etc.). We ignored this part filled by the participant due to the higher subjectivity of some criteria and because our experiments assessed different tasks. Maximum scores for each section were respectively, 80, 32, and 28. Since this scale is not specific to ET evaluation, a low score in some items is expected like rest tremor, uncommon in ET.

2.2.2 Tasks

The study was composed of two experiments: a saccadic adaptation task (Figure 2.1 & 2.2) and a reaching adaptation task to a force field (Figure 2.3 & 2.4). During the saccadic adaptation task inspired from Xu-Wilson et al. (Xu-Wilson et al., 2009), participants sat in a dark room on a height-adjustable chair in front of a screen. Head movements were restricted using a chin rest bar and forehead support. Eye movements were recorded using an Eyelink 1000 Tower-mounted eye tracker (SR Research, Ottawa, Canada) at a sampling rate of 1kHz, and stored for offline analyses. Participants gazed at the green targets (0.8 visual degrees wide) displayed on the screen. After a series of baseline trials containing a fixation target and a goal target, a jump of the goal target was introduced as a perturbation for the adaptation trials (Figure 2.1 a&b). We divided the experiment into 7 blocks: oblique (30 trials), horizontal (30 trials), and five adaptation blocks (60 trials each). Coordinates are expressed in degrees of visual angle both for the horizontal and vertical component, with the center (0°,0°) being straight ahead of the participants.

During the oblique trials, a fixation target (F: (-10°,0°)) was projected on the left side of the screen. After a random wait time between 2 sec and 3 sec distributed uniformly, a new target was projected 20° away

from the fixation target in the horizontal direction and 5° above the meridian vertically (T1: (10°,5°)). For the horizontal trials, the same fixation target (F) was used, and the final target was 20° away in the horizontal direction but aligned vertically (T1: (10°,0°)). We refer to the initial measurements of oblique and horizontal trials as baseline trials. The adaptation trials started with the same initial fixation target (F). A second target displayed 20° to the right appeared (T1: (10°,0°)), and participants were instructed to direct their gaze to the new target. As soon as the saccade was detected, the target jumped 5° away in the vertical direction (T2: (10°,5°)). The target T2 served as a fixation target for the next trial, the jump continued to be counterclockwise (F = (10°,5°); T1: (-10,5°); T2: (-10,0°)). See Figure 2.1 a&b for a sketch of the different targets coordinates. The saccades were detected based on a horizontal velocity threshold of 150°/s computed online using backward 2nd order finite differences. Because of the perturbation, the saccade towards T1 was followed by a corrective saccade towards T2. An inter trial time of 2.3 sec was used in all cases. Participants took a short break between each block (15sec to 1min).

For the reaching adaptation task, participants sat on a height-adjustable chair in front of an End Point KINARM device (KINARM, Kingston, Ontario). They grabbed the handle of the robotic arm and performed reaching movements toward the target projected on the screen (Figure 2.3 a). All participants performed the experiment with their right arm, independently of their laterality based on recent observation that adaptation on each side for the same task is very similar (Córdova Bulens et al., 2023). The device recorded the participants' hand cursor position and forces applied to the handle. An occluder blocked the direct vision of the hand, but a hand-aligned cursor was always represented (white dot, radius 0.6 cm). The radius of the targets was 1.2 cm. A criterion on movement time was applied to encourage consistent velocities, but all movements crossing the target at least once and finishing within less than 3 cm from its center were kept for analyses. Good movement time ([600 ms – 1500 ms]) was indicated by a green target at the end of the trial. If the participant was too slow, the target remained red and full. For movements too quick, the target switched to red and hollow. The experiment was composed of two trial types: null-field trials, and force field trials. During the null-field block

(40 trials), participants were instructed to reach and stop at the displayed target. Two goal targets were used to avoid potential bias liked to the repetition of one target and to make the task less repetitive. The two goal targets and the start target formed an equilateral triangle. Targets centers were 10 cm apart. The start target, closest to the participant, was aligned with their elbow. For each trial, one of the two possible goal target was randomly selected and displayed on the screen. Each set was composed of the same number of trials towards each target. The adaptation blocks (4 blocks) featured trials with similar instructions but performed in the presence of a clockwise velocity-dependent curl field applied throughout the whole movement. The force field was defied as followed: $f_x = 15\ \dot{y}$ and $f_y = -15\ \dot{x}$ (N). Each block was composed of 66 trials: 30 trials towards each target with the force field, and 3 catch trials per target during which the force field was unpredictably turned off. The trials were presented in random order. The inter-trial time was 1sec. Participants were encouraged to take short breaks between the blocks to reduce fatigue (15 sec to 1 min).

2.2.3 Data Analysis

Raw measurements of eye position were filtered with a dual-pass 4th order low pass Butterworth filter with a cut-off frequency of 50 Hz. Eye velocity was computed based on position signals using 4th order finite differences. The beginning and end of each saccade were defined using a threshold on the horizontal eye velocity of 16°/s for at least 10 ms. Additional criteria for saccade inclusion were: (1) its duration, within 50 to 200 ms, (2) its peak velocity, above 100°/s, and (3) a minimum amplitude of 10°, corresponding to one-half of the instructed horizontal displacement. These inclusion/exclusion criterions were adapted from (Xu-Wilson et al., 2009). On average, NI volunteers had 11.7% of their trials excluded (min: 3.9%, max: 38.9%), ET patients 14.7% excluded (min: 3.9%, max: 31.4%). Non-detected saccades were mainly due to blinks and fatigue leading to poor detection of the pupil by the eye-tracking system. The mean velocity was computed on a 40 ms window, centered around the trial's peak velocity. The curvature of saccades was approximated using the same method as Chen-Harris and colleagues (Chen-Harris et al., 2008). Each saccade was divided into 4

equal segments along the horizontal direction, the slope of the line extending the end of each segment was computed and was referred to as S1-S4 (see Figure 2.2 c-g). The timing of each segment was in average 21.7 ms, 11.8 ms, 13.2 ms and 28.5 ms. After observing no qualitative differences between the left and right saccades, adaptation trials in both directions were combined for analyses.

For the reaching adaptation task, the data was filtered using a dual-pass 6th order low pass Butterworth filter with a cut-off frequency of 25 Hz. Movement onset and end were defined using a speed threshold of 3 cm/s. Movements were included in the dataset if their duration was above 300 ms, crossed at least once the target, and ended less than 3cm from the target center. Based on this criterion, we excluded in average 1.1% of the trials for NI participants (min: 0.3%, max: 2.3%) and 4.9% of the trials for ET patients (min: 0%, max: 21.1%). Adaptation was quantified using Pearson's correlation between the force orthogonal to straight path measured at the interface between the hand and the robot handle (measured force), and the force field commanded by the robot and extracted offline based on velocity signals of each trial (commanded force). Intuitively, if the measured force and the commanded force are equal and opposite, one expects high values of correlation between these signals. In contrast, a lack of knowledge of the force field producing only approximate or poorly tuned compensation for the perturbation should yield lower correlation values. It was also verified empirically that this metric was indeed sensitive to adaptation in the same setup and task (Crevecoeur et al., 2020). Initial angles, between the hand path and the straight line connecting the two targets, were computed at 200 ms after movement initiation, with a counter-clockwise angle being defined as positive. We verified that there was no qualitative difference between the two targets, thus movements were remapped and combined for all analyses. We used a constant bin width of 8 trials for illustration purposes to show the effect of the perturbations.

2.2.4 Statistical Analysis

In both experiments, Student's t-tests were used to compare performances between groups during baseline condition (endpoint and maximum velocity of the saccade, movement duration, and path length of

the reaching movement) and for the initial angles from catch trials in the reaching adaptation task. T-tests were also used to compare average group age. Adaptation was evaluated using two techniques: exponential fits and Linear Mixed Effects (LME) models. A standard exponential model of adaptation was fitted on group average and 95% confidence intervals of each parameter were compared between ET and NI. The parameter a corresponds to the final offset to which the exponential curve converges, b is the amplitude of adaptation which therefore impacts the starting point of the curve, and c to the learning rate. The variable i was the trial number. The exponential fit was as follows:

$$y = a + b * e^{-c*i} . \tag{2.1}$$

Because the exponential fits were not significant in all cases, we also used linear mixed models to assess the evolution of the dependent variables across trials and group while taking inter-individual variance as a random factor. More precisely, LME models were fitted with factors Trial Number (i) and Group (2 level factor) as fixed predictors, and a random intercept to capture idiosyncrasy. LME and exponential fits were used for vertical end-point, vertical velocity, and saccades slopes in the first experiment, and maximum perturbation forces, normalized deviation, initial angle, and forces correlations in the second experiment. For each dependent variable the formulae of LME was:

$$Y_{ij} = \beta_0 + \beta_1 * i + \beta_2 * Group + \beta_3 * Group * i + b_j + \epsilon_{i,j}, \tag{2.2}$$

where Y_{ij} represents the dependent variable of trial number i from participant j, β_i are the coefficient of the fixed predictors including trial number, group (control or ET), and interaction between them, and b_j is the random intercept for participant j, and $\epsilon_{i,j}$ is the residual.

To measure the variability of the movements, we investigated several bins across the movement and kept the bin with the highest variability which corresponded to 20 ms around the midpoint between peak velocity and target crossing for the reaching adaptation and 20 ms around the midpoint between peak velocity and movement end for the saccadic adaptation. Variability of each person was computed using their movement in each block. We compared variability of participants

using Wilcoxon rank-sum tests. For the unpaired comparisons between groups, due to the limited number of participants and the inherent variability of our populations we defined the significance threshold at 0.05. This includes Spearman's and Pearson's correlations, Wilcoxon rank-sum tests and Student's t-test. Concerning the LME, where all trials are considered we expect increased statistical power and therefore assessed the significance of each effect using an F-test and a significance threshold of 0.005 (Benjamin et al., 2017; Lakens et al., 2018).

Finally, a linear support vector machine classifier was trained on the final performances of each participant in a 2-dimensional space that contained the learning indices that exhibited strong differences across trials and groups. The purpose of the classification technique was to quantify the overlap between the two groups in this two-dimensional space, however the accuracy of the model was still assessed based on leave-one-out cross-validation. In addition to quantifying the overlap between the distributions, the support vector machine was also used to illustrate that the boundary between the two groups separated the plane into overall better or worse performances in the two groups. All analyses were performed offline with Matlab 2020b. The data will be available in Zenodo following the publication of the article.

2.3 Results

2.3.1 Experiment 1: Saccadic Adaptation

We instructed participants to perform visually guided saccades to a target projected on a screen. The time course of a trial followed standard protocols of saccadic adaptation (Chen-Harris et al., 2008; Xu-Wilson et al., 2009): after an initial fixation delay, the target was projected, and participants initiated a saccade (Figure 2.1 a&b). During movement, the goal target jumped vertically, inducing a terminal error that was gradually reduced as adaptation progressed. The experiment started with baseline trials, during which the target did not jump (see Methods). A total of 40 volunteers took part to this experiment, 20 Essential Tremor (ET) patients (14 F, 6 M) and 20 neurologically intact (NI) volunteers (14 F, 6 M). There was no significant difference in age between ET patients ($M = 58.6$, $SD = 15.4$) and NI volunteers ($M = 56.8$, $SD = 12.4$);

(t-test; $t_{38} = -0.4013$, $p = 0.69$). We assessed tremor severity in all participants using the Fahn-Tolosa-Marin Tremor Rating Scale (FTM-TRS). ET patients obtained an average score of 8.8 ± 5 (mean $\pm$ SD) points in part A assessing tremor amplitude and 14.6 ± 7.6 points for part B which assesses drawings and pouring (part B). The average score of NI participants was 1 ± 1.3 (part A) and 1.5 ± 1.7 (part B).

The average eye trajectories of the baseline phase of the experiment are depicted in Figure 2.1 c, left panel. No significant differences of vertical (t-tests; oblique: $t_{38} = 0.47$, $p = 0.64$; horizontal: $t_{38} = 0.55$, $p = 0.58$) and horizontal (t-tests; oblique: $t_{38} = 0.23$, $p = 0.82$; horizontal: $t_{38} = 0.79$, $p = 0.43$) end-point were observed between the two participants groups during these baseline trials. Likewise, average vertical (t-tests; oblique: $t_{38} = 0.39$, $p = 0.7$; horizontal: $t_{38} = 1.04$, $p = 0.31$) and horizontal (t-tests; oblique: $t_{38} = -0.19$, $p = 0.85$; horizontal: $t_{38} = -0.28$, $p = 0.78$) velocities were similar across the two groups. Mean velocity was computed on a 40 ms window centered on the trial's peak velocity. No statistical differences were observed regarding the fixation prior to the saccade, which was assessed by comparing averaged position and velocity across a 100 ms window prior saccade initiation.

During the adaptation phase of the experiment, the target jumped vertically (5 visual degrees up/down) depending on the saccade direction (right/left respectively). The perturbation resulted in an endpoint error corrected by a second saccade. Both groups adapted their saccades to the target jump by increasing the vertical endpoint coordinate of the first saccade, but the extent of adaptation was significantly smaller for ET patients. The average eye trajectories at the beginning and the end of adaptation trials are plotted for each participant in Figure 2.1 d. First, the vertical end-point of saccade increased with trial repetitions to reach an average of 2.06° (visual degrees) for NI participants, and only 1.83° for ET patients as can be seen in Figure 2.2 a. Exponential fits were generally non-significant for the saccadic adaptation task (except for the 3rd slope), we therefore only present LME analyses for this task. A linear mixed-effect (LME) model revealed a significant main effect of the trial ($F_{(10,356)} = 24.20$, $p < 10^{-4}$), no effect of the group (NI or ET) on the vertical end point was observed ($F_{(38)} = -0.44$, $p = 0.66$) but there was a clear interaction effect between these two

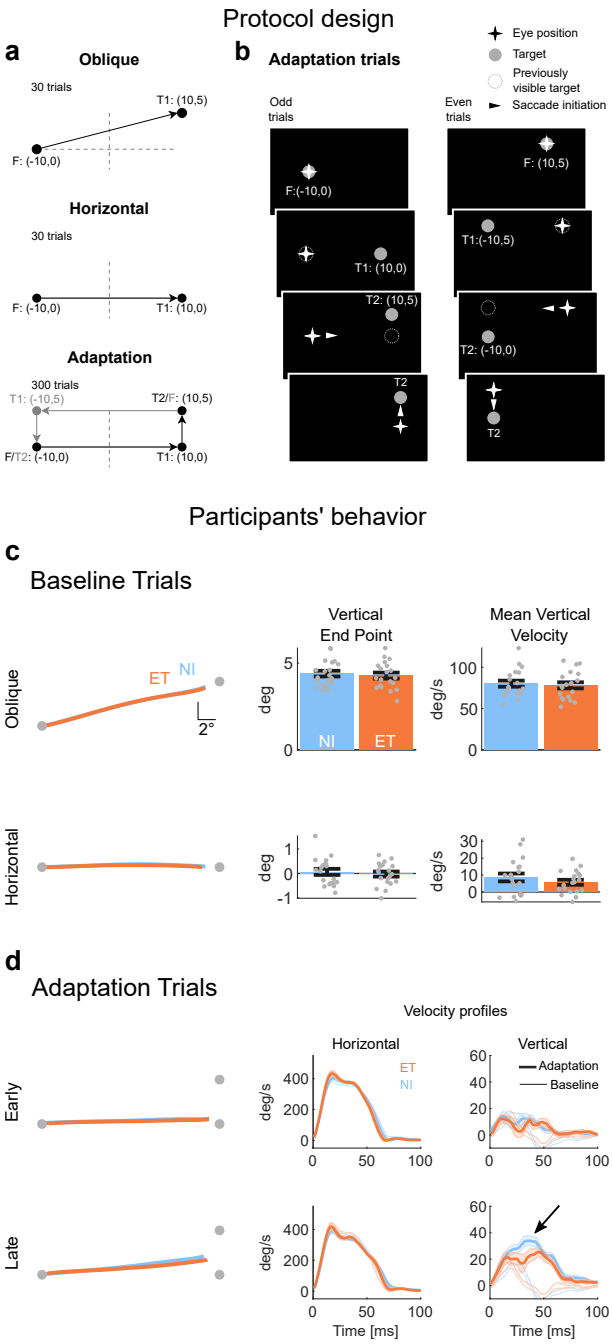
Protocol design
a
Oblique
30 trials
T1: (10,5)
F: (-10,0)
Horizontal
30 trials
F: (-10,0)
T1: (10,0)
Adaptation
300 trials
T1: (-10,5)
T2/F: (10,5)
F/T2: (-10,0)
T1: (10,0)
b
Adaptation trials
Odd trials
Even trials
Eye position
Target
Previously visible target
Saccade initiation
F:(-10,0)
T1: (10,0)
T2: (10,5)
T2
F: (10,5)
T1:(-10,5)
T2: (-10,0)
T2
Participants' behavior
c
Baseline Trials
Oblique
ET
NI
2°
Vertical End Point
deg
NI
ET
Mean Vertical Velocity
deg/s
Horizontal
d
Adaptation Trials
Velocity profiles
Early
Late
Horizontal
Vertical
ET
NI
Adaptation
Baseline
deg/s
Time [ms]

FIGURE 2.1: Schematic representation of the saccadic adaptation protocol design (a,b) & behavior in saccadic adaptation task (c,d). **a** Time course of a trial in the saccadic -adaptation task. Participants (n=40) were asked to perform saccades to gaze at a target visible on the screen. The experiment was divided into 3 trial types: oblique saccades, horizontal saccades, and adaptation saccades. Each trial began with a fixation target (F), followed by the appearance of the goal target (T1) after a random delay. Locations are indicated in visual degrees. During adaptation trials, the goal target was shifted by 5 degrees (T2). These trials occurred in two directions, to the right (black) and the left (grey). Target jump was counterclockwise. The dashed lines depict the axes centered straight ahead. **b** Target sequence from an adaptation trial. Arrows indicate when a saccade was initiated. Target jump (T1 to T2) occurs when the saccade is initiated. At the end of the trial, T2 served as fixation for the next trial (grey in 2.1 a). **c** (Left) Group average of participants' eye trajectories averaged over the oblique and horizontal blocks. Grey dots represent the targets. (Right) Vertical end point and mean vertical velocity of saccades, across all trials, and averaged for the two groups. Error bars represent the SEM. Grey dots represent individual datapoints. **d** (Left) Saccades averaged over the first and last 10 trials to highlight differences between early and late adaptation phases. (Right) Average velocity traces are plotted for the horizontal and vertical components. Thin traces correspond to the horizontal baseline trials. Shaded areas represent the SEM.

factors with a negative coefficient ($F_{(10,356)} = -5.22$, $p < 10^{-4}$). This model shows that even if both groups started at the same level (no main effect, thus no offset on average) ET patients adapted at a lower rate to the perturbation than neurologically intact volunteers (interaction effect). The mean vertical velocity increased with trials for both groups, but with a smaller increase for the ET group (Figure 2.2 b, LME; Trial :$F_{(10,356)} = 0.07$, $p < 10^{-4}$; Group:$F_{(38)} = -2.16$, $p = 0.51$; Group-by-Trial :$F_{(10,356)} = -6.14$, $p < 10^{-4}$). Participants performed a corrective saccade, in order to reach the final target T2. The amplitude of this saccade decreased with trial repetition, in accordance with the increase in the vertical endpoint coordinate of the first saccade. Similar to the first saccade, there was no group effect for the amplitude of the corrective saccade, but there was a significant interaction between the group and trial number, reflecting that ET patients adapted less to the perturbation

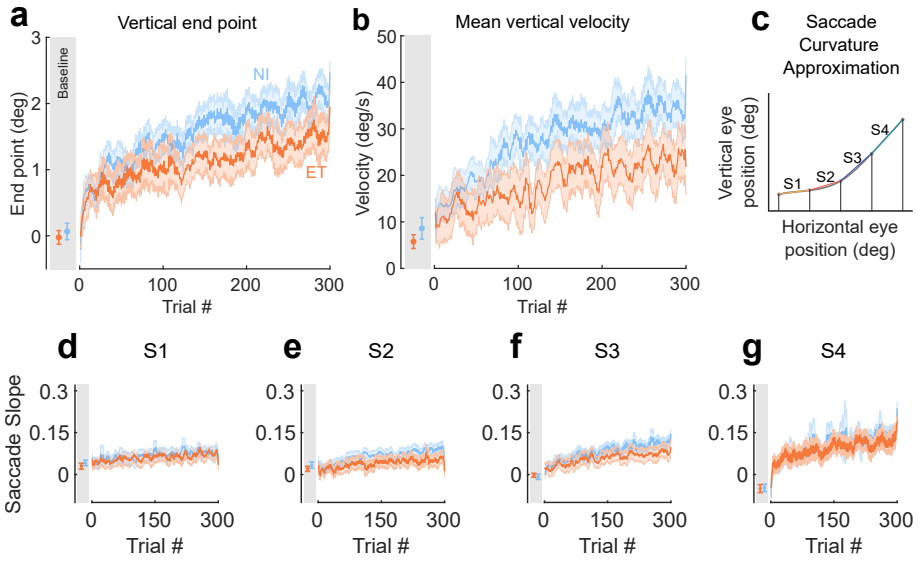

FIGURE 2.2: Participants' behaviour during the saccadic adaptation task ET patients showed reduced saccadic adaptation **a**, **b**, Evolution of the vertical end point (**a**) and peak vertical velocity (**b**) averaged over each group. Shading indicates SEM. **c**, The curvature was approximated by dividing saccade into 4 segments along the horizontal axis and by computing the slope of each segment (labeled S1 – S4). **d-g**, Evolution of the segment slopes with adaptation. **a**,**b**,**d-g**, grey area: Behavior in the horizontal baseline trials, error bars depicts the SEM.

(LME: Trial: $F_{(9497)} = -17.4$, $p < 10^{-4}$; Group:$F_{(38)} = 0.29$, $p = 0.78$; Group:Trial: $F_{(9255)} = 3.89$, $p < 10^{-3}$).

Previous studies on saccadic adaptation (Chen-Harris et al., 2008; Xu-Wilson et al., 2009) reported a specific pattern in the evolution of saccades curvature, differentiating adapted saccades from oblique saccades with the same amplitude. Using the same technique, we approximated the saccade curvature by dividing the saccade into four equal segments along the horizontal axis and analyzed the evolution of the slope of each segment (S1-S4) (Figure 2.2 c-g, see Methods). The differences between the slopes of segments is a proxy of the curvature since highly curved movements should display large variations in consecutive slopes. We observed an altered adaptation pattern in

ET patients. The LME model revealed a significant effect of the trial and of the interaction between group and trial for all segments but the first one (LME; S1: Trial:$F_{(10,356)} = 8.41$, $p < 10^{-4}$; Group:$F_{(38)} = -0.25$, $p = 0.8$; Group-by-Trial:$F_{(10,356)} = -1.25$, $p = 0.21$; For S2-S4 Trial:$F_{(10,356)} > 15.01$, $p < 10^{-4}$; Group:$F_{(38)} > 0.09$, $p > 0.24$; Group-by-Trial:$F_{(10,356)} < -2.88$, $p < 0.004$). Differences between NI and ET participants were maximal during S2 and S3. Interestingly, the fact that the first segment of the saccade was similar across groups suggested the preservation of the initial component of saccadic adaptation -which could be seen as a proxy of anticipatory compensation-, whereas differences in S2 and S3 indicated impairment in the time course of saccadic execution supported by internal feedback. We studied whether any relationship existed between anticipation and real-time execution performances. For the patient group, we computed the correlation between the slope of the first segment and the end point, the correlation coefficient was 0.5 with a p-value of 0.03 (Spearman correlation). This relationship was expected as reported in Chen-Harris study where S1 was responsible of 75% of the total adaptation (Chen-Harris et al., 2008).

Finally, we compared the variability of participants' behaviour during the baseline blocks, and during the last trial of adaptation to observe participants' consistency during the task. We only report the results for the horizontal position, but similar results were observed for the other metrics (including vertical position as well as velocities in each direction). The variability was the most important towards the end of the movement, midway between peak horizontal velocity and the end of the movement. For the horizontal, oblique and last block of adaptation, patients were respectively 28.8%, 27.6% and 18.3% significatively more variable than controls (Wilcoxon rank-sum test: $T > 489$, $z > 2.12$, $p < 0.03$). This variability was not correlated with the FTM-TRS score nor the task performance.

2.3.2 Experiment 2: Adaptation of reaching movements to a force field

For this experiment, we tested 20 ET patients (15 F, 5 M) and 20 NI participants (14 F, 6 M). The NI group was identical to the saccadic adaptation experiment, whereas the ET group involved 18 participants that

were also tested in the saccadic adaptation task and 2 new participants. As for the saccadic adaptation task, we verified that there was no significant difference in age between the two groups (ET patients : M: 57.7, SD: 16.1, t-test: $t_{38} = -0.19$, $p = 0.85$). ET patients obtained an FTM-TRS score of 9 ± 4.8 for part A (tremor amplitude) and 13.7 ± 6.5 for part B (drawings/pouring).

Participants first performed 40 movements moving the robotic handle of an instrumented device (KINARM, Kingston, ON) in a null field. These movements were used as control trials to measure differences between the two groups when no perturbation occurred (Figure 2.3 a-d). We decomposed the trials into a reaching and a stabilization phase that were defined based on the time at which participant's hand crossed the target for the first time. The last movement of each participant in this field is depicted in grey in Figure 2.3 f. The reaching phase was exempt of oscillations: movement duration and path length were similar for both groups (Figure 2.3 e, t-test; Movement duration: $t_{38} = -0.16$, $p = 0.87$; Path length: $t_{38} = -0.66$, $p = 0.51$). The stabilization phase was, however, directly impacted by the tremor with longer movement duration and path length (Figure 2.3 e, t-test; Movement duration: $t_{38} = -2.95$, $p = 0.005$; Path length: $t_{38} = -3.3$, $p = 0.002$). Initial assumptions were not made regarding differences between reaching and stabilization. Nevertheless for the subsequent analyses, we focused on the reaching phase of the movement – similar across groups in the absence of perturbation – as adaptation indices taken from this window would likely not be directly affected by the tremor.

When participants were exposed to the force field for the first time, they all experienced large lateral hand deviations (Figure 2.3 f). After a few trials, they quickly adapted their movements to the perturbation, and a reduction of the deviation relative to a straight line was observed: the path length decreased and the forces applied by the participant paralleled the one applied by the robot, a good compensation being the opposite of the perturbation (Figure 2.3 c).

Similar to the saccadic adaptation task, both groups showed an adaptation of their movements to the force field, however, this adaptation was reduced for ET patients. The ET patients were slower in the task (Figure 2.4 a&b; Movement duration – LME: Trial: $F_{(9255)} = -2.73$, $p < 10^{-2}$; Group: $F_{(38)} = 2.19$, $p = 0.03$; Group:Trial: $F_{(9255)} = -3.6$,

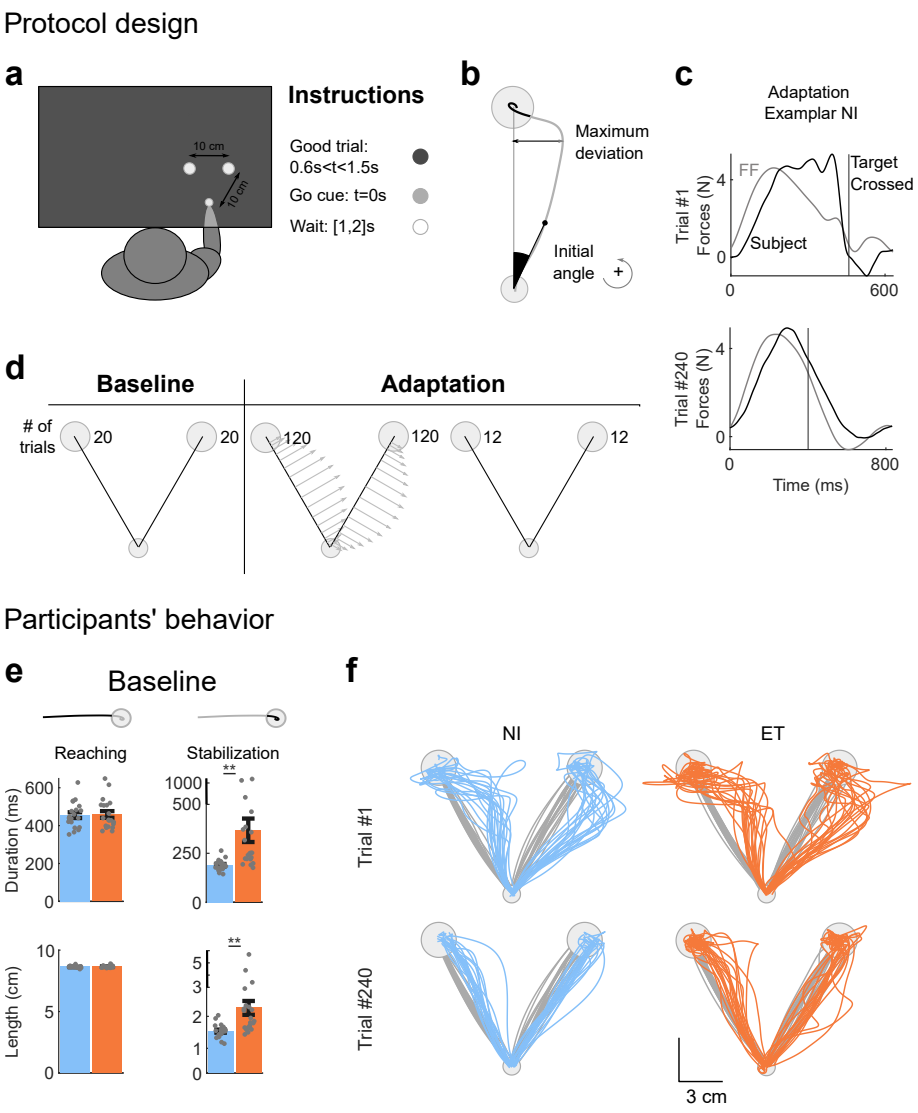

FIGURE 2.3: Schematic representation of the upper limb adaptation protocol design (**a-d**) and participants behavior during the reaching adaptation task (**e,f**). **a**, Participants (n=40) were asked to perform reaching movement to one of two goal targets displayed on the screen 10 cm away from the start target with hand-aligned cursor. Direct view of the limb was blocked. The timing of the movement was constrained, the go cue was given by the filling of the goal target. Visual feedback about movement

Figure 2.3: cont. timing was provided (see Methods). **b**, Parameters extracted from individual traces: the initial angle was defined as the angle between the straight line connecting the two targets and the hand position at 200 ms. Counter-clockwise angle is defined as positive. Maximum deviation was computed between hand path and the straight line connecting the targets. **c**, Lateral Forces applied by participant on the handle (solid traces) and applied by the robot (grey traces) for an exemplar participant from the control group. Top and bottom panels illustrate the difference between early and late phases of the adaptation blocks. It can be observed that the applied force was closer to the perturbation force at the end of the adaptation phase. **d**, Time course of the protocol: 20 baseline trials towards each target (no force field). Adaptation trials were composed of 120 trials in each direction perturbed by a velocity dependent clockwise curl force field. Randomly interleaved catch trials (no force field) were included during the adaptation blocks. Target presentation order was randomized for each block. **e**, Movements were divided into reaching and stabilization. The end of reaching corresponded to the time at which the cursor crossed the target boundary. Significant differences between the two groups in movement duration and hand path lengths were observed only during the stabilization part. Error bars represent SEM. Note the modified scale for the stabilization measures. **f**, Participants' hand paths during the first (top) and last (bottom) force field trial. The differences between the trials illustrate adaptation. Grey traces correspond to the last baseline trial of each participant.

$p < 10^{-3}$). This resulted in a significantly smaller perturbation (Figure 2.4 c; LME: Trial: $F_{(9255)} = -13.11$, $p < 10^{-4}$; Group: $F_{(38)} = -1.65$, $p = 0.11$; Group:Trial: $F_{(9255)} = 6.62$, $p < 10^{-4}$). To account for this difference, the maximum deviation measured during each trial (Figure 2.4 d) was normalized by the maximum perturbation force during the trial. The normalized deviation (Figure 2.4 e) was significantly higher in the ET group as revealed by the exponential fits, where all fitted parameters revealed reduced adaptation in the ET population (Figure 2.4 e, asymptote (a) ET: $a = 0.33$ (95% CI: 0.32-0.34), $p < 10^{-4}$, NI: $a = 0.23$ (0.22-0.24), $p < 10^{-4}$, amplitude (b) ET: $b = 0.30$ $(0.24 - 0.37)$, $p < 10^{-4}$, NI: $b = 0.21$ $(0.19 - 0.23)$, $p < 10^{-4}$ and learning rate ET: $c = 0.10$ (0.07-0.14), $p < 10^{-4}$, NI: $c = 0.02$ $(0.015 - 0.025)$, $p < 10^{-4}$). LME confirmed these results with a significant interaction between the group and the

trial number (Figure 2.4 e; LME: Trial: $F_{(9255)} = -19.78$, $p < 10^{-4}$; Group: $F_{(38)} = 0.91$, $p = 0.37$; Group:Trial: $F_{(9256)} = 5.60$, $p < 10^{-4}$).

The initial reach angle is defined as the angle between the position of the hand at 200 ms and the straight line connecting the home and the goal target (Figure 2.3 b). It is a proxy of participants' anticipation of the perturbation as the earliest modulation of motor commands within movement was previously reported at $\sim$ 250 ms after movement onset (Crevecoeur et al., 2020; Mathew & Crevecoeur, 2021). It suggests that movement parameters prior to this time must be linked to anticipation. It is expected that the force field produces negative values of initial angles early in the adaptation phase, with gradual changes towards 0 as adaptation progresses. Exponential fits reported similar learning rates and amplitude for both groups but a significant difference in the asymptote (ET: $a = -2.5$ (95% CI: $-2.8, -2.3$), $p < 10^{-4}$, NI: $a = -1.7$ $(-1.9, -1.5)$, $p < 10^{-4}$). Mixed models analyses reported a small difference in learning rate for the initial angles (Figure 2.4 f), suggesting that both groups had slight differences in initial angles (LME: Trial: $F_{(9255)} = 5.35$, $p < 10^{-4}$; Group: $F_{(38)} = 0.03$, $p = 0.98$; Group:Trial: $F_{(9255)} = -3.40$, $p < 10^{-3}$). However, no difference in initial angles was observed during the catch trials (Figure 2.4 g; t-test; $t_{(38)} = 0.83$, $p = 0.41$). Similarly, the distributions were not significantly different (Kolmogorov-Smirnov test: $D_{(38)} = 0.2$, $p = 0.77$). Overall, these results reflected no significant differences between the two groups in anticipating the perturbation.

In contrast, the compensation for the force field during movement was more strongly impacted. We computed the correlation between the perturbation force and the force measured at the handle, a high correlation highlighting a good compensation for the force field (Crevecoeur et al., 2020). We found an increase across trials for both groups, while remaining significantly smaller for ET patients than for NI participants (Figure 2.4 h). Exponential fits reported a difference of asymptote (ET: $a = 0.81$ $(0.8 - 0.82)$, NI: $a = 0.86$ $(0.85 - 0.87)$) and no significant differences in amplitude or learning rate. This result was also confirmed by LME models (Trial: $F_{(9020)} = 20.41$, $p < 10^{-4}$; Group: $F_{(37)} = -2.41$, $p = 0.021$; Group:Trial: $F_{(9020)} = 0.74$, $p = 0.46$). Interestingly, the reaching adaptation experiment revealed impairments qualitatively similar to the saccadic adaptation task: first, ET patients

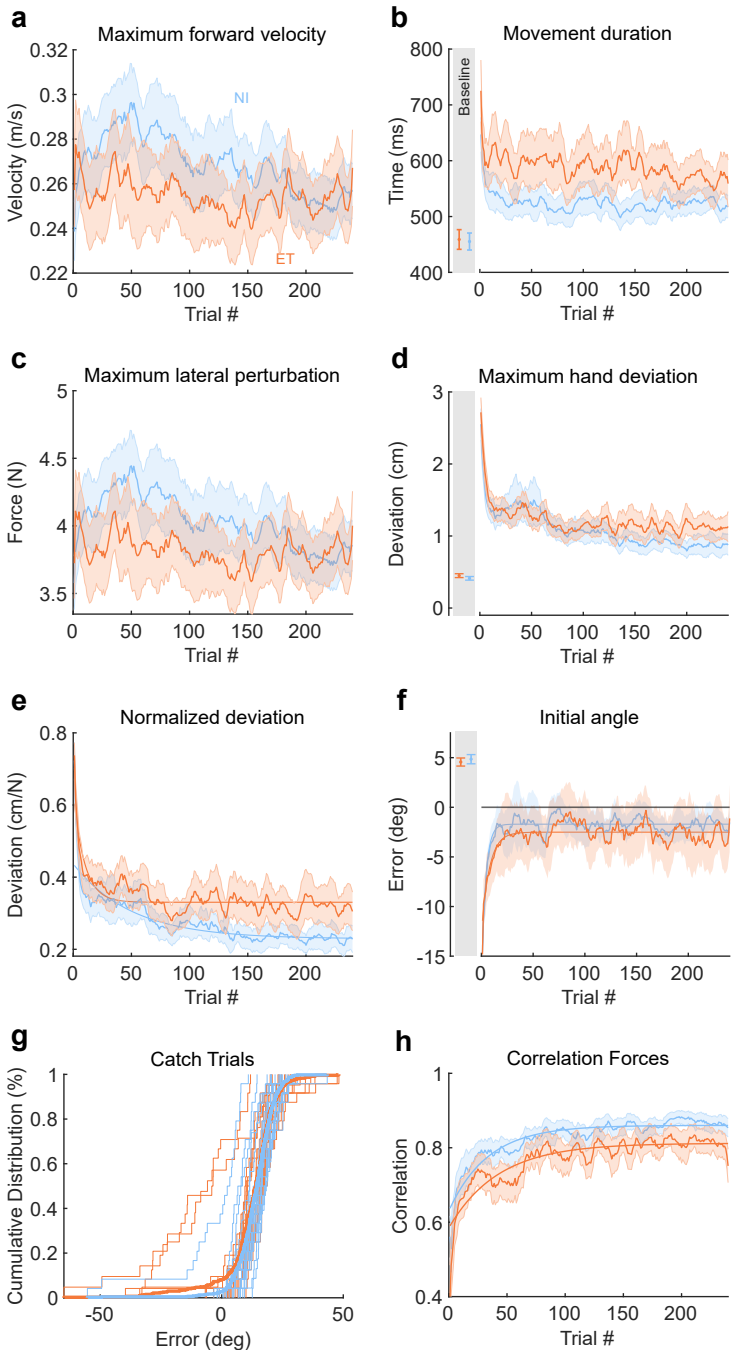
a
Maximum forward velocity
Velocity (m/s)
NI
ET
Trial #
b
Movement duration
Time (ms)
Baseline
Trial #
c
Maximum lateral perturbation
Force (N)
Trial #
d
Maximum hand deviation
Deviation (cm)
Trial #
e
Normalized deviation
Deviation (cm/N)
Trial #
f
Initial angle
Error (deg)
Trial #
g
Catch Trials
Cumulative Distribution (%)
Error (deg)
h
Correlation Forces
Correlation
Trial #

FIGURE 2.4: Participants' adaptation during the reaching task **a**, Maximum forward velocity during the adaptation trials, used to compute the lateral perturbation. **b**, Movement duration during the reaching phase **c**, Maximum lateral perturbation received by the participants during the adaptation trials. Averaged over each group. **d**, Maximum hand deviation observed during force field trials. **e**, Maximum lateral deviation, normalized by the averaged force received during reaching. **f**, Initial angle between the hand and the line connecting the start-target centers at 200 ms after movement initiation. **g**, Cumulative distribution of the initial angle during the catch trials for the ET and NI participants. **h**, Trial by trial correlation between the force field applied by the robot and the forces applied by the participant. Averaged over participants of each group. **a-f, h,** Shaded areas represent the SEM, grey area: average behavior in the baseline trials, error bars depicts the SEM. **e,f,h**, Significant exponential fits.

were able to adapt, but they exhibited reduced adaptation in comparison with the control group. In both experiments, it appeared that the aspects linked to anticipation were preserved (S1 for the saccadic adaptation, the catch trials initial angles for the reaching task), whereas the metric closely linked to online execution exhibited a reduced compensation for the perturbation (S2 and S3 for the first task, and the correlations computed on continuous force traces for the reaching task). We did not find any significant correlation between the initial angle and the correlations (Spearman's correlation for the patient group; 0.38, $p = 0.12$), suggesting an absence of interaction between both adaptation mechanisms.

We also compared participants' variability during the baseline block and the last block of adaptation. Variability peaked close to the end of the movement, midway between peak forward velocity and target crossing. During the baseline and the last block of adaptation, for the lateral velocity, ET patients were in average 51.4% and 49.6% significantly more variable than NI participants (Wilcoxon rank-sum test: $T > 519$, $z > 2.93$, $p < 0.003$). This variability was not correlated with the FTM-TRS score nor the task performance. Similar results were observed for the lateral and forward position and velocity with a difference for the Spearman's correlations in the forward position where

the variability positively correlated with the tremor score (Spearman correlation; baseline: 0.54, $p = 0.01$, last block of adaptation: 0.45, $p = 0.046$) and negatively with task performances during the baseline block (Spearman correlation; baseline: -0.75, $p < 10^{-3}$, last block of adaptation: -0.46, $p = 0.057$). We also observed trends in two other conditions for both comparisons ($p < 0.10$).

2.3.3 Correlations between task performances and FTM-TRS scores

We investigated the correlation of tremor severity with the impairment for each task. Despite ET patients' significant impairment of saccadic adaptation, the FTM-TRS score (part A+B) was not correlated with the vertical end-point at the end of the adaptation (Figure 2.5 a; Pearson's correlation = 0.11, $p = 0.65$). Concerning the force field adaptation task, a trend between the correlation of forces and the FTM-TRS score was observed (Figure 2.5 b; Pearson's correlation = -0.47, $p = 0.047$), suggesting that most affected ET patients were also those showing the larger impairment in reaching adaptation. It is clear that one participant with lowest task performance score both epitomizes and drives this effect. One the one hand, there was no anomaly with their data meaning that the result is likely valid. On the other hand, the correlation diminished to -0.40 with a p-value of 0.11 after removing this data point. In any case, additional data may be necessary to address the robustness of this relationship.

Finally, we sought to quantify the differences between the two-dimensional distributions of adaptation indices to measure the overlap across NI and patient's groups. We used a linear support vector machine, trained on the vertical end-point error and the continuous correlations, to visualize which task performances regions were associated with each group and quantify the overlap between the two populations taking two-dimensional linear separation in the space of adaptation indices. The classifier separated our performance space into reduced performances in both tasks for ET patients and higher performances in both tasks for NI volunteers, as shown in Figure 2.5 c. In this dataset, participants classified in the blue region had an average FTM-TRS score of 7.1 points; participants classified in the orange region had

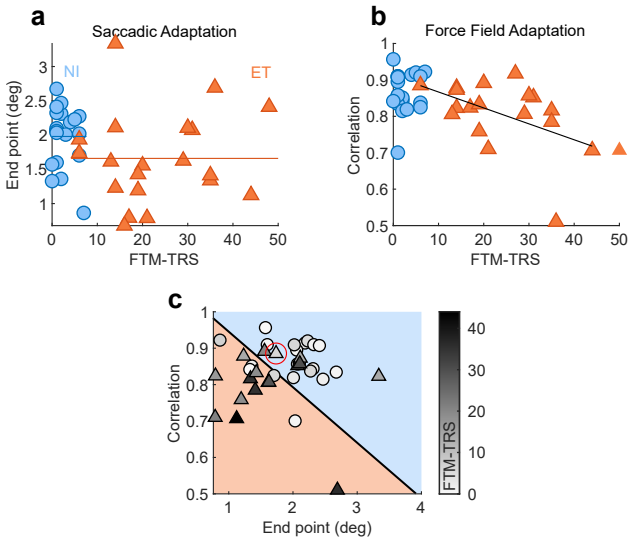

FIGURE 2.5: Correlation between performance and tremor score **a**, **b**, Relationship between the score obtained during late adaptation (**a**, Saccadic adaptation, **b**, Force field adaptation) and the Tremor Score measured via the FTM TRS scale (Part A+B). Each dot represents the average score obtained over the last 10% trials. **c**, Relationship between the performances in the two tasks for each participant. Color gradient represents the FTM TRS Score. The separation between the two groups was computed by training a linear support vector machine to discriminate populations based on the scores obtained in each task (accuracy: 67.6%). Red circle highlight a misclassification error for a less severely affected ET participant.

an average score of 18.6 points. The support vector machine leave-one-out cross-validation accuracy was 67.6%. Classification errors mainly occurred for patients with a lower FTM-TRS score. Misclassifications happened more frequently for ET patients with lower FTM-TRS scores, closer to NI participants' scores. An example of misclassification for a less severely affected ET patient is highlighted on Figure 2.5 c.

2.4 Discussion

Our study aimed to better understand the origin of the sensorimotor adaptation deficits previously reported in ET patients. To do so, we selected standard reaching and saccadic adaptation tasks known to be altered in patients with cerebellar deficits. As expected, ET patients experienced a deficit of adaptation in both tasks when compared with the control group. Importantly, our study revealed that the aspects linked to the anticipation of the perturbation, namely the initial saccade slope, the catch trials, and the initial reach angles, clearly evolved across trials and were intact for ET patients. In contrast the deficits seemed to be linked to markers of online control (intermediate saccade slopes and correlations in the reaching task).

Our results are consistent with previous adaptation studies performed with ET patients in various tasks (Bindel et al., 2022; Chen et al., 2006; Hanajima et al., 2016; Kronenbuerger et al., 2007). Here we reproduced the results of Chen et al. (Chen et al., 2006), and added to this line of evidence that the impairment in adaptation in ET patients may reflect a general sensorimotor deficit as it also impacts adaptation of saccades despite the absence of ET symptoms in unperturbed saccades (Helmchen et al., 2003; Wójcik-Pedziwiatr et al., 2016).

Although a linear correlation was not observed between the tremor score and the performance in the saccadic adaptation task, a trend was observed indicating that higher tremor score were related to lower performance in the force field adaptation task. This result might be explained by the fact that the FTM-TRS scale mostly evaluates upper limb sensorimotor function and tremor, whereas eye movements are not included or evaluated in this clinical scale. The overall tendency was an ordering of the patient's group in the region of the space of parameters used to quantify adaptation corresponding to lower performances in both tasks.

A previous study reported an interaction between noise and adaptation performances (Van Der Vliet et al., 2018). They reported a decreased adaptation rate when execution noise (noise originating from the sensorimotor pathway) was more important and increased adaptation rate when planning noise was more important. A parallel can be

made here between execution noise and the increased variability observed in the population with ET. Interestingly, a negative trend was observed between variability and task performances and a positive trend between variability and tremor score for half of the metrics studied in the reaching adaptation task.

Our study is not without limitation but they may not have a strong impact on our interpretations. First, participants did not stop their medications before the evaluation, which may influence the FTM-TRS score. Our analyses of the correlations between performance and the tremor score were computed based on this score, and might therefore suffer from the heterogeneity of patients and treatments. Severely affected patients with efficient treatments might have a lower tremor score than less severely affected patients and therefore have an impact on the correlations computed. Accounting for the medication was however difficult due to the variety of treatments and dosages taken by the participants. Studying sensorimotor deficits while taking medication into account is likely a challenge for prospective studies. Besides the heterogeneity inherent with clinical population and the diversity of treatments, our conclusions are still supported by the fact that the components of motor control prior to the adaptation tasks were similar across groups. Another point of attention concerns the performance of our classifier, which requires validation and should not be hastily generalized. The classifier was used here to quantify the overlap between two distributions, and not to perform prediction on unseen data. The performance of such an approach must be validated with larger datasets before becoming a candidate test to improve the diagnosis of ET. Finally, previous work has reported the existence of cognitive or explicit strategies during adaptation to force fields accounting for a fraction of force produced against a force field (Schween et al., 2020). It is clear that the initial movement angle could be composed of an explicit component, however it was likely similar across groups and our data do not allow us to isolate it. In addition, the main deficit again was linked to movement control which is difficult to relate to a cognitive bias or strategy in both tasks. We believe that quantifying the contribution of explicit components in ET is an interesting topic for follow-up studies.

In contrast with cerebellar ataxia, patients who showed dramatic

impairments and almost complete absence of adaptation in the tasks performed in this present study, ET patients showed only reduced adaptation in both tasks (Smith & Shadmehr, 2005; Xu-Wilson et al., 2009). When comparing the results of the control group obtained by Xu-Wilson et al. with our control group, it must be noted that adaptation in this study appears to be slightly reduced. This difference could be potentially attributed to variations in the experimental setup and protocols. Our motivation to conduct the present study was to parse out potential cerebellar deficits in ET patients. However, it is important to keep in mind that even if cerebellum seems to be involved, it does not exclude other causes. A clear difficulty in documenting these cerebellar deficits was that cerebellum has been associated with a wide range of sensorimotor functions, including motor adaptation and control (Baizer et al., 1999; Ojakangas & Ebner, 1992; Smith & Shadmehr, 2005; Tseng et al., 2007; Xu-Wilson et al., 2009). A common ground between adaptation and control is the use of internal models that have been also associated with cerebellum (Diedrichsen & Bastian, 2014; McNamee & Wolpert, 2019; Therrien & Bastian, 2015). It is widely assumed that the brain uses these internal models to produce an estimation of the next state based on the current state estimate and the sensory feedback. This estimation is required to perform fast and accurate movements in an unpredictable environment despite sensorimotor noise and delayed sensory feedback. Online monitoring of the movement and corrections inflight linked to cerebellar mechanisms was shown in saccadic eye movements (Crevecoeur & Kording, 2017; Lefèvre et al., 1998; Quaia et al., 1999; Schreiber et al., 2006; Xu-Wilson et al., 2011), as well as reaching movements (Miall et al., 2007). It is therefore possible that internal models for control hosted in cerebellum would be responsible for tremor and for reduced online compensation in adaptation tasks. Such internal models can take several forms, including aspects linked to sensorimotor coordination, as well as operations linked to timing representations (Bo et al., 2008; Diedrichsen et al., 2007; Kilteni et al., 2019; Martin et al., 1996). In this regard, it is known that oscillations, explaining the low frequency components of ET tremor, can arise in a system that incorrectly compensates for sensorimotor delays (Crevecoeur & Gervers, 2019; Stein & Oğuztöreli, 1976). Thus, we suggest that tremor arises from incorrect internal models in

cerebellum likely associated with delay compensation, producing the well documented oscillations and deficits in online control.

The possible dissociation between anticipation and online control is important for interpreting ET disorders, and also potentially on the underlying dysfunction of the cerebello-thalamo-cortical loop (Helmich et al., 2013; Muthuraman et al., 2018). Our proposed interpretation is that the cerebello-thalamo-cortical pathway conveys an estimate of the state of the system that combines an efferent copy of motor commands with sensory feedback and current estimates that compensates for sensorimotor delays. When the movement was initiated from a static posture, errors had not yet accumulated and movement started in the correct direction, but later in the trial, the faulty delay compensation accumulates errors and the closed-loop system starts producing erroneous control signals potentially leading to oscillations. This view suggests a very specific cause of tremor in ET patients, which is linked to errors in real-time state-estimation based on internal feedback of motor commands. Orienting future research on online feedback control in ET should bring novel insights to validate or invalidate the hypothesis of impaired delay compensation as candidate root cause of oscillations in this population.

To conclude, our contribution is twofold: on the one hand we replicate the presence of cerebellar-dependent adaptation deficits in ET population, adding to the line of evidence that this disorder is linked to cerebellar dysfunction. On the other hand, we proposed a movement decomposition suggesting a specific functional consequence of the altered cerebellar pathways, which affects online control more than anticipation.

Data availability

The data will be available in Zenodo after the publication of this article.

Supplemental material

Supplemental Table S1: doi.org/10.6084/m9.figshare.24072213

Grants

Florence Blondiaux is a FRIA grantee of the Fonds de la Recherche Scientifique–FNRS (Be). The FNRS provided salary and research support for Bernard J. Hanseeuw under Grants No. CCL40010417 and No. FRFS-WELBIO40010035. Frédéric Crevecoeur is supported by a grant from the FNRS under Grant No. 1.C.033.18.

Disclosures

No conflicts of interest, financial or otherwise, are declared by the authors.

Chapter 3

Erroneous compensation for long-latency feedback delays as origin of Essential Tremor

Published as : Blondiaux F., Colmant L., Lebrun L., Hanseeuw B., and Crevecoeur F., Erroneous compensation for long-latency feedback delays as origin of Essential Tremor, *Journal of Neuroscience*

ESSENTIAL tremor (ET), a movement disorder characterized by involuntary oscillations of the limbs during movement, remains to date not well understood. It has been recently suggested that the tremor originates from impaired delay compensation, affecting movement representation and online control. Here we tested this hypothesis directly with 24 ET patients (14 female; 10 male) and 28 neurologically intact (NI) human volunteers (17 female; 11 male) in an upper limb postural perturbation task. After maintaining their hand in a visual target, participants experienced perturbations of unpredictable direction and magnitude, and were instructed to counter the perturbation and steer their hand back to the starting position. In comparison with NI volunteers, ET patients' early muscular responses (Short and Long-Latency Responses, 20-50 ms and 50-100 ms respectively) were preserved or even slightly increased. However, they exhibited perturbation-dependent deficits when stopping and stabilizing their hand in the final target supporting the hypothesis that the tremor was generated by the feedback controller. We show in a computational

model that errors in delay compensation accumulating over time produced the same small increase in initial feedback response followed by oscillations that scaled with the perturbation magnitude as observed in ET population. Our experimental results therefore validate the computational hypothesis that inaccurate delay compensation in long-latency pathways could be the origin of the tremor.

Significance Statement Essential Tremor origin remains poorly understood. In the present study, we focused on motor impairments associated with feedback control. Following a mechanical perturbation applied to their arm, patients' short and initial long-latency stretch responses were preserved. However, we observed clear impairments during the stabilization phase that scaled with the perturbation magnitude. These results were reproduced in a computational model where delay compensation was inaccurate, suggesting that the origin of the tremor may lie in an underestimation of the delays impacting the internal monitoring of the motor commands.

3.1 Introduction

Essential Tremor (ET), among the most frequent movement disorders (Louis & Ferreira, 2010), typically manifests as involuntary oscillations of the upper limbs and less frequently head, legs and trunk, mainly during movement (Bhatia et al., 2018; Shanker, 2019). While tremor characteristics, such as frequency and lack of impact of loading, have been described extensively, the underlying pathophysiology remains poorly understood (Elble, 2003). Several clinical, postmortem and neuroimaging studies pointed out that ET could originate from the cerebello-thalamo-cortical loop (Ibrahim et al., 2021), without characterizing how the movement deficits arise from a functional perspective. Identifying preserved and impaired cerebellar functions in ET would therefore help to better understand the mechanisms at the origin of the tremor (Butler et al., 2023; Louis & Faust, 2020b; Trillenberg et al., 2006).

From a computational perspective, it is well known that the presence of delays in a feedback control system can induce oscillations if the impact of the delay is not taken into account (Miall et al., 1993; Stein

& Oğuztöreli, 1976). This parallels with the way we control our limbs. Indeed, the sensory feedback, used in motor control, is delayed due to the conduction time of sensory signals and motor commands through the nerves. The delay depends on the feedback loop: in the upper-limb, short-latency delays associated with spinal stretch reflex are in the range of 20-30 ms, and long-latency delays involving a transcortical loop are in the range of 50-60 ms (Scott, 2016). Importantly, it has been also suggested that state estimation, and therefore compensation for temporal delays, is performed in the long-latency feedback pathway (Crevecoeur & Scott, 2013). Assuming erroneous delay compensation in this sensorimotor system, previous simulations reproduced oscillations in the frequency range observed in ET (Crevecoeur & Gervers, 2019), allowing us to formulate the hypothesis that ET originates from errors in the long-latency feedback loop.

Indeed, Long-Latency Responses (LLRs) refer to the burst of muscular activity observed 50-100 ms (for upper-limbs) post-perturbation (Pruszynski & Scott, 2012). This activity helps to counteract perturbations and is likely supported by transcortical feedback. LLRs are not only elicited for large perturbations but are also present for very small perturbations, with a magnitude close to the magnitude of errors observed during voluntary control (Crevecoeur et al., 2012), and parallels unperturbed movement in the tendency to exploit target redundancy (De Comite et al., 2021). This suggests that LLRs could therefore be present constantly during movements to compensate for the undesirable effects of motor variability. If LLRs continuously contribute to movement control, errors in this pathway could lead to general movement deficits affecting both voluntary movements and feedback responses to perturbations. This hypothesis is also supported by our previous study showing that ET patients could learn to anticipate the effect of a perturbation but exhibited adaptation impairments linked to online control (Blondiaux et al., 2023). Together, there is strong evidence that movement execution is impaired in ET, and errors in the long-latency feedback loop is a candidate model for their deficits.

We tested this hypothesis directly by investigating feedback control in both ET patients and in a neurologically intact (NI) control

group using a postural perturbation task. We observed similar initial perturbation-related limb displacement and intact short (R1: 25-45 ms post-perturbation) and initial LLR (R2: 45-75 ms), suggesting preserved peripheral system and initial stretch responses. However, perturbation-dependent deficits arose during the later phase of the feedback correction and during stabilization, which followed an enhanced stretch response in the late LLR epoch (R3: 75-105 ms) dependent on the load magnitude. We reproduced both movement kinematics and transient perturbation-related increase in the stretch response in a computational model considering an error in the delay parameter. Together our analyses suggest that ET could arise from partial or inaccurate compensation of long-latency delays, leading to oscillations in movements caused by accumulation of error over time.

3.2 Methods

3.2.1 Participants

A total of 24 ET patients (14 females, mean age: 61.1 ± 13.1) and 28 NI volunteers (17 females, mean age: 62.7 ± 12.6) were recruited for this study. The ethics committee at the host institution (Comité d'Éthique Hospitalo Facultaire, UCLouvain, Belgium) approved the experimental protocol and all participants provided written informed consent following standard procedures. All participants were evaluated using the Fahn-Tolosa-Marin Tremor Rating Scale (FTM-TRS) and participants with other neurological disorders were excluded. The FTM-TRS scale was divided into 3 sections. Part A quantified the tremor amplitude of the limbs at rest, during postural control, and during action. Part B assessed writing, drawing and pouring liquids. Finally, Part C evaluated the impact of the tremor in daily life activities (eating, drinking, getting dressed, working, ...) (Fahn et al., 1993). The latter part was filled by the participant and was not considered during this study due to its inherent subjectivity. ET patients did not interrupt their medication prior to the evaluation. The FTM TRS Score for part A and B was 2.3 ± 0.38 (mean $\pm$ SEM) for the NI group and 21.6 ± 1.98 for the ET group.

3.2.2 Task

Participants sat on a height-adjustable chair and grabbed the robotic handle of an End-Point KINARM device (KINARM, Kingston, Ontario). Direct vision of volunteers' hands was blocked and a semitransparent mirror that reflected the virtual reality screen (VPixx, 120 Hz), allowing them to interact with virtual targets (Figure 3.1 a). A hand-aligned cursor was always represented (white dot, radius 0.6 cm). The experiment was composed of 2 trial types: voluntary movements and perturbation trials.

Participants started with a block of 60 voluntary movements. A home target of radius 1 cm was presented approximately 30 cm ahead of the participant's torso, aligned with the right hand. They had to maintain the hand in the home target (coordinates: [x, y] = [0, 0]), after a random time uniformly distributed between 1 and 2 sec, an external target was lit and used as a go signal. Participants were instructed to pass through the external target (radius 2.5 cm) and to finish their movements inside the home target. The goal target was randomly selected within 4 targets with coordinates [10,0], [-10,0], [0,7.5], and [0,-7.5]. Each target was presented 15 times during the block. Participants were encouraged to finish their movements in less than 2 s. This initial block with voluntary movements was performed to collect information about movement kinematics without perturbations, but the results were consistent with the main experiment and with previous reports on reaching movements in this population (Blondiaux et al., 2023). Because these results did not provide specific additional information, we do not show the corresponding dataset here.

Perturbation trials started with the same home target (Figure 3.1 b): participants maintained the hand in the home target, after a random time between 1 and 2 s, the robot applied a step force (rise time: 5 ms) in one of 4 directions [+x,-x,+y,-y], with a magnitude of 4, 6.5, or 9 N. The perturbation magnitude and direction were randomly selected. The participants performed a total of 300 trials composed of 25 trials per combination of perturbation direction and magnitude. The trials were divided into 5 blocks of 60. Participants were instructed to return and stabilize in the home target, and they received a positive

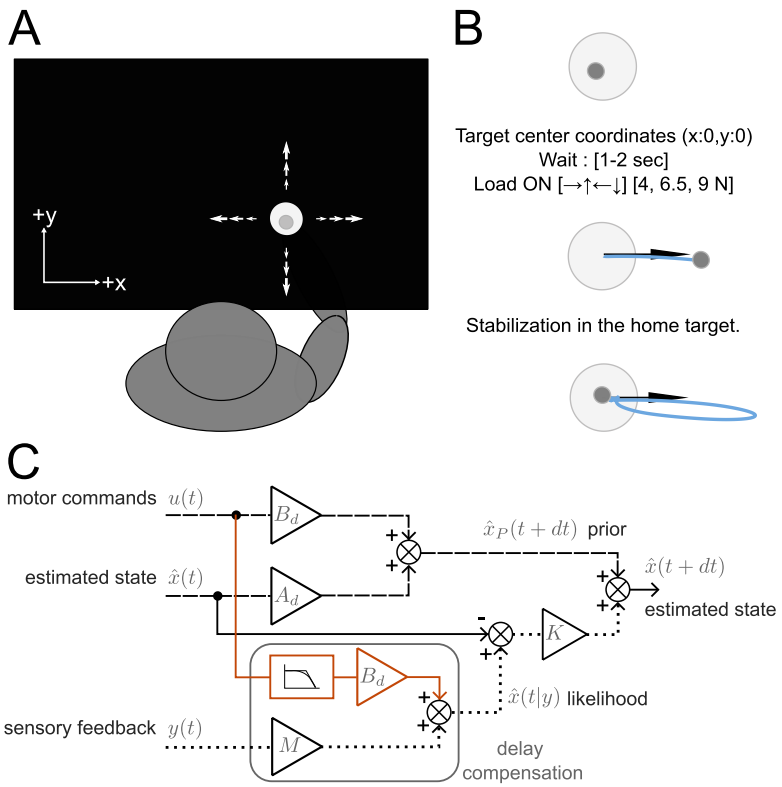

FIGURE 3.1: Schematic representation of the protocol design and theoretical model. **A,** Prior perturbation, participants maintained the hand-aligned cursor in the home target. Direct view of the limb was blocked by an occluder but participants had continuous visual feedback about the hand-aligned cursor. **B,** Perturbation trials started in the home target, participants received one of three perturbation magnitudes (4, 6.5, 9N) in one of four directions (+x,-x,+y,-y). Visual feedback about movement timing was provided via target color (see methods). C, Model pathway adapted from Crevecoeur and Gervers, 2019. Model compensating for the delay in sensorimotor control. The dotted pathway corresponds to the sensory feedback, the dashed pathway corresponds to the internal prior and the orange pathway correspond to the delay compensation that is suspected to be faulty in ET. A_d and B_d define the dynamics of the model, dt is the time step, δt the system delay and K are the Kalman gains. For clarity, we omitted the explicit dependencies of M on δt and K on t, see methods for variable and matrices definitions.

mark indicating good performance (target turned green) if they completed their movement in less than 3 s. The total score was projected on the screen for their motivation. When movements were too slow, the target remained red. Trial timed out after 3 s if the participant was not able to stop their hand. The criterion on movement time was applied to encourage consistent speeds, but all movements that returned to the target were kept for analyses. The step force turned off at the end of the trial and the inter-trial time was 1 s. Participants were encouraged to take short breaks between the blocks to reduce fatigue (15 s to 2 min).

For the perturbations along the y-axis, we did not observe any significant scaling of the EMGs with perturbation magnitude both in the NI and ET group. This was likely due to participants' limb configuration (the arm and forearm were approximately vertical and horizontal, respectively) and of the action of gravity, which in this direction passively brought the hand back to the initial position. Thus, although all perturbations were applied during data collection to reduce anticipation, the following analyses focus on the positive and negative perturbations along the x-axis, for which we collected a clear EMG response that scaled with the perturbation magnitude.

3.2.3 Data collection and analysis

Kinematics data was filtered using a dual pass 4th order low pass Butterworth filter with a cut-off frequency of 20 Hz. Movement velocity was extracted using KINARM's data extraction scripts (version 3.1) and movement path lengths were defined as the integral of the velocity vector norm. Movement onset and end were defined using a speed threshold of 3 cm/s for at least 200 ms. Movements were included in the dataset if the participant returned to the target after perturbation. Movements oscillating around the target at the end were also included in the analysis when possible. Based on these criteria, we kept all trials for ET participants and removed 1 trial for two NI volunteers who did not return to the target. NI volunteers managed to stop all their trials at the end of the trial time, while on average, ET participants managed to stop for a fraction of trials corresponding to $89.42\% \pm 4.36\%$ of the total number of trials. The return time was defined as the duration between

perturbation onset and the moment when the hand re-entered the target. The stabilization phase was defined as the remaining duration of the trial. The Power Spectral Density (PSD) was computed on the acceleration signal during the stabilization phase, and averaged across perturbation trials of similar direction and force magnitude. Subsequently, the average PSD for each participant was averaged across populations (NI and ET), and normalized to the peak PSD observed in ET patients.

Surface EMG electrodes (Bagnoli surface EMG sensor, Delsys INC. Natick, MA, USA) were used to record the muscular activity during movement. The 6 electrodes were located on the Pectoralis Major (PM), Posterior Deltoid (PD), Biceps, Brachialis, and Long and Lateral heads of the Triceps. The electrodes were attached after light abrasion of the skin with cotton and ether. A conductive gel was used to improve data quality. The EMG data was sampled at a frequency of 1000 Hz. The reference electrode was located on the right ankle. Raw EMGs were filtered using a dual pass 6th order Butterworth filter with a passband frequency range of 20 Hz to 250 Hz, rectified and aligned on the perturbation onset for analyses. To normalize EMG data, participants had to apply a force of 15 ± 1 N during 3 s on the handle which was locked by the robot for this calibration procedure. A force gauge was displayed on the screen to help applying the target force. Calibration blocks of 12 trials (3 trials in each direction: $\pm x$, $\pm y$ (unused)), were used at the beginning, middle and end of the experiment (3 blocks in total). We normalized the EMG of each muscle by dividing the signals by the mean value across the calibration trials.

3.2.4 Statistical Analysis

Comparisons across ET and NI populations were performed based on linear mixed models (LME). The fixed predictors were the perturbation *Direction* (2 level categorical factor, -x or +x) and Force (numerical) as well as the *Diagnosis* (2 level categorical factor, NI or ET), plus a random intercept to capture inter-individual variability. We use Y_{ij} to designate the dependent variable of interest, with index i corresponding to the trial number and j to the participant. We used a significance threshold of 0.05 given the higher variability inherent with clinical population, as well as with the between-participants design. LME were

used for the kinematics analyses with Y_{ij} representing respectively for the movement phase the pre-perturbation average speed, displacement at 100 ms, maximum displacement, path length and return time and for the stabilization phase, the stop time, maximum displacement, and path length. LME were also used in the EMGs analyses for the average EMG activity prior the perturbation (-50-0 ms), short latency (R1:25-45 ms), and long-latency bins (R2:45-75 ms and R3:75-105 ms). Effects of the direction and the force (p-value smaller than 10^{-3} in all tests) will not be reported. The statistical model can be written as follow:

$$\begin{aligned} Y_{ij} = \ & \beta_0 + \beta_1 * \ Direction + \beta_2 * Force + \beta_3 \ Diagnosis \\ & + \ \beta_4 * Diagnosis * Force + \ b_j + \epsilon_{i,j} \ . \end{aligned} \quad (3.1)$$

3.2.5 Model

We reimplemented the model described in Crevecoeur and Gevers, and refer the reader to this reference for a fuller description (Crevecoeur & Gervers, 2019). The simulations describe feedback control of a single joint system (Figure 3.1 c). We considered three torque loads acting on the system: a dissipative torque opposite and proportional to the velocity with a constant $G = 0.14$ Nm/rad/s (Crevecoeur & Scott, 2014), a controlled torque T and an external torque T_{ext}. We considered a first-order filter as linear model of the muscle, transforming the command $u(t)$ into the control torque with a time constant $\tau = 60$ ms. The system dynamics is captured by the following system of continuous differential equations:

$$I\ddot{\theta} = -G\dot{\theta} + T + T_{ext}, \quad (3.2)$$

$$\tau\dot{T} = u - T, \quad (3.3)$$

$$\dot{T}_{ext} = 0, \quad (3.4)$$

with the inertia set to $I = 0.15$ Kgm², the joint angle θ, and dots represent time derivatives. We defined the state vector $x(t) = \begin{bmatrix} \theta & \dot{\theta} & T & T_{ext} \end{bmatrix}^T$ and rewrote the three equations as follows:

$$dx(t) \ = (Ax(t) + Bu(t))dt + \ \alpha(t)dW, \quad (3.5)$$

with:

$$A = \begin{bmatrix} 0 & 1 & 0 & 0 \\ 0 & -G/I & 1/I & 1/I \\ 0 & 0 & -1/\tau & 0 \\ 0 & 0 & 0 & 0 \end{bmatrix}, B = \begin{bmatrix} 0 \\ 0 \\ 1/\tau \\ 0 \end{bmatrix} \tag{3.6}$$

The sensory feedback was defined as follows:

$$y(t) = x(t - \delta t) + \sigma(t). \tag{3.7}$$

In Equation 3.5 and 3.7, $\alpha(t)\, dW$ represented signal-dependent and additive sources of noise, $y(t)$ was the current sensory feedback signal, $x(t - \delta t)$ the delayed state with $\delta t = 55\ ms$, and the sensory noise $\sigma(t) \sim N(0, \Sigma_\omega)$. We augmented the state with the target coordinates $x^*(t)$. We then discretized the system using a discretization step of $dt = 5\ ms$. The system became:

$$x_{t+dt} = A_d x_t + B_d u_t + \xi_t, \tag{3.8}$$

$$y_t = x_{t-h} + \omega_t, \tag{3.9}$$

where $A_d \coloneqq M(dt)$, $B_d \coloneqq \left(\int_0^{dt} M(s)ds\right) B$, $M(t) = e^{tA}$, $\xi_t = \alpha(t)dW$ and $h = \delta t/dt$. Because of delayed and noisy sensory feedback, we needed to compute an estimate of the state vector:

$$\hat{x}_{t+dt} = A_d \hat{x}_t + B_d u_t + K_t \left[\hat{x}_{t|y} - \hat{x}_t\right], \tag{3.10}$$

where we define the prior estimate as $x_p = A_d \hat{x}_t + B_d u_t$. The Kalman gains K_t were computed using a forward recursion.

This formulation differs from the standard definition of predictive Kalman filter, by incorporating an explicit extrapolation of the system state given present sensory feedback. Indeed, the standard form of Kalman filters uses an innovation sequence for the non-delayed case equal to $y_t - \hat{x}_t$. Here, because y_t is a delayed state measurement, it is possible to extrapolate this information and compute the current expected state given y_t, the knowledge of limb dynamics and the motor commands during the delay interval. This extrapolation is either performed recursively based on system augmentation, or explicitly in the

formulation that we have chosen here which corresponds to finite spectrum assignment (Mondie & Michiels, 2003). With the discrete time system equations, the extrapolation of delayed sensory signals to the present state takes the following form:

$$\hat{x}_{t|y} = M(\delta t)y_t + \sum_{k=1}^{h} M(kdt)Bu(t-kdt)dt. \tag{3.11}$$

In the sequel, we assume that this operation is performed with a value of the delay δt that underestimated the correct value. Recall that, in addition to the explicit dependency of δt on M, the motor commands were integrated over a smaller delay interval, h being the delay in discretized time steps. Observe this filter is equivalent to a standard Kalman filter when the delay $\delta t = 0$ as $\hat{x}_{t|y} = y_t$. It is also similar to system augmentation (Crevecoeur & Scott, 2013; Fridman, 2014), where the estimation of the system state during the delay interval results from the augmented structure of the state vector. It is important to emphasize that we assumed an output signal of the form of Equation 3.9. If a more general output signal in the form $y\prime(t) = Hx(t-\delta t) + \sigma(t)$ must be considered, then it is possible to reconstruct an estimate of the state vector at $t-\delta t$ with an observer prior the extrapolation step. Such intermediate observer would produce an estimate of the state that corresponds to Eqn. 3.9.

In order to calculate the control signal, we minimized a quadratic cost function penalizing position and velocity error (first term) and control (second term), which writes as follows:

$$J(x,u) = E\left[x_N^T Q_N x_N + \sum_{t=1}^{N-1} x_t^T Q_t x_t + u_t^T R_t u_t\right], \tag{3.12}$$

with $R = 10^{-2}$ and $x^T Qx = w_1(x_1 - x_1^*)^2 + w_2(x_2 - x_2^*)^2$, with $w = [100, 0]$ for $t < N$ and $w = [100, 10]$ for $t = N$.

Based on these assumptions, the optimal motor commands were defined as $u_t = -L_t\hat{x}_t$. The optimal feedback gains L_t were obtained via a backward recurrence following standard technique. For the simulations, to capture errors in the delay estimation, we considered a case for which the delay ($\delta t = 55ms$) was underestimated. We used $\hat{\delta}t = 0.7\delta t$ and $h = \hat{\delta}t/dt$ in Equation 3.11, with h rounded to the closest integer.

A delay error of 70% was used to match qualitatively the experimental data and verified in a sensitivity analysis that our conclusion did not depend on this choice. For the simulations with noisy underestimation of the delay we added or removed up to 10ms to the estimated delay. The noise was randomly and uniformly selected from the set -10, 5, 0, 5, 10ms. For the simulations with an error in the prior estimate (Eqn. 3.10), we multiplied it by a factor larger or lesser than 1 (1.1 and 0.7, respectively). Note that this is not equivalent to multiplying A_d and B_d by a scaling factor, as these matrices are also used in the delay compensation step (Figure 3.1C). The step perturbations amplitudes were 1, 2 and 3 Nm applied at 50 ms. Movement duration was of 800 ms. The figures were produced using the average across 20 simulations in each condition. Similar to the data, the PSD of simulated traces was computed on the acceleration during the stabilization phase and averaged over trial repetitions then perturbation magnitude. Then, the PSD was normalized using the maximum PSD value from the simulations obtained with an error in the delay. An access to working code for the model simulations is provided at the following URL: github.com/fblondiaux/ErroneousDelayCompensationET. The experimental dataset can be accessed at doi.org/10.5281/zenodo.10843311.

3.3 Results

We studied the ability of ET patients (n=24) and NI volunteers (n=28) to respond rapidly to step perturbations of various directions and amplitudes. After holding the handle of a robotic arm in the initial visual target, participants were instructed to counter the perturbations and steer their hand back to the initial target (Figure 3.1). Four directions and three force magnitudes were used for this experiment with a total of 300 randomly interleaved trials (25 repetitions per direction and magnitude). The analyses focus on the lateral perturbations (aligned with positive and negative values along the x-axis, 150 trials, see methods).

Figure 3.2 A-C provides an overview of the hand traces of an exemplar participant of each group for each perturbation. Initially, the perturbation had a similar effect on the ET participants, however, once

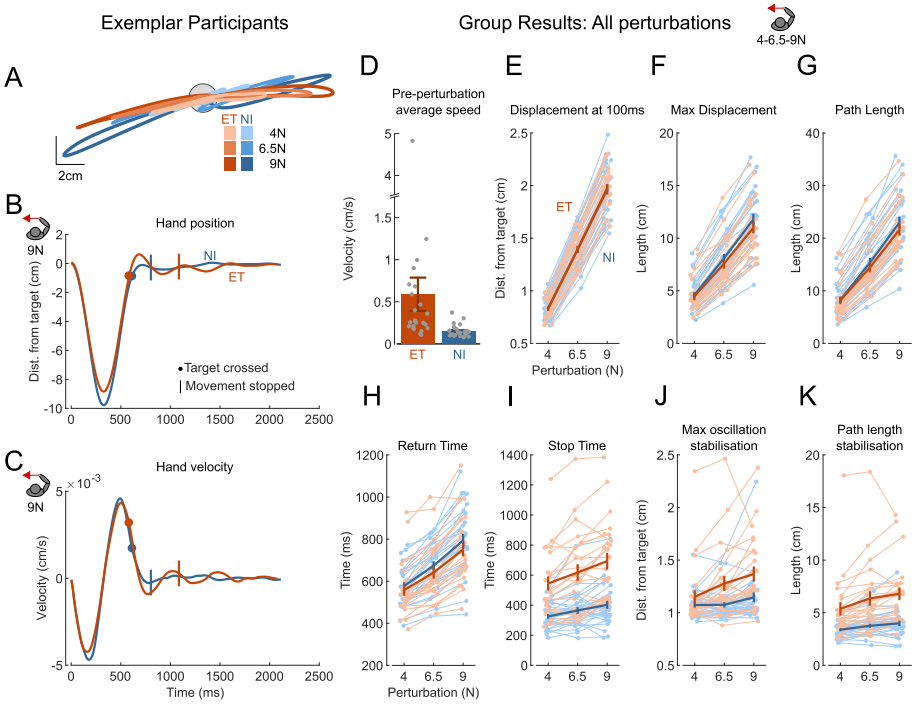

FIGURE 3.2: Perturbation trials, ET patients' difficulties in the stabilization phase are increased with perturbation magnitude. **A,** Exemplar participants' hand path during the last perturbation trial, the 2 analyzed directions and 3 amplitudes are represented. **B,** Distance in the X-axis of the exemplar hand path for the 9 N -x perturbation. **C,** X-Velocity profile of the same trials. **B, C,** Dot: time at which the hand re-entered the target for the first time; Bar: movement stop condition met: velocity$<$3 cm/s for at least 200 ms (see Methods). **D,** Pre-perturbation average speed, averaged over all perturbation magnitudes, gray dots represent individual behavior. **E-H,** Movement phase, prior first target crossing. **E,** Distance of the hand from the target center at 100 ms. **F,** Maximum displacement, **G,** Path length **H,** Time elapsed between perturbation onset and first target crossing. **I-K,** Stabilization phase. **I,** From target re-entering, time required to stop the hand in the target **J,** Maximum displacement from target center along the X-axis. **K,** Path length. **E-K,** Metrics computed on all -x perturbation trials for each perturbation magnitude. Error bar represents the SEM. Light lines represent individual behavior.

participants returned to the target and tried to stop their movements, oscillations around the target became visible. We observed a slightly larger pre-movement speed explained by oscillations within the target in some heavily affected patients, resulting in a significant effect of the diagnosis (Figure 3.2 D; LME: Diagnosis: $F_{(50)} = 2.39$, $P = 0.02$). We decomposed movements in two phases: movement and stabilization, with the cut-off being the first time the participant re-entered the target. Concerning the movement phase, the perturbation initially impacted ET patients and NI volunteers in a similar way. There were no significant differences in hand displacement at 100 ms (Figure 3.2 E; LME: Diagnosis: $F_{(50)} = 0.32$, $P = 0.75$; Diagnosis x Force: $F_{(7743)} = 1.68$, $P = 0.09$), in maximum hand displacement (Figure 3.2 F; LME: Diagnosis: $F_{(50)} = 0.29$, $P = 0.78$; Diagnosis x Force: $F_{(7743)} = -1.79$, $P = 0.07$), in path length (Figure 3.2 G; LME: Diagnosis: $F_{(50)} = 0.25$, $P = 0.80$; Diagnosis x Force: $F_{(7743)} = -1.05$, $P = 0.29$) and return time (Figure 3.2 H; LME: Diagnosis: $F_{(50)} = -0.46$, $P = 0.65$; Diagnosis x Force: $F_{(7743)} = 0.11$, $P = 0.92$). However, during the stabilization phase, ET participants faced clear difficulties, with a longer stopping time (Figure 3.2 I; LME: Diagnosis: $F_{(50)} = 2.83$, $P < 10^{-3}$; Diagnosis x Force: $F(7362) = 5.05$, $P < 10^{-4}$), larger oscillations defined as maximum displacement during the stabilization phase (Figure 3.2 J; LME: Diagnosis: $F_{(50)} = 0.44$, $P = 0.67$; Diagnosis x Force: $F_{(7743)} = 3.66$, $P < 10^{-3}$) and increased path length during that phase (Figure 3.2 K; LME: Diagnosis: $F_{(50)} = 2.18$, $P = 0.03$; Diagnosis x Force: $F_{(7743)} = 4.94$, $P < 10^{-4}$). The interaction between the diagnosis and the force magnitude indicated that performances of the stabilization phase significantly worsened with perturbation amplitude for the three stabilization measures.

In addition to the hand kinematics, we recorded surface muscular activity. We present here recordings of the Pectoralis Major and the Deltoid, respectively the shoulder flexor and extensor stretched by the perturbations aligned with the x-axis. No group effects were observed prior to the perturbation (-50-0 ms; LME: Diagnosis: $F_{(50)} = -0.89$, $P = 0.38$). The initial reflexes elicited by the perturbation were studied and compared between groups shortly after its onset (Figure 3.3). No significant differences between groups were observed in the short latency window (R1: 25-45 ms; LME: Diagnosis: $F_{(50)} = 0.11$, $P = 0.91$; Force: $F_{(7743)} = 4.02$, $P < 10^{-4}$; Diagnosis x Force: $F_{(7743)} = 1.05$,

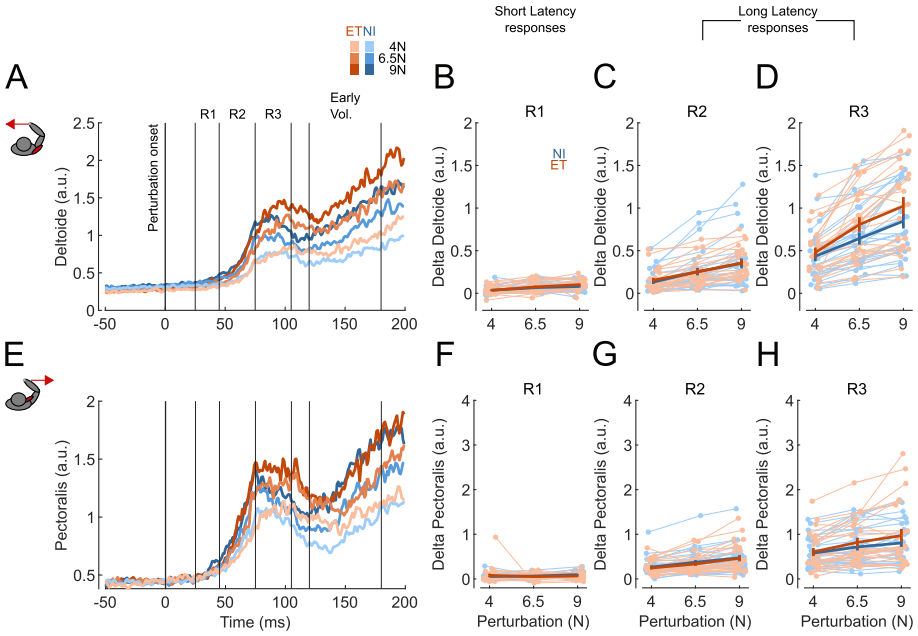

FIGURE 3.3: Short and Long-Latency responses in the perturbation trials. **A,** Early deltoid EMG responses averaged over each group for the 3 perturbation magnitudes aligned with negative direction of the x-axis. Vertical lines delineate the different time windows analyzed. **B-D,** Binned data over the different time windows for the 3 perturbation magnitudes. Average baseline (-50 to 0 ms) was subtracted from the data for illustration purpose. Error bars represent the SEM. Light traces depict individual behavior. **E-H,** Pectoralis response for the perturbations aligned with the positive x-direction. Same format as **A-D**.

$P = 0.30$) and during R2, the first part of the long-latency window (45-75 ms; LME: Diagnosis: $F_{(50)} = 0.43$, $P = 0.74$; Force: $F_{(7743)} = 4.02$, $P < 10^{-4}$; Diagnosis x Force: $F_{(7743)} = -0.06$, $P = 0.95$). Note that the absence of significant differences between NI and ET in R1 and R2 is not due to an absence of response as we observed a strongly significant effect of the Force on the muscular activity. Differences between the two groups are visible starting from R3, the second part of the long-latency window (75-105 ms; LME: Diagnosis: $F_{(50)} = 0.73$, $P = 0.47$; Force: $F_{(7743)} = 4.02$, $P < 10^{-4}$; Diagnosis x Force: $F_{(7743)} = -3.66$,

$P < 10^{-3}$). These results suggest similar initial response following perturbation and highlight intact proprioception in ET. Impairments are visible in the late long-latency responses (LLRs), from 75ms. Surprisingly, this difference was associated with a slightly larger R3 response in the ET group, which was dependent on the perturbation magnitude as indicated by the interaction term. We demonstrate below that this effect is in fact expected in theory, assuming partial delay compensation in ET.

Computational model of feedback control in ET

In order to describe the behavior of ET patients from a theoretical perspective, we reproduced our experimental observations with a closed loop control model featuring a state estimator that compensates for sensorimotor delays. We modeled a Linear-Quadratic-Gaussian (LQG) controller taking into account delayed sensory feedback (Fig 3.1 C: dotted line) and internal representation of the body dynamics (Fig 3.1 C: dashed line) to produce an optimal motor command. The delay in the sensory feedback is compensated by extrapolating the sensory feedback over the delay interval (Fig 3.1 C: orange line), which is performed explicitly in this approach to study the impact of errors in this operation. We considered a scenario in which the sensory feedback delay was underestimated by the controller: the value of the delay used in the controller was 70% of the system's delay ($\delta t = 55\ ms$, $\hat{\delta} t = \ 0.7 \delta t$). This model previously showed that a mismatch in the state estimator associated with long-latency delays could also produce oscillations (Crevecoeur & Gervers, 2019).

In such case, the simulations for which the delay was underestimated produced trajectories bearing striking similarities with those of ET participants. Initially, the arm angle and angular velocity matched the simulations with no errors in delay estimation. We can notice a slightly smaller maximum hand deviation in the underestimated case, a trend that was also observed in the experimental results for the ET population (Figure 3.2 F). An overshoot was observed when bringing the hand back to the target and was followed by oscillations during the stabilization phase (Figure 3.4 B and C). Oscillations amplitude scaled

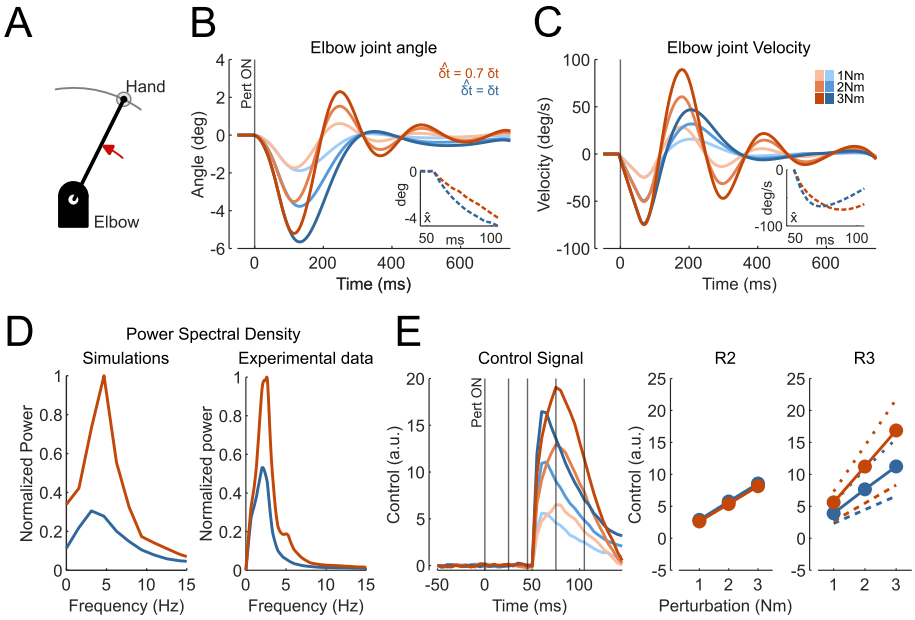

FIGURE 3.4: Computational model of feedback control in ET. **A,** Simulations of step perturbations in a single joint system. **B-E,** Model underestimating the sensory delays ($\hat{\delta t} = 0.7\delta t$, orange) and model with no delay estimation error ($\delta t = 55\ ms$, blue). **B,** Elbow joint angle following perturbation (1, 2 or 3 Nm). Insets represent the estimated state over the long-latency windows for the larger perturbation. **C,** Elbow joint angular velocity following perturbation. Inset same as **B**. **D,** Average normalized power spectral density across all perturbations for the simulated (left) and experimental (right) data. **E,** (Left) Average control signal for the 3 perturbation magnitudes ([1, 2, 3] Nm). Detail of the R2 (45-75 ms, middle panel) and R3 (75-105 ms, right panel) long-latency Windows. Additional traces on the right panel represent the most extreme slope changes following changes in delay and inertia values. Lower limit: $I = 0.2$ Kgm², $\delta t = 45$ ms. Higher limit: $I = 0.1$ Kgm², $\delta t = 65$ ms.

with perturbation magnitude and their frequency matched the oscillations observed with our participants; with a higher power spectral density for ET patients in the range 0 to 15Hz (Figure 3.4 D), and a peak frequency located around 4Hz as in the data. The motor commands produced by the model during the LLR window showed no difference

during R2, and early differences in R3, similarly to what was observed between NI and ET participants (Figure 3.4 E). This effect was robust as the presence of oscillations and increased gains persisted even when varying parameters such as delay and inertia. Simulations with parameters leading to the most extreme changes of slopes are visible on Figure 3.4 E.

We then assessed the sensitivity of the model properties as a function of different parameters. First, we observed that the main frequency of the oscillations remained unaffected when varying the limb inertia (Figure 3.5 A), which reminds ET as tremor frequency is also unaffected by arm loading (Elble et al., 1994). Similarly, varying the delay or delay error had an effect on the amplitude of the oscillations, while keeping the same tremor frequency (Figure 3.5 B&C). To identify the origin of these oscillations, we separated the contribution of a delay estimation error solely in the extrapolation of the state (first term of eq. 3.11) with an error solely in the extrapolation of motor commands (second term of eq. 3.11). We observed that the oscillations mainly arose from errors of the latter component (Figure 3.5 D-G). These results confirm the possibility that the initial pass through the state estimator produced comparable responses, as reflected by intact R2 responses, but errors accumulated over time due to the underestimation of the delay in the extrapolation of motor commands, resulting in oscillations during the later phases of the corrective movement.

All simulations above considered a static error in the delay parameter. To investigate the effect of a noisy error in the delay, we considered a delay composed of a fixed, or mean error, plus a random error drawn from uniform distribution (see Methods). Interestingly, simulations exhibited similar oscillations around the target, and an increase in the early response component compatible with the increase measured in R3. In contrast, a random delay error in the absence of a mean error did not produce oscillations. Thus, it seemed that the mean of the error was more important than a random source of the error, however a fuller treatment of random delay errors with more general sources of noise is needed in future studies.

Finally, we investigated the possibility that oscillations arose from

errors in other parameters of the model and discuss their link to the different pathways associated with state estimation. First, an up- or down-scaling of the Kalman gains accelerated or slowed down the model response to the perturbation, but it did not produce any oscillation. Then, we introduced an error in the prior estimate, x_p (Eqn. 3.10, Figure 3.5

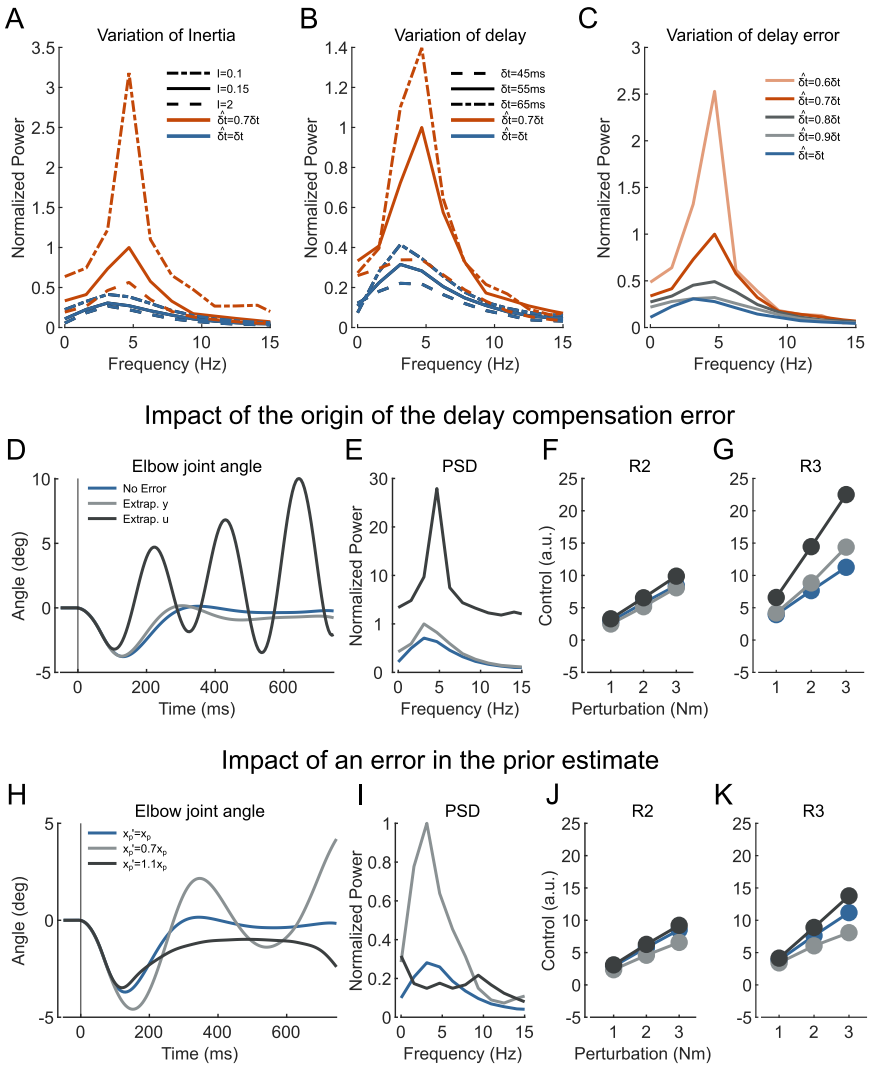

FIGURE 3.5: Sensitivity analyses of our feedback control model of ET. **A,** Variation of PSD under different values of inertia for the model underestimating the sensory delays ($\hat{\delta t} = 0.7\delta t$, orange) and the model with no delay estimation error ($\delta t = 55\ ms$, blue). **B,** same as **A** for different values of delay (δt=45ms/55ms/65ms). **C,** Effect of different delay errors on the PSD. **D-G,** Impact of the origin of the delay estimation error. Three cases were considered: an error ($\hat{\delta t} = 0.7\delta t$) solely in the extrapolation of the sensory feedback over the delay interval (light grey), an error ($\hat{\delta t} = 0.7\delta t$) solely in the extrapolation of the motor commands (dark grey), or no errors ($\hat{\delta t} = \delta t$) in delay estimation (blue). **D,** Elbow joint angle following a 2Nm perturbation. **E,** Average normalized power spectral density across all perturbations. F-G, Average control signal for 3 perturbation magnitudes ([1, 2, 3] Nm). **F,** Detail of the R2 (45-75 ms) and **G,** R3 (75-105 ms) Long Latency Windows. **H-I,** Impact of an error in the prior estimate x_p. Three cases considered: underestimation of the prior estimate ($x'_p = 0.7x_p$, light gray), overestimation of the prior estimate ($x_p\prime = 1.1x_p$, dark grey) or no error ($x_p\prime = x_p$, blue). Subpanels same as **D-G**.

H-K). When an overestimation was made, it reproduces a slight increase in the R3 response, as observed in experimental data. However, it did not lead to oscillations and while the system was unable to reach back to the target (Fig. 3.5 H). We noted that testing higher values of multiplicative errors produced numerical instability (the scaling factor was 1.1). Conversely, underestimating the prior produced oscillations at a lower frequency than observed in ET, and was associated with a decrease in the initial response, which was incompatible with our experimental observations. Finally, we introduced errors in the internal models underestimating A_d or B_d following previous work (Takei et al., 2021). An error in these parameters produced effects that were generally not compatible with the data, except for B_d which impacted the same summation as the delay (Eqn. 3.11). As these parameters impact all operations, we privileged the delay error that had a more specific role in the feedback pathway.

To summarize, based on oscillations and the transient increase in control responses observed in R3 for patients, we conclude that an erroneous delay estimation appears was the only hypothesis that reproduced all experimental features observed in ET patients while varying a single parameter.

3.4 Discussion

We investigated the hypothesis that ET originates from an erroneous compensation of the sensory delays. With a postural perturbation task, we observed feedback control impairments in the ET population. The initial impact of the perturbation was similar for the ET and NI volunteers, in the kinematics as well as the initial stretch responses. However, ET patients experienced perturbation dependent deficits when stabilizing their hand in the target, and they exhibited an increased R3 long-latency response suggesting errors in the feedback controller. We reproduced these results with a computational model erroneously compensating for long-latency delays. The simulations were performed with a value of the delay that was smaller than the true delay, producing an intact initial response to the perturbation followed by an accumulation of errors over time that led to impaired feedback control and to the emergence of oscillations that scaled with the force magnitude and matched the frequency of oscillations measured in ET patients.

To identify which pathway is affected in ET, we can divide our computational model into 3 main processes: 1- the processing of the afferent sensory information, 2- the prior estimate of the state of the system and of the environment (such as the external torque, estimated), 3- and finally the delay compensation pathway requiring internal monitoring of the effect of motor commands during the delay interval. Our results suggest that the sensory feedback is intact in ET. Indeed, because we did not observe any difference in short-latency response, and early long-latency responses (R2), we can conclude that the peripheral system and the early components of the stretch responses are preserved in ET. This result is also consistent with a recent study reporting intact proprioception in ET patients (Butler et al., 2023). Regarding the prior estimate of the state, simulations revealed that introducing an error that over or underestimate the prior did not reproduce the oscillations coupled with the increased R3 response observed in ET (Fig. 3.5 H-K). Additionally, in our previous study, we reported motor adaptation impairments in ET. The anticipation of the perturbation was preserved while the metrics related to motor control were impaired (Blondiaux et al., 2023). Their ability to anticipate an external disturbance suggests the preservation of patients' ability to form an internal prediction of

their movement even in the presence of a perturbation.

Thus, on the one hand, it is possible that both internal priors and sensory feedback are preserved, while, on the other hand, we observed clear deficits that could be linked to the feedback controllers as they scaled with the perturbation magnitude. The third model component, linked to the internal monitoring of motor commands, becomes a unique candidate pathway to account for sensorimotor deficits in this population: it is clearly a component of the state estimator, and therefore, of the feedback controller, and can be dissociated from both the sensory system and the formation of internal priors. Moreover, a selective alteration of the operation performed in this component produced all features observed experimentally, namely preserved R2 response, increased R3 response and impaired stabilization scaling with perturbation magnitude. However, it is important to note that, while an error in delay estimation is also affecting the pathway processing the sensory feedback, we observed that errors solely in this pathway does not lead to the emergence of oscillations. Consequently, we concluded that the impairment was attributable to the erroneous integration of motor commands. A clear added value of our modeling work is to provide a quantitative model of ET based on the simple assumption that their feedback control is not well adjusted to the true value of long-latency delays.

Considering some quantitative differences between our results and the simulations, a note of caution is warranted. First, an approximation of body dynamics was used in our model for the derivation of the controller. The simulations reported in this study are a simplified version of the task as we only modeled single-joint movements around a fixed axis. Our participants performed movements in the 3D space using the handle of the robotic device and therefore responded to the perturbation using more than one joint. In addition, the muscular activity collected during the experiment and the control signal extracted from the simulations did not fully match in terms of temporal profiles. Indeed, the model did not take the details of non-linear muscle dynamics into account nor the effect of antagonist muscles. In spite of these differences, the range of oscillations frequencies was similar across simulations and data, suggesting that the net effect of the muscle responses may correspond to the simulated control signal.

Despite these simplifications, we did observe an increase of the R3 responses both in the experimental data and the simulations, an effect that remained present even when varying several simulation parameters such as the limb inertia, the value of the delay or delay error. While the estimation of the perturbation magnitude was intact, simulations revealed that the velocity was overestimated starting already $\sim$70 ms following the load onset (Figure 3.4 B & C) which resulted in an increased gain in the response despite a small underestimation of the position.

Based on these results, a next challenge is to identify the neural pathways behind these operations to better identify the origin of the deficits in ET. To date cerebellum is one of the main candidates. Traditional views of the role of cerebellum in motor control have considered that this region was involved in forward models (Kawato, 1999). However, it has been also associated with state estimation (Diedrichsen & Bastian, 2014; Franklin & Wolpert, 2011; Miall et al., 1993; Wolpert, Miall, & Kawato, 1998), which is a component of feedback control models and of LLR (Crevecoeur & Scott, 2013; Todorov & Jordan, 2002). We also know from human and animal studies that a suboptimal state estimation leads to incorrect movements or oscillatory behavior (Flament et al., 1984; Miall et al., 2007; Takei et al., 2021). Interestingly, limb-imposed displacement induces changes in cerebellar nuclei activity within 70 ms, aligning with the timing of the long-latency pathway (Strick, 1983). In addition, severe cerebellar dysfunction induced by cerebellar ataxia or dentate nucleus cooling in monkeys is known to reduce drastically LLRs responses (Kurtzer et al., 2013; Meyer-Lohmann et al., 1975), making this structure a contributor to long-latency feedback pathway. Thus, the functional implication of cerebellum in LLR, and the possibility that the corresponding operation corresponds to state estimation, is in our view the candidate mechanism that is potentially altered in ET, while other cerebellar functions linked to forward models and anticipation may be preserved in this population (Blondiaux et al., 2023).

We suggest that instead of a severe cerebellar disruption leading to a substantial response attenuation as reported in cerebellar ataxia, ET could originate from subtle and partial cerebellar dysfunction such as a

small mismatch in delay estimation that is enough to produce sensorimotor deficits. This error in delay estimation does not affect the initial pass of the sensory feedback through the state estimator as observed with the intact initial responses, compatible with the observation that peripheral and spinal contributions seemed intact (R1 and R2). Yet, the accumulation of errors with multiple passes through the state estimator generated oscillations. Future studies should be performed to relate this functional hypothesis with the anatomical structures behind it using for example neuroimaging. Interestingly, the link between state estimation and cerebellum as well as its involvement in LLRs aligns with numerous indicators of a cerebellar origin in ET as highlighted by neuroimaging studies (Holtbernd & Shah, 2021; Mavroudis et al., 2019; Pietracupa, Bologna, Tommasin, Berardelli, & Pantano, 2021; Tikoo et al., 2020), as well as postmortem studies (Louis et al., 2007; Louis & Faust, 2020a) which report pathological cerebellar changes in ET.

Overall, this study reported intact short and initial long-latency responses in ET during a postural perturbation task. However, perturbation dependent deficits were observed when ET participants stabilized their hand in the home target, confirming impairments in feedback control. Based on computational modeling, we suggest that these deficits may stem from an erroneous compensation for sensorimotor delays, attributed to an underestimation of the delay by the controller.

Acknowledgments

The authors want to thank John Aoga for his assistance in sharing the code and Tremblement Essentiel Belgique for their help with patients' recruitment. Florence Blondiaux is a FRIA grantee of the Fonds de la Recherche Scientifique – FNRS (Be). Lise Colmant is a Research Fellow of the Fonds de la Recherche Scientifique – FNRS (Be). The FNRS provided salary and research support for Bernard Hanseeuw under grants n° CCL40010417 and n° FRFS-WELBIO40010035. Frédéric Crevecoeur is supported by a grant from the FNRS under grant number 1.C.033.18.

3.5 Supplementary Material

In addition to testing errors in estimating the feedback delay, we tested whether patients' behavior could originate from other error sources.

First, we generated errors in the state estimation by altering the Kalman gains by a scaling factor (0.2 or 2.5) with a perturbation load of 3 Nm and observed that none of these modifications generated any oscillation (see Figure 3.6 A-C). When the Kalman gains were down-scaled, the response to the perturbation was reduced due to the smaller influence of sensory feedback, which was not consistent with our data in which we observed similar R2 and increased R3 response. In contrast, an increase in the Kalman gains increases the sensibility to noise, as reflected by an increased tail of the power spectral density (PSD), without affecting significantly R2 and R3 responses. These simulations did not produce oscillations. Thus, the dissimilarity between these simulations and our results suggest that this possibility is not a good candidate to explain patients' behavior.

Besides, we also introduced errors in the internal model by underestimating A_d or B_d. Using the same technique as in (Takei et al., 2021), we multiplied A_d or B_d by a scaling factor (0.5). Oscillations obtained when underestimating A_d were also associated with a reduced initial response in R2 and R3, incompatible with experimental data. Errors in the matrix B_d reproduced a similar behavior as reported in erroneous delay estimation (see Figure 3.6 D-F). In fact, this result is expected as, by underestimating B_d, we not only introduced an error in the prior estimate but also in the compensation for sensory delays. Indeed, when down-scaling B_d, we also reduced the term that extrapolates past estimates over the delay interval (equation 3.11), leading to similar effect as when the delay was underestimated. In addition, A_d and B_d impacts almost all stages of the processing, making the interpretation more difficult and not specific to a given pathway. Furthermore an error in the internal model would be incompatible with our previous study which indicated preserved anticipation of the perturbations during a motor adaptation task, suggesting that forward models were not primarily impacted in ET (Blondiaux et al., 2023).

Based on oscillations and the transient increase in control responses, we concluded that an erroneous estimation of the delay was the best

hypothesis that reproduced all features of patients' behavior. Even if other combination can likely reproduce similar trajectories, the advantage of this hypothesis was that it involved an error in a single parameter.

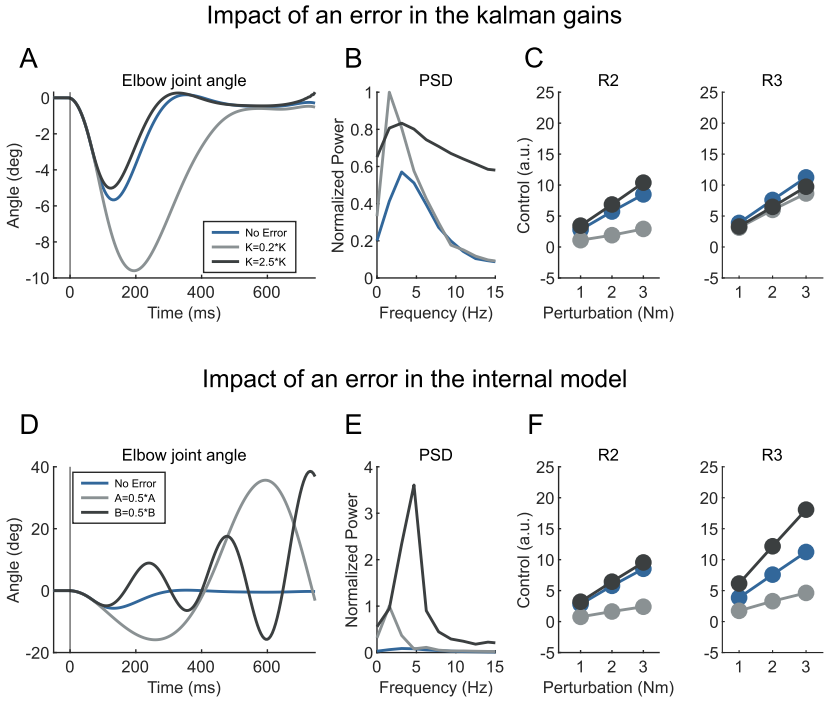

FIGURE 3.6: Impact of errors in the computational model of feedback control. **A-C,** Impact of an alteration of the Kalman gains. Three cases considered: downscaling of the Kalman gains (K' = 0.2K, light grey), upscaling of the Kalman gains (K' =2.5K, dark grey), no errors (blue). **A,** Elbow joint angle following a 3 Nm perturbation. **B,** Average normalized power spectral density across all perturbations. **C,** Average control signal for 3 perturbation magnitudes ([1, 2, 3] Nm). *Left,* Detail of the R2 (45-75 ms) and *Right,* R3 (75-105 ms) Long Latency Window. **D-F** Impact of an error in the internal model. Under-estimation of A or B were considered (A'=0.5A, light grey, B'=0.5B, dark grey). **D-F** same format as A-C.

Chapter 4

Decreased cerebello-thalamo-cortical functional connectivity and thalamic subnuclei atrophy in Essential Tremor

THE origin of Essential Tremor (ET), a movement disorder characterized by tremor during voluntary movements, remains poorly understood. Prior research suggested a pivotal role of the cerebellum and its connections with the cortex in tremor genesis. In this study, we investigated volumetric and functional connectivity changes in ET patients and assessed their relationship with behavioral measurements of the tremor collected outside of the scanner. Nineteen ET patients and 19 age-matched Neurologically Intact (NI) volunteers underwent a 3 T MRI protocol, which included a 3D T1-weighted sequence for volumetric analyses, resting-state functional MRI and three-dimensional multi-echo gradient echo sequence used for manual segmentation of the Dentate Nucleus (DN). Tremor severity was assessed using the Fahn-Tolosa-Marin tremor rating scale (FTM-TRS) and quantified using accelerometers attached to the fingertips of participants during the clinical assessment. We used a seed-based approach to study the functional connectivity of the dentate nucleus (DN), the main output of the cerebellum, and showed that a more precise segmentation

of the DN did not influence the results significantly when compared to using the DN region from the SUIT cerebellar atlas as a seed. DN functional connectivity was significantly decreased in the ET group with cortical, subcortical, and cerebellar areas when compared to NI participants. Connectome-based analyses, in which no specific region is considered a priori, reinforced these results showing group differences of functional connectivity between thalamus and cortical areas. Additionally, we observed a correlation between the FTM-TRS score and reduced functional connectivity between the thalamus and the cerebellum. Using Connectome Predictive Modeling (CPM), we were able to predict the FTM-TRS score and the average power spectral density of the tremor in ET patients. Finally, we found a significant correlation between the FTM-TRS score and atrophy in several thalamic subnuclei. Overall, our findings provide compelling evidence that the functional connectivity of the cerebellum and thalamus, as well as atrophy in the thalamic subnuclei, are associated with Essential Tremor.

4.1 Introduction

Essential tremor is one of the most frequent movement disorders affecting around 0.9% of the general population (Louis & Ferreira, 2010) and up to 4.8% of people above 65 years old (Benito-León et al., 2003). ET typically manifest with bilateral upper limb postural or kinetic tremor disrupting daily life activities. The tremor frequency typically ranges from 4 to 12 Hz. However, the tremor can also spread to other regions affecting the head, tongue, torso, lower limbs or voice (Clark & Louis, 2018; Gruol et al., 2016). The mechanisms underpinning this disorder remains poorly understood although the cerebello-thalamocortical pathway has often been identified as a potential circuit responsible for tremor genesis (Holtbernd & Shah, 2021). Postmortem studies also reported cerebellar abnormalities in ET patients (Cerasa & Quattrone, 2016; Pan & Kuo, 2022).

Magnetic resonance imaging (MRI) has been used by numerous researchers to try to identify deficits, anomalies, or biomarkers of ET. With the progress in acquisition and analyses techniques, we are now

able to generate images of the brain with a good contrast between tissues (white matter, grey matter and cerebrospinal fluid) (McRobbie et al., 2017). Using structural imaging, researchers and clinicians can quantify brain volumes, identify abnormalities or lesions, and explore structural changes associated with diverse pathological conditions.

In patients with ET, volumetric alterations have been studied extensively as outlined in the comprehensive review by Holtbernd and Shah (Holtbernd & Shah, 2021). Among these studies, previous research focusing on cerebellar volumes reported inconsistent findings. While some studies reported cerebellar atrophy in ET (Bagepally et al., 2012; Cerasa et al., 2009; Gallea et al., 2015), others have found no morphological changes (Archer et al., 2018; Nicoletti et al., 2015; Pietracupa et al., 2019). In addition, volumetric analyses of the cerebral cortical and subcortical structures exhibited even more heterogeneous results across studies. Grey matter atrophy or hypertrophy was documented in some studies while others did not identify any differences between NI and ET (Archer et al., 2018; Benito-León, Serrano, et al., 2019; Nicoletti et al., 2015; Pietracupa et al., 2019; Prasad et al., 2019). A recent meta-analysis supported the absence of consistent alterations of grey matter in this population (Luo et al., 2019).

Alongside structural imaging, functional imaging is commonly used to infer brain activity by capturing changes associated with blood flow via the blood oxygenation level-dependent (BOLD) signal. Increased brain activity increases energy consumption, inducing variation of the ratio between oxygenated and deoxygenated hemoglobin in the blood. Given the diamagnetic nature of oxygenated hemoglobin and the paramagnetic nature of deoxygenated hemoglobin, these alterations induce variations in the BOLD signal. Increased brain activity induces an immediate alteration in the oxygenated/deoxygenated hemoglobin ratio, followed a couple of seconds later by vasodilation and increased blood flow within the activated brain region. This typical response pattern is called the Hemodynamic Response Function (HRF). Using models of HRFs and BOLD signal, dynamic maps illustrating the activation of specific brain regions can be generated. Strong correlations between BOLD signal across the brain suggest that these regions are jointly activated (Bijsterbosch, 2017; Soares et al., 2016). Functional connectivity can be assessed at rest, but can also be coupled with tasks

performed within the scanner, offering insights into brain functions under diverse conditions.

Task-based studies, using motor tasks such as performing arm and wrist movements, maintaining the arm against gravity, or continuous writing of "8" with the dominant hand, reported altered activity in the cerebello-thalamo-cortical pathway for ET patients (Buijink et al., 2015; Muthuraman et al., 2018; Nicoletti et al., 2015). Interestingly, resting-state fMRI reported diminished and altered connectivity in the same circuits (Benito-León et al., 2015; Fang et al., 2016; Gallea et al., 2015; Tikoo et al., 2020).

Finally, diffusion imaging relies on the movement of water molecules to elucidate brain's microstructure. The diffusion of water molecules varies across tissues depending on tissue type, integrity and architecture. This movement provides insights into anisotropy, indicating whether water molecules can diffuse in all directions or are restricted to a single direction, as well as orientation of fibers within the tissue. Different tissues are associated with different diffusion properties: white matter tends to be anisotropic, with water molecules preferentially moving along axons; grey matter tends to be less anisotropic; and cerebrospinal fluid manifests isotropic diffusion, with unrestricted movement in all directions. One of the mostly used approaches, Diffusion Tensor Imaging (DTI), models from diffusion weighted images the diffusion process of each voxel using ellipsoids also known as tensors. Parameters derived from these tensors include Fractional Anisotropy (FA), indicating the directional preference of diffusion, and mean diffusivity (MD), which can be further categorized into axial and radial diffusion components (Soares et al., 2013). These reconstructed maps enable the investigation of tissue microstructural properties. In addition, anatomical connectivity can be explored through tractography, tracing fiber bundles from a specific location to other regions of the brain (Jenkinson & Chappell, 2018).

Diffusion studies more consistently reported cerebellar anomaly in ET compared with conventional volumetric MRI studies. Consistent microstructural alterations of the cerebellum have been reported, with changes mainly in cerebellar peduncles (Klein et al., 2011; Novellino et al., 2020; Tikoo et al., 2020). In addition to these cerebellar changes, widespread microstructural alterations have been reported in various

tracts related both to motor and non-motor functions (Gallea et al., 2015; Klein et al., 2011; Pietracupa et al., 2019).

In this study, our primary objective was to replicate the findings of Tikoo and colleagues who reported a diminished functional connectivity of the DN in ET patients with cortical and subcortical areas (Tikoo et al., 2020). In addition, we tested whether a more precise segmentation of the DN would impact the outcomes. We investigated cerebellar, cortical and subcortical volumes in both groups, including volume of the Dentate Nucleus and finally, we explored whether behavioral measurements of the tremor were correlated with functional connectivity or brain volume.

4.2 Methods

4.2.1 Participants

A total of 20 Essential Tremor (ET) patients and 22 Neurologically Intact (NI) volunteers of similar demographic repartition were enrolled in this study. All participants provided informed consent following standard procedures and the ethics committee of the host institution (Comité d'Éthique Hospitalo Facultaire, UCLouvain, Belgium) validated the protocol. Participants were evaluated using the Fahn-Tolosa-Marin Tremor Rating Scale (FTM-TRS) (Fahn et al., 1993). ET participants who received surgical treatment for their tremor or ET participants with co-existing neurological disorders were not enrolled in the study. The control group consisted of participants who self-reported the absence of known neurological disorders. Due to incidental findings, we excluded three participants of this group of NI volunteers. One participant presented a leukoaraiosis, and two participants had a mega-cisterna magna. One ET participant was excluded of the study because of important artifacts in the images caused by ferromagnetic surgical material in the patient's jaw. Analyses were therefore performed on 19 ET patients (11 females; age: M: 61,8 $\pm$ SD: 11,9) and 19 NI volunteers (11 females; age: 64 $\pm$ 14).

4.2.2 Tremor Assessment

During the FTM-TRS evaluation, participants wore wearable Inertial Measurements Units (device described in (El Khoury et al., 2021)). The setup was composed of accelerometers attached to the tip of the index fingers used to compute the tremor frequency during hand extension and finger-to-finger position (Figure 4.1 a). We computed the tremor frequency by considering the Power Spectral Density (PSD) as a density function and computed the expected value of the distribution to find the frequency associated with the peak in the PSD (Vertical line Figure 4.1 b). We also extracted the mean PSD of the oscillations between 4 and 12 Hz (Grey area Figure 4.1 b). We then averaged these measurements across left and right arms. This acquisition was performed the same day as the neuroimaging assessment.

4.2.3 Neuroimaging Assessment

MRI acquisition was performed at the Cliniques Universitaires Saint-Luc (UCLouvain, Belgique) using a 3.0 Tesla head scanner (Signa Premier, General Electric Company, United States) equipped with a 48-channel coil. ET patients and NI volunteers were positioned in the scanner, cushions were used to enhance comfort and to limit movement artifacts, and we used earplugs and noise-reduction headphones. Participants were instructed to remain eyes closed for the resting state as well as not to engage in cognitive or motor activities.

A **three-dimensional (3D) T1-weighted** data set encompassing the whole brain was selected to provide detailed anatomy (1 mm^3) thanks to MPRAGE sequence: inversion time = 900 ms, repetition time (TR) = 2188.16 ms, echo time (TE) = 2.96 ms, flip angle (FA) = 8°, field of view (FOV) = 256*256, 156 slices, slice thickness = 1 mm, no gap, total scan time = 5 min 36 s.

Resting state MRI T2*-weighted sequences of brain activity was collected with echo-planar imaging: FOV = 220*220 mm^2, matrix size = 110*110, TE = 30 ms, TR = 1700 ms, FA = 90°, 75 slices (order ascending and interleaved), slice thickness = 2 mm, parallel imaging (ARC2) and hyperband factor = 3. The whole brain slices were scanned 217 times (=6 min 09s)

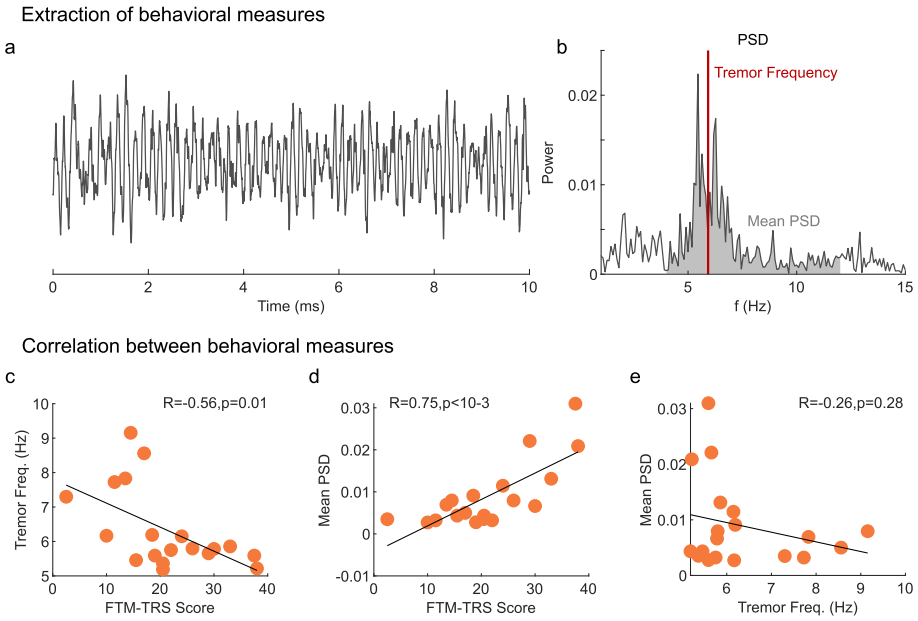

FIGURE 4.1: **a,** Principal component of the accelerometer signals. **b,** Power Spectral Density of the principal component. Grey area corresponds to the values used to compute the mean PSD. Red vertical line corresponds to the tremor frequency computed as the expected value of the PSD considered as a density function. **c,** Correlation between Tremor Frequency and FTM-TRS Score. **d,** Correlation between Mean PSD and FTM-TRS Score. **e,** Correlation between Mean PSD and Tremor Frequency.

A **three-dimensional multi-echo gradient echo (GRE)** sequence was utilized to obtain T2*-weighted images. These images were used to delineate DN. Imaging parameters for the multi-echo GRE sequence were the following: repetition time=47.1 ms, echoes = 16, first echo time =2.76 ms, echo time spacing = 2.78 ms, bandwidth = 651.02 Hz/pixel, flip angle = 12°, field of view = 24 x 24 cm, matrix size = 256 x 256, resolution = 0.94 x 0.94 x 1.0 mm^3, acceleration factor = 2, slices = 76, and total acquisition time = 5 min and 32 s. Slices in the multiecho GRE sequence were oriented axially and centered on cerebellum.

A **Multishell diffusion-weighted** sequence was employed to acquire data for diffusion MRI (dMRI) analysis. The imaging parameters for this sequence were as followsFOV = 220*220 mm^2, matrix size= 110*110, TE=77 ms, TR= 5200 ms, 64 gradients at b=1000, 32 at b=2000, 3000, 5000 and 7 b=0 s/mm2, 75 slices with slice thickness = 2 mm, with reversed phase encoding (=14 min 34 s). dMRI data not presented here.

4.2.4 Neuroimaging Data Processing

We analyzed fMRI data using BrainVoyager (Version 22.2.2, Brain Innovation, Maastricht, Netherlands). Preprocessing of the resting-state data consisted of linear trend removal to exclude scanner-related signal drift, a temporal high-pass filter to remove frequencies lower than 0.005 Hz and correction for head movements using a rigid body algorithm for rotating and translating each functional volume in 3D space. Additionally, we dropped the initial 7 volumes. The data was also corrected for time differences in the acquisition of the different slices and movement corrections were optimized using a sinc interpolation. As spontaneous low-frequency fluctuations can arise from non-neural signals and not only from BOLD-related fluctuations we performed additional pre-processing steps to remove undesirable sources of variance. Regression analyses were performed to remove artifacts due to residual motions (using the six movement regressors obtained during the previous motion correction) and changes in the ventricles (the signal from the ventricular mask defined in each participant). To perform comparisons between subjects, the data was spatially normalized in the Montreal Neurological Institute (MNI) space. All co-registrations were manually verified.

The whole brain was segmented using Freesurfer 7.0 image analysis pipeline (https://surfer.nmr.mgh.harvard.edu/). The resulting segmentation is based both on subject-independent probabilistic atlas and subject-specific measured values. We performed a visual inspection of the segmentation results and manual editing was made when needed. We only found and corrected minor skull strip errors before running the data through the pipeline again. In addition to whole brain segmentation, we also ran automatic labeling and volume estimation of the thalamic nuclei (25 ROIs per hemisphere, Iglesias et al., 2018) and estimation of the volume and cortical thickness of the regions defined by the Brainnetome atlas (Fan et al., 2016), which we also used for the functional connectivity analyses. Segmentation of the thalamus for one exemplar NI participant is visible on Figure 4.2 a, the Brainnetome atlas is displayed in Figure 4.2 d. We used a residual correction approach and corrected the results of the segmentation for intracranial volume (ICV), age and gender by fitting a linear regression model on all participants:

$$y = \beta_0 + \beta_1 \times \text{ICV} + \beta_2 \times \text{Age} + \beta_3 \times \text{Gender} + \varepsilon, \tag{4.1}$$

with β_0 the intercept; $\beta_1, \beta_2, \beta_3$ the coefficients associated with the independent variables and ε the residuals that captures the difference between predicted and actual values of y; y being the volume or the cortical thickness of a region of the Brainnetome or the CERES segmentation. The analyses were performed on the residuals.

We used the SuscEptibility mapping PIpeline tool for phAse images (SEPIA) pipeline to reconstruct Quantitative Suscpetibility Mapping (QSM) maps from the 3D multi-echo GRE phase data (Chan & Marques, 2021). Bilateral masks of the Dentate Nucleus were drawn manually in the QSM images using ITK-SNAP (www.itksnap.org) (Yushkevich et al., 2006) and verified by a neurosurgeon. Segmentation for one NI participant is displayed on Figure 4.2 b.

Cerebellar lobe volumes were estimated using the CEREbellum Segmentation (CERES) pipeline. This patch-based multi-atlas segmentation tool (Romero et al., 2017) divides the cerebellum into 12 lobules in the native space. Bilateral volume of each lobule was extracted from the results. A sample of segmentation results for one NI participant is visible on Figure 4.2 c.

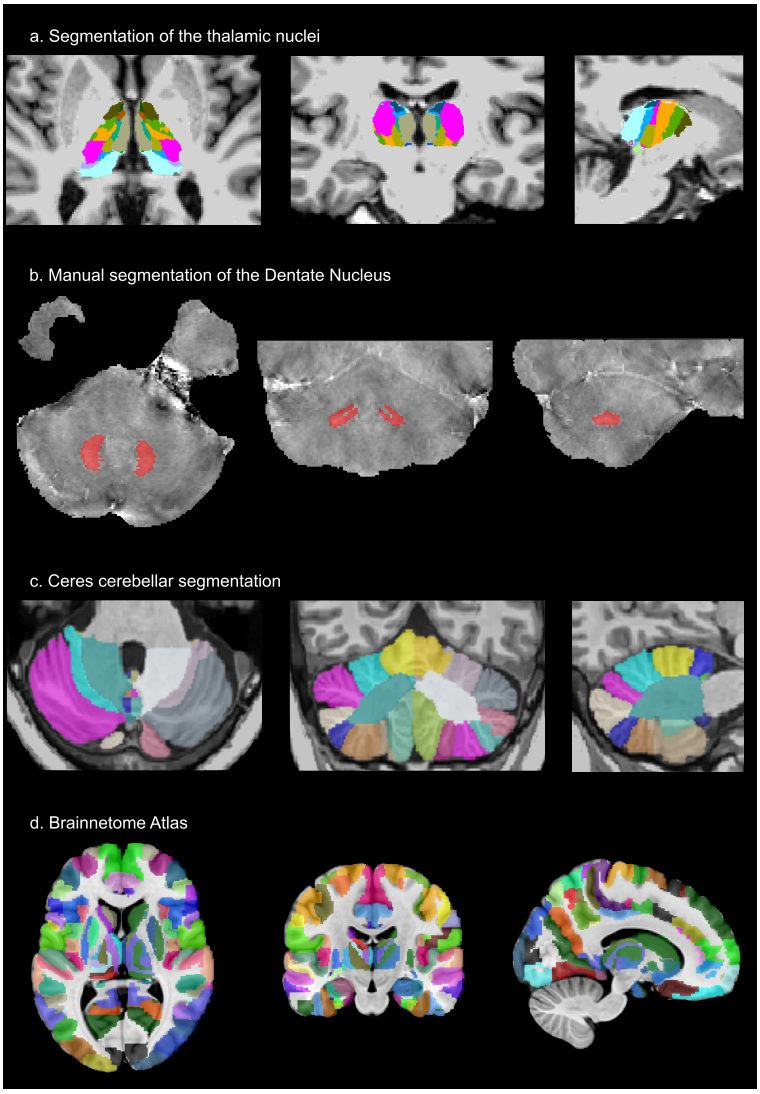

FIGURE 4.2: **a, b, c,** Segmentation for an exemplar NI participant in axial, coronal and sagittal views (Native space); **a,** Segmentation of the thalamic nuclei. Labels can be found in (Iglesias et al., 2018); **b,** Manual segmentation of the Dentate Nucleus on the susceptibility maps; **c,** CERES segmentation of the cerebellar lobules. Labels can be found in (Romero et al., 2017); **d,** Brainnetome atlas in standard MNI space. Labels can be found in (Fan et al., 2016).

4.2.5 Data Analysis

Seed-based analyses Differences between NI and ET were investigated via voxel-wise t-tests. P-values were corrected against multiple comparisons using a False Discovery Rate (FDR) of 0.01. Similarly, the relationship between DN functional connectivity and behavioral measures were evaluated using a multiple regression model (general linear model; GLM), using the behavioral measure of interest as predictor. P-values were corrected against multiple comparisons using a qFDR of 0.1. The data were smoothed in the spatial domain (Gaussian filter, FWHM – 5 mm). Behavioral measures considered were the FTM-TRS score and the frequency of the tremor measured with the accelerometers.

Connectome Functional Connectivity analyses 279 ROIs seeds, with defined shape and locations, were derived using the Brainnetome atlas composed of 246 regions of the bilateral hemispheres (Fan et al., 2016) and the SUIT cerebellar atlas composed of 33 regions (Diedrichsen, 2006). We modified the SUIT atlas to group the left and right Dentate Nucleus into a unique region. We assessed the connectivity between the different regions by computing the bivariate Pearsons' correlation between the time series of the extracted mean BOLD signal for each pair of ROIs, resulting in a 279 x 279 connectivity matrix per individual. We converted the resulting coefficients to normally distributed scores using Fisher's transformation. This transformation improves the normality assumptions of the second-level analysis. These matrices were then used for second-level analysis using the Conn toolbox (Whitfield-Gabrieli & Nieto-Castanon, 2012). We performed two-sided interdependent t-test to investigate differences between the two groups. A severe p-uncorrected $< 5 * 10^{-4}$ was used at the connection level and no corrections were made at the cluster level. In addition to group analyses, we investigated the influence of the tremor score on the functional connectivity by including this variable as a second-level covariate. We identified significant networks in our data using Network Based Statistics. The matrix of T-statistics estimated from the correlations between

the functional connectivity and the FTM-TRS score was thresholded using an a-priori p-uncorrected value of $< 5 * 10^{-4}$. The remaining connections are then used to identify sub-graphs that define the different clusters with a p-uncorrected of 0.05.

In addition, using the same connectivity matrices, we performed connectome-based predictive modeling (CPM). We extracted the most relevant features from the brain functional connectivity data allowing us to construct a predictive model of the group or behavioral measures (Shen et al., 2017). To construct this model, we first controlled for ICV, age and gender by performing a partial correlation on the connectivity matrices, we then extracted the most relevant features using a threshold of $2.5*10^{-4}$. We formed a binary mask of the most relevant features and applied it on individual matrices. We computed the sum of positive and negative significant correlations for each participant to summarize these features. Using leave-one-out we built a model predicting the behavioral score based on the sum of positive and negative correlations for the participants in the training set which resulted in a prediction of the behavioral feature for the tested participant. We reproduced this step for every individual. We finally assessed the prediction significance by reapplying the same steps 3000 times on randomly permuted behavioral measures. We compared our predictions made with the actual behavioral measures with those obtained with random permutations to assess the significance of our results. Behavioral measures considered for this analysis were the group, the FTM-TRS score, tremor frequency and tremor mean PSD.

Volumetric Analyses We used Pearson's correlation coefficient to measure linear association between volume of brain regions and participants' group or behavioral measurements (FTM-TRS score and tremor frequency). We corrected for multiple comparisons using the Benjamini-Hochberg method (Benjamini & Hochberg, 1995).

4.3 Results

4.3.1 Demographic and clinical characteristics of participants

There were no significant differences in age ($p = 0.61$, $t_{36} = 0.52$) or gender distribution ($p = 1$, $t_{36} = 0$) between the two groups. ET participants had a FTM-TRS score of 21.18 ± 2.16 (mean $\pm$ SEM) while the NI participants had a score of 2.82 ± 0.59. Scores significantly differed between groups ($p < 10^{-4}$, $t_{36} = -8.2$). ET participants had a tremor frequency of 6.33 ± 0.27 Hz. Correlations between the different behavioral measures are depicted on Figure 4.1 c-e.

4.3.2 Seed-based analysis of the DN functional connectivity

In this study, we aimed at reproducing previous results on functional connectivity of the dentate nucleus (DN) using a seed-based approach (Tikoo et al., 2020). Our first question was whether using a manual and more precise segmentation of the DN as a seed would influence the results compared to the simpler approach consisting in approximating this structure by a sphere, as in the original study. We also included a comparison of results obtained with the DN from the SUIT atlas. For the functional connectivity analyses, we did not observe any difference across these three definitions of the seed (manual drawing, sphere approximation or SUIT atlas). We computed the average t-statistic obtained when comparing NI and ET participants over all regions of the Brainnetome and SUIT atlas. We then computed the correlation between the values obtained with the 3 seeds and obtained a high and significant correlation for every combination (SUIT-Sphere: 0.85, $p < 10^{-4}$; Sphere-Manual segmentation: 0.78, $p < 10^{-4}$ and Suit-Manual segmentation= 0.83, $p < 10^{-4}$) suggesting that the different approaches were similar. In addition, when comparing the maps of significant differences between groups obtained with the seed defined by the manual segmentation or with the seed extracted from the SUIT atlas, we observed only minor differences despite considering a very loose uncorrected significance threshold of 0.05 and no spatial smoothing (Figure 4.3 a).

Based on these results, we decided to use a more general approach using the DN obtained from the SUIT atlas as a seed and spatial

smoothing of 5 mm for the following analyses. We observed a decreased functional connectivity in ET patients between the DN and the bilateral thalamus, bilateral basal ganglia, supplementary motor area, right primary motor area, right temporal lobe (inferior and transverse temporal gyrus), left precuneus and left superior frontal gyrus. We found increased functional connectivity in the ET group between the DN and the cerebellar lobes and the medulla oblongata (Figure 4.3 b). Finally, we found a negative association of the FTM-TRS score in the thalamus (Figure 4.3 c). All cluster coordinates and sizes are reported on Table 4.1.

4.3.3 Connectome Functional Connectivity

To confirm the choice of the seed from previous work (Tikoo et al., 2020) as well as to ensure we did not miss any important results not implicating the DN, we studied differences of functional connectivity between groups or correlations between functional connectivity and behavioral scores using connectivity matrices of 279 brain regions defined using atlases of the hemispheres and cerebellum (Figure 4.4 a). Unlike seed-based analyses, which focused on DN connectivity, this exploratory approach allowed us to investigate whole-brain functional connectivity without any prior hypothesis about specific regions of interest. Group-wise resting state differences were observed with a decreased connectivity between the left thalamus and the right angular gyrus for ET patients, and an increased connectivity between the left insula and the right pregenual areal in ET patients (p-uncorrected $< 5*10^{-4}$, Figure 4.4 b). The observed results did not remain statistically significant after applying multiple comparisons correction. These connections are reported in Table 4.2.

A negative association was found between the FTM-TRS score and functional connectivity of the bilateral interposed nuclei, DN, thalamus nuclei, vermis and between left superior temporal sulcus and DN (Figure 4.4 c). These connections are part of a significant network identified by NBS ($p<0.05$). These results indicate a weaker connectivity of these connections for participants with a high tremor score. Connections and strengths of the effects are reported in Table 4.2.

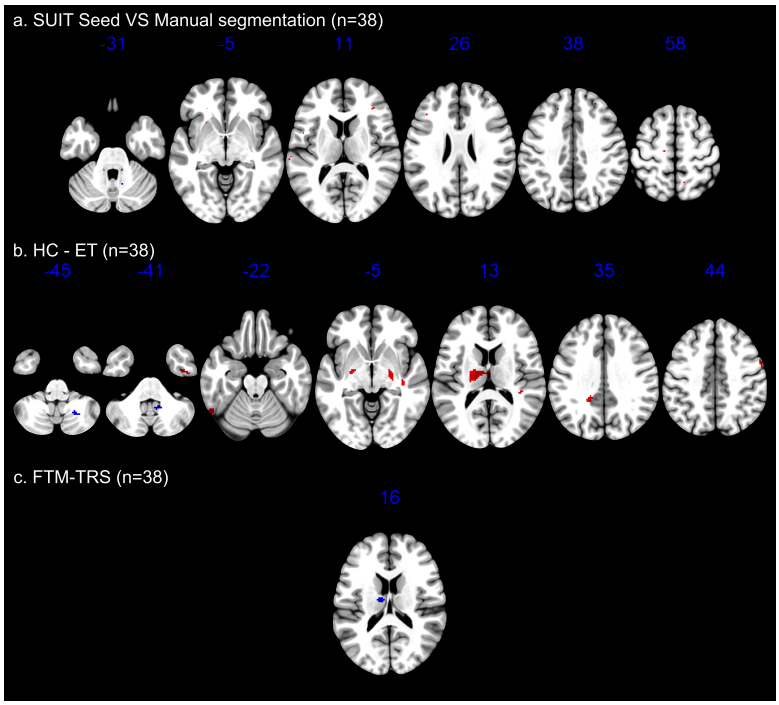

FIGURE 4.3: **a,** Subtraction of the maps of significant group differences obtained using two different seeds, DN extracted from the SUIT atlas and DN segmented manually on the QSM maps (no spatial-smoothing, p-uncorrected < 0.05, no corrections against multiple comparisons); **b,** Group differences in the DN functional connectivity between ET and NI. Maps of significant differences superimposed on T1 MNI template, red clusters imply higher DN functional connectivity for NI participants, blue clusters imply higher DN functional connectivity for ET patients (two-sample t-test, two-tailed, p-uncorrected < 0.005, FDR corrected using 0.01 threshold). **c,** Correlation of the DN functional connectivity with the FTM-TRS score in all participants. Blue clusters imply lower DN functional connectivity in participants with high FTM-TRS score (p-uncorrected $< 10^{-6}$, FDR corrected using 0.1 threshold), **a-c,** All maps are superimposed on T1 MNI template.

	Brain regions	MNI Coordinates			Cluster
		X	Y	Z	size mm³
NI>ET	Right pre-central gyri, primary motor area (BA4)	56.72	0.61	42.5	144
	Right inferior temporal gyrus (BA20)	42.68	-9.62	-41.56	136
	Right transverse temporal gyrus	38.4	-35.3	15.9	160
	Right putamen	38.64	-22.36	-3.36	112
	Right thalamus	26.1	-9.8	18.2	160
	Right lateral globus pallidus	22.83	-14.26	-3.32	528
	Superior frontal gyrus, supplementary motor area (BA6)	16.17	29.06	59.5	144
	Right Thalamus	10.27	-13.65	1.5	104
	Left thalamus, ventral lateral nucleus	-11.95	-12.79	12.26	1624
	Left thalamus	-1.83	-22.97	19.5	120
	Medial frontal gyrus, supplementary motor area (BA6)	-6.95	-4.68	73.32	176
	Left precuneus	-17.34	-42.13	34.76	152
	Left superior frontal gyrus	-18.64	66.79	0.5	112
	Left lateral globus pallidus	-24.19	-9.5	-4.04	104
	Left cerebellum	-55.25	-59.13	-22.63	256
ET>NI	Right cerebellum	23.5	-60.42	-45.27	104
	Right cerebellum	9.64	-52.93	-40.79	112
	Medulla oblongata	-7.04	-41.77	-55.15	296
FTM-TRS	Thalamus, anterior nucleus	-10.32	-11.32	15.05	176

TABLE 4.1: Brain regions that showed significant differences of DN functional connectivity between groups or significant correlations between DN functional connectivity and FTM-TRS. FTM-TRS = Fahn-Tolosa-Marin Tremor Rating Scale. BA = Brodmann Area. The results for group comparisons are corrected for multiple comparisons using a qFDR of 0.01 and correlations with tremor scores using a qFDR of 0.1. Cluster sizes are expressed in mm^3 and coordinates are expressed in MNI152 space.

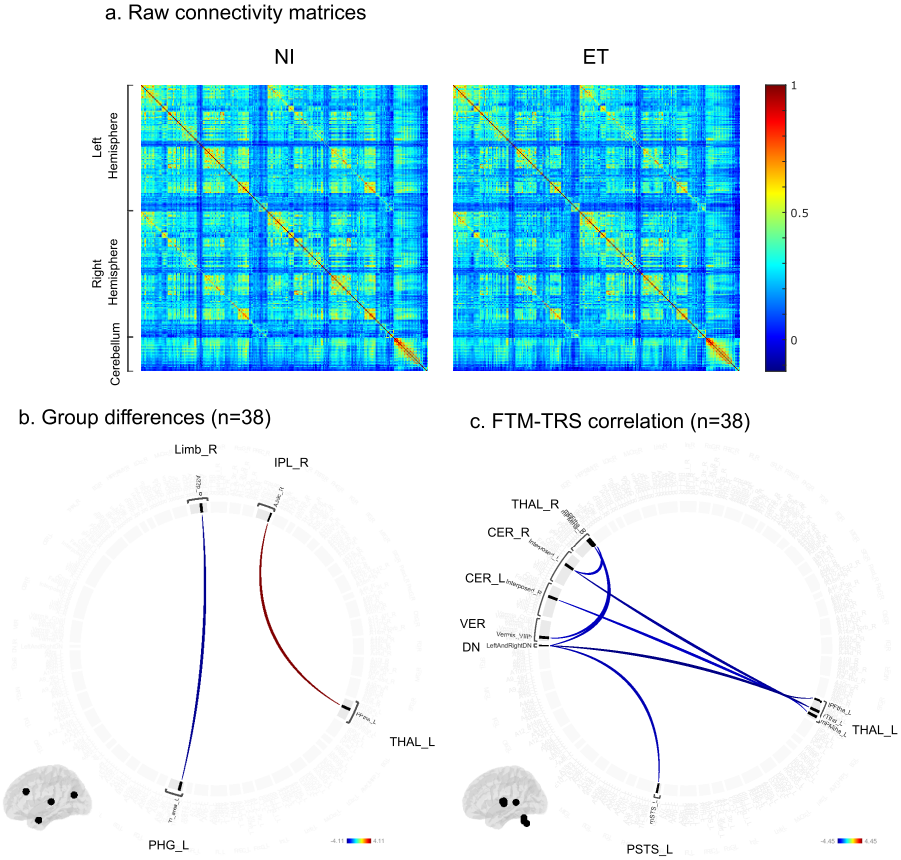

FIGURE 4.4: **a,** Average connectivity matrix reporting correlation between 279 regions of interest. Parcellation was made using Brainnetome atlas and SUIT cerebellar atlas; **b,** Connectome ring of the connections that were significantly different between groups ($p < 5{*}10^{-4}$, uncorrected for multiple comparisons). Increased functional connectivity in the NI group is depicted in red and increased functional connectivity in the ET group is depicted in blue; **c,** Connectome ring of the connections that were significantly associated with the FTM-TRS score ($p < 5{*}10^{-4}$, network-level p<0.05). Blue represents negative correlation between FTM-TRS score and the functional connectivity.

Effect of the group		
Connection	t-stat	p-value of the connection
PPtha_L-A39c_R	T(36)=4.41	0.000220
TI_area_L-A32p_R	T(36)=-3.97	0.000325
Effect of the FTM-TRS score (NBS, p<0.05)		
Connection	t-stat	p-value of the connection
rTtha_L-DN	T(36)=-4.45	0.000079
lPFtha_L-DN	T(36)=-4.39	0.000095
rTtha_L-Interposed_L	T(36)=-4.2	0.000170
rpSTS_L-DN	T(36)=-4.01	0.000290
mPMtha_L-DN	T(36)=-3.96	0.000342
mPMtha_R-DN	T(36)=-3.95	0.000345
mPFtha_R-DN	T(36)=-3.95	0.000346
mPMtha_R-Vermis_VIIIb	T(36)=-3.87	0.000443
mPFtha_R-Interposed_L	T(36)=-3.87	0.000443
rTtha_L-Interposed_R	T(36)=-3.86	0.000450

TABLE 4.2: Effect of the group on the functional connectivity, connections that significantly differed between groups ($p < 5 * 10^{-4}$), a positive t-statistic implies an increased connectivity in the NI group. Significance does not hold multiple comparison corrections. Network correlates with FTM-TRS scores. Significant connections ($p < 5 * 10^{-4}$) negatively correlated with the tremor score. These connections are part of the network identified by NBS (p<0.05).

4.3.4 Connectome-Based Predictive Modeling

Using CPM, we developed predictive models of the behavioral metrics (see Methods). This method is based on the same correlation matrices as the previous analyses, however, when using all participants' data, we were not able to form significant predictions. When working on ET patients only, we were able to predict the tremor score using the functional connectivity data. Correlation between predicted and actual FTM-TRS score was 0.57 (p=0.01, Figure 4.5 a). The significance of this correlation, computed on 3000 permutations, was $p < 10^{-3}$. The connections that best predicted FTM-TRS score are the left dorsal caudate with the right ventromedial putamen, the right occipital polar cortex with the right X lobule, and the right lateral pre-frontal thalamus with the left lobule VIIa (connections depicted on Figure 4.5 b&c).

We were also able to predict the mean PSD of the tremor. The correlation between predicted and actual values was 0.68 ($p< 10^{-3}$, Figure 4.5 d, significance computed on 3000 permutations $p < 10^{-3}$). The predictions were based mainly on connections between the occipital cortex and the right lobule X of the cerebellum (connections depicted on Figure 4.5 e&f).

4.3.5 Volumetric Analyses

Thalamic Nuclei As first analyses reported several impaired connections with the thalamus, using anatomical imaging we studied the volume of thalamic subnuclei in both groups as well as the relationship with behavioral measures. There was no significant change between the ET and NI groups. However, we found a negative association between the tremor score and the volume averaged over both hemispheres for the AV, VA, PuM, PuA, VAmc, LD, CL, VLa, and for the whole thalamus, implying a smaller volume for participants more affected by the tremor. Significant results are reported in Table 4.3 and displayed on Figure 4.6. Results for the 25 subthalamic nuclei are reported in the supplementary Table 4.4.

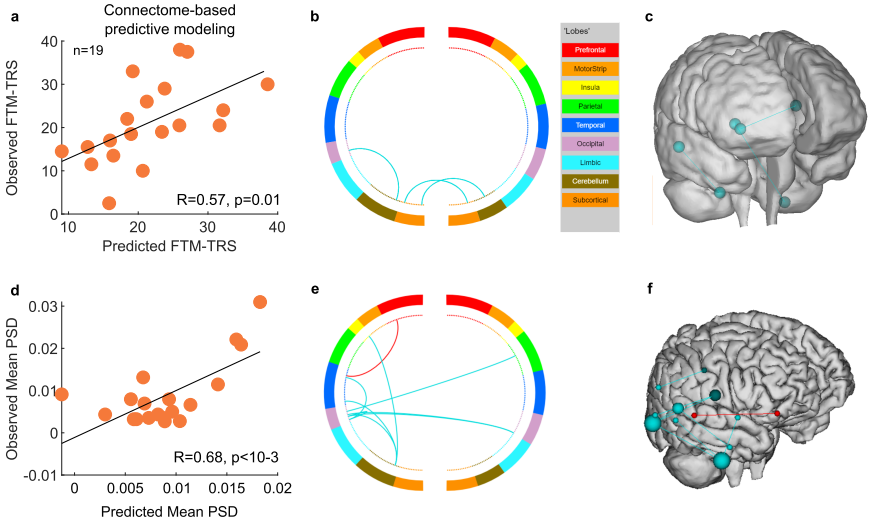

FIGURE 4.5: **a,** Correlation between actual and predicted FTM-TRS score based on CPM ; **b,** Left: Significant connections used to predict the FTM-TRS score. Blue lines indicate negative correlations and red lines indicate positive correlations (all $p<0.00025$). Right: Bain lobes color code; **c,** Projected node on a schematic representation of the brain. **d**, Correlation between actual and predicted mean PSD based on CPM; **e-f**, same as **b-c**.

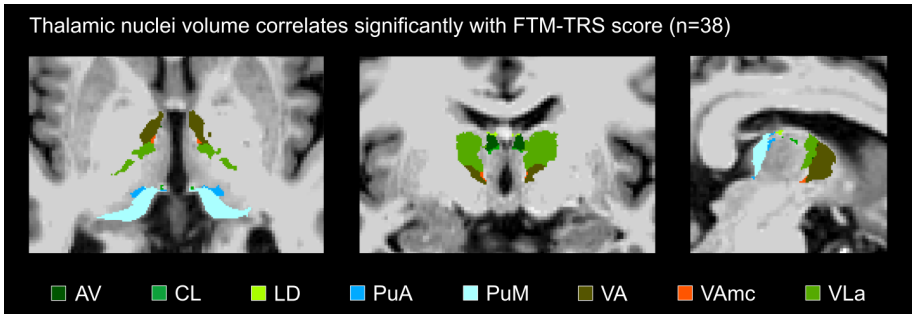

FIGURE 4.6: Thalamic nuclei that significantly correlate with FTM-TRS score, segmentation for an exemplar NI participant in native space in axial, coronal and sagittal views.

Correlations with FTM-TRS score	Region	R	uncorrected p-value
Thalamus	Anteroventral (AV)	-0.45	0.005
	Central lateral (CL)	-0.34	0.037
	Laterodorsal (LD)	-0.34	0.037
	Pulvinar anterior (PuA)	-0.39	0.014
	Pulvinar medial (PuM)	-0.40	0.013
	Ventral anterior (VA)	-0.45	0.005
	Ventral anterior magnocellular (Vamc)	-0.35	0.030
	Ventral lateral anterior (VLa)	-0.32	0.047
	Whole thalamus	-0.38	0.018
Dentate Nucleus	No significant correlations		
Cerebellum	Lobule X	-0.40	0.014
Brainnetome	No significant correlations		

TABLE 4.3: Correlations between FTM-TRS score and volumes of the thalamus nuclei, dentate nucleus, cerebellum and Brainnetome regions, corrected for ICV, age and gender. The significance level of 0.05 was adjusted for multiple comparisons using the Benjamini-Hochberg method using a qFDR of 0.2.

Dentate Nucleus Using QSM images, we manually segmented the dentate nucleus of our participants, an exemplar healthy control is displayed on Figure 4.2 b. We did not find significant differences between groups (t-test: $t_{36} = 0.21$, $p = 0.84$), neither a correlation with the tremor score (Pearson's correlation: 0.16, $p = 0.32$).

Cerebellum No significant changes of cerebellar volume were found between the two groups. A significant negative correlation was found between the FTM-TRS Score and the volume of the lobule X (r=-0.4, p-uncorrected=0.014, adjusted for multiple comparisons using a qFDR of 0.2). Results for all lobules are available in Supplementary Table 4.5.

Brainnetome Regions No significant changes of cortical thickness were found between the two groups neither significant correlation between the cortical thickness and any of the behavioral measures.

4.4 Discussion

In this study, we identified altered functional connectivity for ET patients in the cerebello-thalamo-cortical pathway. We used a seed-based approach to study DN connectivity alongside with connectome-based analyses, eliminating potential bias brought by the requirement to form an a-priori hypothesis. Using the functional connectivity data, we were able to predict the FTM-TRS score in the ET group, focusing on the connections involving the thalamus and cerebellum and we were able to predict the mean PSD of the tremor using connections between the occipital lobe and the cerebellum. Furthermore, we observed a negative correlation between thalamic nuclei volume and tremor severity, while the volume of the DN did not differ between groups, nor correlated with tremor severity. Altogether, these results support the pathophysiological significance of the cerebello-thalamo-cortical pathway in ET.

We first demonstrated that a more precise segmentation of the DN did not significantly influence the results of the seed-based analysis. Indeed, the maps of significant differences between groups, generated from the different seeds only marginally differed. Consequently, we suggest that, for functional connectivity analyses, incorporating an extra sequence requiring extra acquisition time and time-consuming preprocessing may not offer substantial advantages.

Seed-based analyses corroborated the findings of Tikoo and colleagues (Tikoo et al., 2020). We observed reduced functional connectivity of the DN with both cortical and subcortical regions, including basal ganglia, thalamus, primary motor cortex and premotor cortex. In addition, we observed increased DN functional connectivity with cerebellar peduncles. This alteration in functional connectivity within the cerebello-thalamo-cortical pathway aligns with evidence from previous fMRI studies implicating this pathway in the pathogenesis of ET tremor (Buijink et al., 2015; Fang et al., 2016; Holtbernd & Shah, 2021; Nicoletti et al., 2015). The DN, as principal cerebellar output, sends projections to the thalamus, serving as a relay station for transmitting information to the cortex (Haines & Dietrichs, 2012). These connections make cerebellum prone to be centrally involved in the generation of the tremor. Moreover, Deep Brain Stimulation of the ventral intermediate nucleus of the thalamus has demonstrated efficacy in tremor reduction among

these patients (Chandra et al., 2022; Iorio-Morin et al., 2020).

Interestingly, similar results were obtained when conducting analyses on the connectivity matrices, which did not require to form any a-priori hypotheses. Across the 279 regions in which we segmented the brain, we examined whether some connections differed between groups. We observed a significant effect of the connection between the left posterior parietal thalamus with the right angular gyrus. That later region is involved in numerous cognitive processes, including visuospatial processing. The second connection identified was between the left parahippocampal gyrus and the right cingulate cortex. The parahippocampal gyrus is involved in visuospatial processing and episodic memory, with prior fMRI studies indicating impairments in this region among ET patients (Benito-León, Sanz-Morales, et al., 2019). The cingulate cortex, strongly connected to the parahippocampal gyrus, receives inputs related to spatial and action-related information (Rolls, 2019). Alterations in the connectivity between these regions provide support for the documented impairments in visuo-motor integration reported in ET (Bareš et al., 2010).

Using the same connectivity matrices, we analyzed connections that exhibited significant correlations with the FTM-TRS score. Several connections between the deep cerebellar nuclei and the thalamus were significant. Direct connections between these regions exist and have been frequently implicated in ET pathogenesis (Haines & Dietrichs, 2012; Pan & Kuo, 2022). Additionally, significant connections were identified with the lobule VIIIb of the cerebellum, involved in motor processing (Stoodley & Schmahmann, 2010, 2018) and with the superior temporal sulcus.

Using CPM, we were able to predict the tremor score from the connectivity matrices in the patient subgroup. The resultant model indicated that the tremor score could be predicted based on the connectivity between the thalamus and the left lobule VIIa of the cerebellum, a region associated with working memory and executive function (Stoodley & Schmahmann, 2010, 2018). Impairments in these cognitive functions have been documented in ET (Bermejo-Pareja & Puertas-Martín, 2012; Louis et al., 2019). The connection between the left caudate nucleus and the right putamen was used to predict the FTM-TRS score. Together they form the striatum, which plays an important role

in movement control (Tewari et al., 2016). This is particularly relevant as our recent study evidenced impaired feedback control during a postural perturbation task in ET (Blondiaux et al., 2024). Finally, the connection between the right occipital polar cortex and the right lobule X was also used to predict the FTM-TRS score. Previously reported alterations in the functional connectivity of the occipital polar cortex in ET align with this finding (Benito-León, Sanz-Morales, et al., 2019; Benito-León et al., 2015), Lobule X is involved in vestibular functions and eye movements (Diedrichsen & Bastian, 2014; Stoodley & Schmahmann, 2018). Interestingly, the same connections between the occipital lobe and the lobule X were used to predict the mean PSD of the tremor.

Due to the numerous findings implicating the thalamus, we decided to investigate the volume of its subnuclei and discovered a correlation between decreased volume and the tremor severity. Some studies have reported smaller thalamus volume in ET (Benito-León, Sanz-Morales, et al., 2019; Pietracupa et al., 2019; Prasad et al., 2019), while other found no differences (Novellino et al., 2020) or even increased volume in young ET participants (Qi et al., 2020). To our knowledge, our study is the first one to study thalamus subnuclei volume in ET. We identified several nuclei whose atrophy correlated with the FTM-TRS score. Nuclei ventral anterior (Va), ventral anterior magnocellular (Vamc) and ventral lateral anterior (VLa) are involved in motor control, receiving afferents from the basal ganglia (Mai & Majtanik, 2019). The anteroventral (AV) nuclei of the thalamus receive afferents from the hippocampal formation and project to the cingulate cortex (Mai & Majtanik, 2019) which relates to the impaired connection between these regions discussed earlier. The laterodorsal (LD) nuclei receive afferents from visual structures and play an important role in spatial navigation by providing key visual inputs to the hippocampal system and the entorhinal cortex (Perry & Mitchell, 2019; Peyrache, 2022). The central lateral (CL) nuclei have an influence on mental and cognitive functions by relaying information between the brainstem and the cortex (Kumar et al., 2023). Finally, the pulvinar anterior (PuA) and medial (PuM) nuclei play a role in multisensory integration, relaying information from various sensory areas to the premotor cortex (Cappe et al., 2012). Lesions in the pulvinar nuclei can affect visually guided movements such as reaching and grasping movements (Kastner & Arcaro, 2022).

The absence of DN atrophy in ET is supported by previous studies that reported no differences in volume and magnetic susceptibility of the DN assessed using QSM images (Y. Zhang et al., 2023), as well as no disparity in iron deposition using swan imaging (Pietracupa, Bologna, Tommasin, Elifani, et al., 2021). These results suggest that the impairments in the DN are more likely functional than caused by an atrophy. As we mentioned in the introduction, results regarding cerebellar, cortical and subcortical atrophy or hypertrophy are highly heterogeneous. In this study, we found no differences between groups nor correlations with behavioral scores for Brainnetome regions. Regarding cerebellar volume, we only found an association between lobule X volume and FTM-TRS score. The absence of differences between groups suggests that connectivity impairments observed are not a direct consequence of morphological differences.

Interestingly, these results are in line with our previously proposed hypothesis regarding the origin of ET (Blondiaux et al., 2024). Indeed, the observed impairments that are more related to motor functions align with a potential deficit in delay compensation in ET, where errors propagate from cerebellum to primary and pre-motor cortex via the thalamus. In addition, our analysis using CPM reveled a correlation between the mean PSD of the tremor and functional connectivity. This result relates to our previous modeling work which demonstrated that larger errors in delay estimation were associated with an increased tremor amplitude and higher mean PSD. Integrating this behavioral measurement to the rest of the analyses used in this paper would be interesting. All participants of this study also participated to the postural perturbation task conducted in our previous study (Chapter 3). However, we did not observe correlations between behavioral metrics extracted from our feedback control task -specifically, the frequency and average PSD of oscillations during the stabilization phase- and functional connectivity or volumetric differences. Several factors could account for this absence of correlations. The assessment was not conducted on the same day, and for some participants, were conducted up to 16 months apart. Additionally, summarizing task performances into two simple metrics may not accurately reflect the complex impairments observed during the task.

In the present study, we mostly observed significant correlations

with the FTM-TRS score but fewer group differences. This could be attributed to the fact that differences between groups are not pronounced, as some ET patients were only affected by a mild tremor. However, it suggests that changes in brain structure and functional connectivity are subtle and progressive, worsening with more severe symptoms.

Finally, one major limitation of our study is the relatively small number of participants included, which limits the statistical power of our analyses. Another limitation is the absence of treatment withdrawal before the assessments, which might alter the behavioral measurements for example by decreasing the tremor score if the treatment is efficient for those patients.

In conclusion, the present study revealed group differences of functional connectivity within the cerebello-thalamo-cortical circuit and revealed differences correlated with tremor severity within the same circuit. Furthermore, using the functional connectivity matrices, we were able to predict the tremor score in ET patients. Additionally, volumetric analyses reported atrophy in several subnuclei of the thalamus that correlated with the FTM-TRS score. Overall, these results support the hypothesis that cerebellum and its projections play an important role in the tremor genesis in ET.

4.5 Supplementary Material

Region	R	uncorrected p-value
Anteroventral (AV)	**-0.45**	**0.005**
Central medial (CeM)	-0.31	0.055
Central lateral (CL)	**-0.34**	**0.037**
Centromedian (CM)	-0.20	0.236
Laterodorsal (LD)	**-0.34**	**0.037**
Lateral geniculate (LGN)	-0.32	0.052
lateral posterior (LP)	-0.30	0.066
Limitans (suprageniculate) (LSg)	0.01	0.958
Mediodorsal lateral parvocellular (MDl)	-0.27	0.100
Mediodorsal medial magnocellular (MDm)	-0.23	0.170
Medial Geniculate (MGN)	-0.04	0.822
Reuniens (medial ventral) (MV_RE)	-0.29	0.076
Paracentral (Pc)	-0.31	0.057
Parafascicular (Pf)	-0.12	0.462
Paratenial (Pt)	-0.13	0.432
Pulvinar anterior (PuA)	-0.39	0.014
Pulvinar inferior (PuI)	-0.24	0.143
Pulvinar lateral (PuL)	-0.13	0.433
Pulvinar medial (PuM)	**-0.40**	**0.013**
Ventral Anterior (VA)	**-0.45**	**0.005**
Ventral Anterior magnocellular (Vamc)	**-0.35**	**0.030**
Ventral lateral anterior (VLa)	**-0.32**	**0.047**
Ventral lateral posterior (VLp)	-0.21	0.209
Ventromedial (VM)	-0.11	0.501
Ventral posterolateral (VPL)	-0.16	0.344
Whole Thalamus	**-0.38**	**0.018**

TABLE 4.4: Correlations between thalamic nuclei and FTM-TRS score, corrected for ICV, age and gender. The significance level of 0.05 was adjusted for multiple comparisons using the Benjamini-Hochberg method using a qFDR of 0.2. Significance denoted in bold.

Region	R	uncorrected p-value
Cerebellum	-0.23	0.16
I-II	-0.11	0.52
III	-0.08	0.62
IV	-0.01	0.93
V	0.07	0.69
VI	0.00	0.98
Crus I	-0.27	0.10
Crus II	-0.02	0.91
VIIB	-0.20	0.23
VIIIA	-0.32	0.05
VIIIB	-0.26	0.12
IX	-0.34	0.03
X	**-0.40**	**0.014**

TABLE 4.5: Correlations between cerebellar lobes volume and FTM-TRS score, corrected for ICV, age and gender. The significance level of 0.05 was adjusted for multiple comparisons using the Benjamini-Hochberg method using a qFDR of 0.2. Significance denoted in bold.

Chapter 5

Discussion

5.1 Summary of contributions

The underlying mechanisms driving Essential Tremor remain unclear, while a cerebellar origin is often suggested, further investigation is still required for a more precise understanding. In this thesis, we used the movement control framework to explore and better document the impaired and preserved mechanisms in ET. Specifically, we focused on tasks relying on cerebellar integrity, such as saccadic adaptation to sudden changes in the location of visual stimulus, adaptation of upper limb movements to force fields, and a feedback control. Through these assessments, we aimed to study whether cerebellar-dependent mechanisms contribute to tremor genesis. Additionally, we conducted a neuroimaging study to investigate impaired pathways in ET, examining functional connectivity and volumetric alterations. In addition, we studied how these findings correlated with behavioral measures and tremor severity.

Firstly, we studied motor adaptation in our ET population, as we know that is it an ability that is impaired in cerebellar patients. We found that ET patients did adapt to the perturbations, contrasting with the drastic impairments often documented in cerebellar patients. However, the degree of adaptation in ET patients was diminished compared with neurologically intact participants. When decomposing the mechanisms contributing to motor adaptation, we observed that ET patients' ability to anticipate the perturbation was preserved. The impairments appeared to stem from erroneous movement execution during the task.

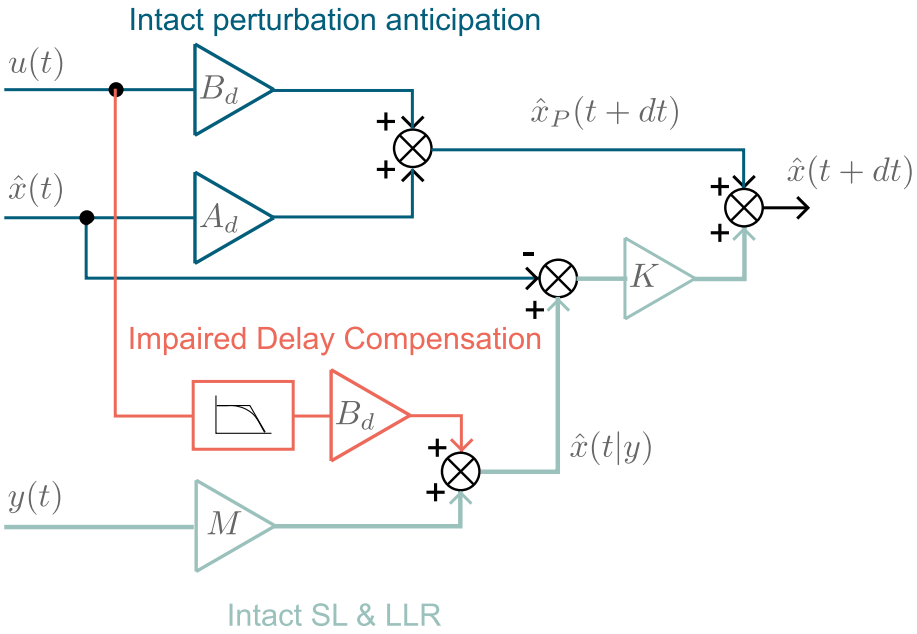

FIGURE 5.1: Model pathway adapted from Crevecoeur and Gervers, 2019. Model compensating for the delay in sensorimotor control. The light blue pathway corresponds to the sensory feedback, the dark blue pathway corresponds to the formation of an internal prior $\hat{x}_P$ and the red pathway corresponds to the delay compensation that is suspected to be faulty in ET. A_d and B_d define the dynamics of the model, dt is the time step, δt the system delay, K are the Kalman gains, u are the motor commands, $\hat{x}$ the estimated state and y the sensory feedback. For more details about the model see Chapter 3.

Referring to our scheme of motor control, this suggests that the formation of the prior estimate of the state (dark blue pathway in Figure 5.1) remains intact in ET patients, allowing them to anticipate the perturbation, despite observed difficulties in the movement execution.

Building upon these findings, our second study focused specifically on feedback control in ET. During a postural perturbation task, we observed oscillations in ET patients' movements when stopping and stabilizing the hand in the target. These perturbation-dependent deficits suggested that the tremor was generated by the feedback controller. Interestingly, the initial muscular responses were intact, implying that

the feedback received was intact (light blue pathway in Figure 5.1). This left us with only one pathway that could be potentially faulty: the delay compensation pathway (red pathway in Figure 5.1). Using computational modeling, we showed that introducing an error in the estimation of the feedback delay leads to oscillations during the movements. The oscillations replicated all features observed in ET patients' movements during the task, including an intact initial response followed by oscillations scaling with perturbation magnitude. This reinforces the hypothesis that oscillations in ET arise from the feedback controller, and that these oscillations result from an erroneous compensation for sensory delays, an ability that is believed to be performed by cerebellum.

In our final study, we studied functional connectivity using resting-state fMRI in ET patients. Our findings revealed impairments within the cerebello-thalamo-cortical loop, which aligns with the assumptions raised with our computational model as these same structures are involved in movement control. In addition, our model predicted an increase in oscillations' PSD for simulations with higher error in delay estimation. Interestingly, we observed a relationship between functional connectivity and the mean PSD of the tremor. We also observed a correlation between the tremor score and reduced functional connectivity between cerebellar and thalamic structures. Moreover, we also studied volumetric changes in these patients and identified a correlation between an atrophy of subnuclei of the thalamus and tremor severity, further emphasizing the central role of cerebellum and its connections in the etiology of the disorder.

These works all emphasize the significant role played by cerebellum in the origin of the tremor, as all identified impairments are related to cerebellar mechanisms. The observed deficits in motor adaptation,feedback control and functional connectivity support the hypothesis of an erroneous delay compensation in ET, a process predominantly mediated by cerebellum. Additionally, from a different perspective, the fMRI study further strengthens the implication of cerebellum in the disorder, as many significant results were closely associated with cerebellar regions. Overall, these results contribute to a better understanding of the mechanisms at the origin of ET.

5.2 Limitations

One of the main limitations of this thesis is the limited sample size. The relatively small number of participants in each group can impact the generalization of our findings. With a limited sample, it becomes challenging to draw a robust conclusion that applies to a larger population. However, the consistency of our findings across multiple tasks and methodologies strengthens our confidence in our hypothesis of impaired delay compensation in ET. Nevertheless, caution should be exercised when extrapolating these findings to broader populations.

Another limitation of this study is the overlap between the control group and the ET group, particularly for patients with mild symptoms that might have a clinical score similar to the participants in the control group. While including patients with mild symptoms enables us to better capture behavior in this population, including early-stage manifestations of the disorder, it complicates differentiation between groups. In particular when results indicate that impairments observed in the behavioral tasks and imaging results tend to progress with the disease severity.

The absence of treatment withdrawal in all the studies could have potentially impacted the results. Treatments might have reduce the tremor and therefore clinical scores or impacted behavioral measurements and brain functional connectivity. To address these limitations, future research could focus on expanding the sample size to obtain a more comprehensive understanding of these impairments and how they evolve with disease severity.

In addition, conducting a longitudinal study that monitor patients over time could provide valuable insights into the progression of essential tremor. With increasing references to ET as an evolutionary disorder and limited documentation on its pattern of evolution (Louis, 2021), there is a clear need for longitudinal investigations. Understanding how behavior in tasks, functional connectivity and brain volume evolve over time could shed light on the disorder. Moreover, assessing whether these measures could serve as objective indicators of the disease evolution could greatly enhance diagnostic accuracy and ease the follow-up of the disorder. Incorporating such assessments in future

studies is crucial for advancing our understanding of ET and improving patient care.

It is important to note that all analyses were conducted at the population level. However, averaging across populations of patients can sometimes lead to misleading or generic conclusions. Specifically, averaging over individuals can obscure different subtypes of the disease or mask heterogeneity in patient's behavior, even if the patients exhibit the same symptoms (Caramazza & McCloskey, 1988). In our studies, we report statistically significant impairments at the group level; however, some ET patients achieve similarly to healthy control in some tasks. To further investigate these nuances, it would be valuable to conduct single-case studies focusing on patients whose performances aligns with that of healthy controls, this time comparing their behavior to a control group that maximizes the same features as the patient of interest. If the patient's behavior remain in the range of controls it would suggest that the hypothesis of ET arising from erroneous delay compensation might explain the disorder in some patients, but not all. This findings could complement the results of this thesis, and would align with the observed heterogeneity of the disorder, as seen in age of onset, cognitive symptoms, and treatment responsiveness, suggesting different underlying mechanisms for ET.

5.3 Open questions & suggestions for future works

Our results seem to point towards impaired delay compensation in ET. But could ET stem from a broader deficit in estimating timings?

This question has been discussed in the review by (Bareš et al., 2012), highlighting a couple of studies that have investigated timing in ET. Britton and colleagues studied fast wrist movements towards several visual targets (Britton et al., 1994). These fast movements are controlled by a triphasic pattern of agonist - antagonist - agonist muscle activity, a pattern also present in ET patients. However, ET patients second agonist EMG burst was delayed. This delay resulted in unopposed action of the antagonist muscle leading to overshoots of the target followed by damped oscillations. This delay of the second agonist EMG

burst evidences abnormalities in the timing of the anticipatory muscle activity required to stop the movement.

Impairments have also been documented in ET patients when performing rhythmic movements. Farkas et al. evaluated rhythmic finger tapping in a group of ET patients (Farkas et al., 2006). These patients were not able to synchronize to the auditory cues and experienced increased variability in their rhythmic movements, variability being defined as the standard deviation of the movement onset with the pacing signal. The same result was observed for alternating hand movements, in both hands, and for fast and slow conditions, suggesting a central origin for this deficit. Avanzino et al. corroborated these findings in a study evaluating repetitive finger tapping at various frequencies also indicated by an audio cue (Avanzino et al., 2009). The temporal variability, defined as the coefficient of variation of the inter-tapping interval, was increased in the ET group. Interestingly, repetitive transcranial magnetic stimulation (rTMS) applied on cerebellum reduced the variability of the rhythmic movements, improving ET patients' performances. Anderson et al. demonstrated that tapping regularity in ET patients improved following DBS or thalamotomy, suggesting the implication of the cerebello-thalamo-cortical pathway in this process (Anderson et al., 2009). Finally, during a rhythmic finger tapping task performed in the MRI scanner, reduced functional connectivity was observed in the cerebellum as well as in the parietal and frontal cortex in ET patients, further emphasizing the role played by these regions in ET.

In addition to the role played by cerebellum in these timing tasks, our fMRI study revealed impaired functional connectivity of the basal ganglia in ET. Interestingly, these regions have been associated with the accuracy of time estimates (Fung et al., 2021). Furthermore, pathologies associated with basal ganglia, such as Parkinson's disease and Huntington's disease, have been shown to impair timing perception (Avanzino et al., 2016).

Bares and colleagues demonstrated that prediction of motor timings during a dynamic precise timing task was also affected in ET. In this task, participants aimed to intercept a moving target, requiring the integration of visual prediction of the moving target with motor response. To mitigate the effect of the tremor, the motor response consisted of a single button press, releasing a "fireball" at a constant

speed. ET patients had fewer hits and delayed responses compared to the control group. Moreover, performances were the most affected in the subgroup of patients with head tremor, indicating a more advanced severity of the disease. These results suggest an impaired ability to integrate feedback with timings. Furthermore, eye-hand coordination appears to be impaired in ET. In healthy controls, thanks to multisensory integration, performing simultaneously saccadic eye movement with arm movements reduces the latency of saccades. However, in ET patients, no difference of saccadic latency was observed between eye-hand movements and eye movements alone, suggesting an inappropriate integration or use of the sensory feedback (Trillenberg et al., 2006). Finally, some studies even revealed increased tremor with increased visual (Archer et al., 2018) or auditory feedback (Welzel et al., 2024). During these tasks, participants were required to apply a specific force while receiving feedback about their performances. Different gains were applied on the feedback to evaluate performances in high or low feedback conditions. These studies revealed an increased tremor severity in the high feedback condition in the ET patients' group.

All these elements seem to support the hypothesis of an erroneous timing estimation in ET. In order to gather more evidence to confirm or infirm this hypothesis as well as to relate to the hypothesis of erroneous delay estimation supported by the second chapter, we suggest investigating whether individuals with ET are capable of learning new artificial sensory delays. A study by Kilteni et al. demonstrated that individuals can learn and unlearn predicted sensory delays in the context of self-generated touch (Kilteni et al., 2019). Somatosensory attenuation occurs during self-generated stimulus, explaining that self-generated touch feels less intense and less ticklish than externally generated identical stimulus. This phenomenon relies on brain's ability to predict the consequences and timing of our actions. Moreover, Kileteni and Ehrsson have linked somatosensory attenuation with the suppression of activation in cerebellum, suggesting its involvement in modulating sensory processing during self-generated touch (Kilteni & Ehrsson, 2020). When introducing an additional delay between the movement and the resulting touch, people can rapidly learn to attenuate delayed touch. Future research could test whether essential-tremor patients sensory attenuation mechanisms are intact but also test whether they are able

to adapt to artificial sensory delays.

Continuing research on this topic is important to continue clarifying the mechanisms behind the tremor genesis in ET. Alongside to elucidating these mechanisms, there is a crucial need to identify biomarkers of the disease and develop more objective behavioral measurements of the disorder. These elements are essential to improve diagnosis and improve the monitoring of the progression of the disorder.

5.4 Concluding words

In this thesis, we approached Essential Tremor from a motor control perspective, providing valuable insights into the underlying mechanisms of the disorder. Through the lens of motor adaptation, we uncovered intact predictions of perturbations in ET patients, coupled with erroneous movement execution. Subsequent investigations into pure feedback control tasks revealed impairments in ET patients. These impairments were replicated by a computational model of motor control erroneously compensating for sensory delays, an operation typically associated with cerebellum. Finally, our imaging study revealed impaired functional connectivity of the cerebellum and its thalamocortical connections in ET, with observed impairments between groups and correlations with tremor severity. Collectively, our results strongly support the hypothesis of a cerebellar origin in ET. We believe that this work lays a solid foundation for future studies on Essential tremor.

Bibliography

Anderson, V. C., Burchiel, K. J., Hart, M. J., Berk, C., & Lou, J.-S. (2009). A randomized comparison of thalamic stimulation and lesion on self-paced finger movement in essential tremor. *Neuroscience Letters*, *462*(2), 166–170. https://doi.org/10.1016/j.neulet.2009.07.003

Archer, D. B., Coombes, S. A., Chu, W. T., Chung, J. W., Burciu, R. G., Okun, M. S., Wagle Shukla, A., & Vaillancourt, D. E. (2018). A widespread visually-sensitive functional network relates to symptoms in essential tremor. *Brain*, *141*(2), 472–485. https://doi.org/10.1093/brain/awx338

Avanzino, L., Bove, M., Tacchino, A., Ruggeri, P., Giannini, A., Trompetto, C., & Abbruzzese, G. (2009). Cerebellar involvement in timing accuracy of rhythmic finger movements in essential tremor. *European Journal of Neuroscience*, *30*(10), 1971–1979. https://doi.org/10.1111/j.1460-9568.2009.06984.x

Avanzino, L., Pelosin, E., Vicario, C. M., Lagravinese, G., Abbruzzese, G., & Martino, D. (2016). Time Processing and Motor Control in Movement Disorders. *Frontiers in Human Neuroscience*, *10*. https://doi.org/10.3389/fnhum.2016.00631

Bagepally, B. S., Bhatt, M. D., Chandran, V., Saini, J., Bharath, R. D., Vasudev, M., Prasad, C., Yadav, R., & Pal, P. K. (2012). Decrease in Cerebral and Cerebellar Gray Matter in Essential Tremor: A Voxel-Based Morphometric Analysis under 3T MRI. *Journal of Neuroimaging*, *22*(3), 275–278. https://doi.org/10.1111/j.1552-6569.2011.00598.x

Baizer, J. S., Kralj-Hans, I., & Glickstein, M. (1999). Cerebellar Lesions and Prism Adaptation in Macaque Monkeys. *Journal of Neurophysiology*, *81*(4), 1960–1965. https://doi.org/10.1152/jn.1999.81.4.1960

Bareš, M., Husárová, I., & Lungu, O. V. (2012). Essential tremor, the cerebellum, and motor timing: Towards integrating them into one complex entity. *Tremor and Other Hyperkinetic Movements (New York, N.Y.)*, *2*, tre-02-93-653–1.

Bareš, M., Lungu, O. V., Husárová, I., & Gescheidt, T. (2010). Predictive Motor Timing Performance Dissociates Between Early Diseases of the Cerebellum and Parkinson's Disease. *The Cerebellum*, *9*(1), 124–135. https://doi.org/10.1007/s12311-009-0133-5

Bastian, A. J., Martin, T. A., Keating, J. G., & Thach, W. T. (1996). Cerebellar ataxia: Abnormal control of interaction torques across multiple joints. *Journal of Neurophysiology*, *76*(1), 492–509. https://doi.org/10.1152/jn.1996.76.1.492

Benito-León, J., Bermejo-Pareja, F., Morales, J.-M., Vega, S., & Molina, J.-A. (2003). Prevalence of essential tremor in three elderly populations of central Spain. *Movement Disorders*, *18*(4), 389–394. https://doi.org/10.1002/mds.10376

Benito-León, J., Louis, E. D., Romero, J. P., Hernández-Tamames, J. A., Manzanedo, E., Álvarez-Linera, J., Bermejo-Pareja, F., Posada, I., & Rocon, E. (2015). Altered Functional Connectivity in Essential Tremor: A Resting-State fMRI Study. *Medicine*, *94*(49), e1936. https://doi.org/10.1097/MD.0000000000001936

Benito-León, J., Sanz-Morales, E., Melero, H., Louis, E. D., Romero, J. P., Rocon, E., & Malpica, N. (2019). Graph theory analysis of resting-state functional magnetic resonance imaging in essential tremor. *Human Brain Mapping*, *40*(16), 4686–4702. https://doi.org/10.1002/hbm.24730

Benito-León, J., Serrano, J. I., Louis, E. D., Holobar, A., Romero, J. P., Povalej-Bržan, P., Kranjec, J., Bermejo-Pareja, F., Del Castillo, M. D., Posada, I. J., & Rocon, E. (2019). Essential tremor severity and anatomical changes in brain areas controlling movement sequencing. *Annals of Clinical and Translational Neurology*, *6*(1), 83–97. https://doi.org/10.1002/acn3.681

Benjamin, D. J., Berger, J. O., Johannesson, M., Nosek, B. A., Wagenmakers, E.-J., Berk, R., Bollen, K. A., Brembs, B., Brown, L., Camerer, C., Cesarini, D., Chambers, C. D., Clyde, M., Cook, T. D., De Boeck, P., Dienes, Z., Dreber, A., Easwaran, K., Efferson, C., … Johnson, V. E. (2017). Redefine statistical significance. *Nature*

Human Behaviour, *2*(1), 6–10. https://doi.org/10.1038/s41562-017-0189-z

Benjamini, Y., & Hochberg, Y. (1995). Controlling the False Discovery Rate: A Practical and Powerful Approach to Multiple Testing. *Journal of the Royal Statistical Society Series B: Statistical Methodology*, *57*(1), 289–300. https://doi.org/10.1111/j.2517-6161.1995.tb02031.x

Bermejo-Pareja, F., & Puertas-Martín, V. (2012). Cognitive Features of Essential Tremor: A Review of the Clinical Aspects and Possible Mechanistic Underpinnings. *Tremor and Other Hyperkinetic Movements*, *2*(0), 02. https://doi.org/10.5334/tohm.106

Bhatia, K. P., Bain, P., Bajaj, N., Elble, R. J., Hallett, M., Louis, E. D., Raethjen, J., Stamelou, M., Testa, C. M., Deuschl, G., & the Tremor Task Force of the International Parkinson and Movement Disorder Society. (2018). Consensus Statement on the classification of tremors. from the task force on tremor of the International Parkinson and Movement Disorder Society. *Movement Disorders*, *33*(1), 75–87. https://doi.org/10.1002/mds.27121

Bijsterbosch, J. (2017). *Introduction to resting state fMRI functional connectivity* (First edition). Oxford University Press.

Bindel, L., Mühlberg, C., Pfeiffer, V., Nitschke, M., Müller, A., Wegscheider, M., Rumpf, J.-J., Zeuner, K. E., Becktepe, J. S., Welzel, J., Güthe, M., Classen, J., & Tzvi, E. (2022). Visuomotor Adaptation Deficits in Patients with Essential Tremor. *The Cerebellum*, *22*(5), 925–937. https://doi.org/10.1007/s12311-022-01474-5

Blondiaux, F., Colmant, L., Lebrun, L., Hanseeuw, B., & Crevecoeur, F. (2024). Erroneous compensation for long-latency feedback delays as origin of Essential Tremor. *The Journal of Neuroscience*, e0069242024. https://doi.org/10.1523/JNEUROSCI.0069-24.2024

Blondiaux, F., Lebrun, L., Hanseeuw, B. J., & Crevecoeur, F. (2023). Impairments of saccadic and reaching adaptation in essential tremor are linked to movement execution. *Journal of Neurophysiology*, *130*(5), 1092–1102. https://doi.org/10.1152/jn.00165.2023

Bo, J., Block, H. J., Clark, J. E., & Bastian, A. J. (2008). A Cerebellar Deficit in Sensorimotor Prediction Explains Movement Timing

Variability. *Journal of Neurophysiology*, *100*(5), 2825–2832. https://doi.org/10.1152/jn.90221.2008

Britton, T. C., Thompson, P. D., Day, B. L., Rothwell, J. C., Findley, L. J., & Marsden, C. D. (1994). Rapid wrist movements in patients with essential tremor: The critical role of the second agonist burst. *Brain*, *117*(1), 39–47. https://doi.org/10.1093/brain/117.1.39

Buijink, A. W. G., Van Der Stouwe, A. M. M., Broersma, M., Sharifi, S., Groot, P. F. C., Speelman, J. D., Maurits, N. M., & Van Rootselaar, A.-F. (2015). Motor network disruption in essential tremor: A functional and effective connectivity study. *Brain*, *138*(10), 2934–2947. https://doi.org/10.1093/brain/awv225

Butler, A. A., Diong, J., Lidman, K., Adler, J., Wardman, D. L., Gandevia, S. C., & Héroux, M. E. (2023). Upper Limb Function but Not Proprioception is Impaired in Essential Tremor: A Between-Groups Study and Causal Mediation Analysis. *Tremor and Other Hyperkinetic Movements*, *13*(1), 1. https://doi.org/10.5334/tohm.731

Cappe, C., Rouiller, E. M., & Barone, P. (2012). Cortical and Thalamic Pathways for Multisensory and Sensorimotor Interplay. In M. M. Murray & M. T. Wallace (Eds.), *The Neural Bases of Multisensory Processes*. CRC Press/Taylor & Francis.

Caramazza, A., & McCloskey, M. (1988). The case for single-patient studies. *Cognitive Neuropsychology*, *5*(5), 517–527. https://doi.org/10.1080/02643298808253271

Carey, M. R. (2024). The cerebellum. *Current Biology*, *34*(1), R7–R11. https://doi.org/10.1016/j.cub.2023.11.048

Cerasa, A., Messina, D., Nicoletti, G., Novellino, F., Lanza, P., Condino, F., Arabia, G., Salsone, M., & Quattrone, A. (2009). Cerebellar atrophy in essential tremor using an automated segmentation method. *American Journal of Neuroradiology*, *30*(6), 1240–1243. https://doi.org/10.3174/ajnr.A1544

Cerasa, A., & Quattrone, A. (2016). Linking Essential Tremor to the Cerebellum—Neuroimaging Evidence. *Cerebellum*, *15*(3), 263–275. https://doi.org/10.1007/s12311-015-0739-8

Chan, K.-S., & Marques, J. P. (2021). SEPIA—Susceptibility mapping pipeline tool for phase images. *NeuroImage*, *227*, 117611. https://doi.org/10.1016/j.neuroimage.2020.117611

Chandra, V., Hilliard, J. D., & Foote, K. D. (2022). Deep brain stimulation for the treatment of tremor. *Journal of the Neurological Sciences*, *435*, 120190. https://doi.org/10.1016/j.jns.2022.120190

Chen, H., Hua, S. E., Smith, M. A., Lenz, F. A., & Shadmehr, R. (2006). Effects of human cerebellar thalamus disruption on adaptive control of reaching. *Cerebral Cortex*, *16*(10), 1462–1473. https://doi.org/10.1093/cercor/bhj087

Chen-Harris, H., Joiner, W. M., Ethier, V., Zee, D. S., & Shadmehr, R. (2008). Adaptive control of saccades via internal feedback. *Journal of Neuroscience*, *28*(11), 2804–2813. https://doi.org/10.1523/JNEUROSCI.5300-07.2008

Clark, L. N., & Louis, E. D. (2018). *Essential tremor* (Vol. 147). Elsevier B.V. https://doi.org/10.1016/B978-0-444-63233-3.00015-4

Cluff, T., & Scott, S. H. (2015). Apparent and Actual Trajectory Control Depend on the Behavioral Context in Upper Limb Motor Tasks. *Journal of Neuroscience*, *35*(36), 12465–12476. https://doi.org/10.1523/JNEUROSCI.0902-15.2015

Córdova Bulens, D., Cluff, T., Blondeau, L., Moore, R. T., Lefèvre, P., & Crevecoeur, F. (2023). Different Control Strategies Drive Interlimb Differences in Performance and Adaptation during Reaching Movements in Novel Dynamics. *eneuro*, *10*(4), ENEURO.0275–22.2023. https://doi.org/10.1523/ENEURO.0275-22.2023

Crevecoeur, F., Cluff, T., & Scott, S. H. (2014, October). Computational Approaches for Goal-Directed Movement Planning and Execution. In M. S. Gazzaniga & G. R. Mangun (Eds.), *The Cognitive Neurosciences* (5th ed.). The MIT Press. https://doi.org/10.7551/mitpress/9504.003.0051

Crevecoeur, F., & Gervers, M. (2019). Filtering compensation for delays and prediction errors during sensorimotor control. *2954*, 2925–2954. https://doi.org/10.1162/NECO

Crevecoeur, F., & Kording, K. P. (2017). Saccadic suppression as a perceptual consequence of efficient sensorimotor estimation. *eLife*, *6*, 1–15. https://doi.org/10.7554/eLife.25073

Crevecoeur, F., Kurtzer, I., & Scott, S. H. (2012). Fast corrective responses are evoked by perturbations approaching the natural variability of posture and movement tasks. *Journal of Neurophysiology*, *107*(10), 2821–2832. https://doi.org/10.1152/jn.00849.2011

Crevecoeur, F., Mathew, J., Bastin, M., & Lefevre, P. (2020). Feedback adaptation to unpredictable force fields in 250ms. *Eneuro*, ENEURO.0400–19.2020. https://doi.org/10.1523/eneuro.0400-19.2020

Crevecoeur, F., & Scott, S. H. (2013). Priors Engaged in Long-Latency Responses to Mechanical Perturbations Suggest a Rapid Update in State Estimation. *PLoS Computational Biology*, *9*(8). https://doi.org/10.1371/journal.pcbi.1003177

Crevecoeur, F., & Scott, S. H. (2014). Beyond Muscles Stiffness: Importance of State-Estimation to Account for Very Fast Motor Corrections (F. J. Valero-Cuevas, Ed.). *PLoS Computational Biology*, *10*(10), e1003869. https://doi.org/10.1371/journal.pcbi.1003869

De Comite, A., Crevecoeur, F., & Lefèvre, P. (2021). Online modification of goal-directed control in human reaching movements. *Journal of Neurophysiology*, *125*(5), 1883–1898. https://doi.org/10.1152/jn.00536.2020

Desmurget, M., Epstein, C. M., Turner, R. S., Prablanc, C., Alexander, G. E., & Grafton, S. T. (1999). Role of the posterior parietal cortex in updating reaching movements to a visual target. *Nature Neuroscience*, *2*(6), 563–567. https://doi.org/10.1038/9219

Diedrichsen, J., Criscimagna-Hemminger, S. E., & Shadmehr, R. (2007). Dissociating Timing and Coordination as Functions of the Cerebellum. *Journal of Neuroscience*, *27*(23), 6291–6301. https://doi.org/10.1523/JNEUROSCI.0061-07.2007

Diedrichsen, J. (2006). A spatially unbiased atlas template of the human cerebellum. *NeuroImage*, *33*(1), 127–138. https://doi.org/10.1016/j.neuroimage.2006.05.056

Diedrichsen, J. (2007). Optimal Task-Dependent Changes of Bimanual Feedback Control and Adaptation. *Current Biology*, *17*(19), 1675–1679. https://doi.org/10.1016/j.cub.2007.08.051

Diedrichsen, J., & Bastian, A. (2014, October). Cerebellar Function. In M. S. Gazzaniga & G. R. Mangun (Eds.), *The Cognitive Neurosciences* (5th ed.). The MIT Press. https://doi.org/10.7551/mitpress/9504.003.0050

Diedrichsen, J., Verstynen, T., Lehman, S. L., & Ivry, R. B. (2005). Cerebellar Involvement in Anticipating the Consequences of Self-Produced Actions During Bimanual Movements. *Journal of Neurophysiology*, *93*(2), 801–812. https://doi.org/10.1152/jn.00662.2004

El Khoury, G., Penta, M., Barbier, O., Libouton, X., Thonnard, J.-L., & Lefèvre, P. (2021). Recognizing Manual Activities Using Wearable Inertial Measurement Units: Clinical Application for Outcome Measurement. *Sensors*, *21*(9), 3245. https://doi.org/10.3390/s21093245

Elble, R. J. (2003). Characteristics of physiologic tremor in young and elderly adults. *Clinical Neurophysiology*, *114*(4), 624–635. https://doi.org/10.1016/S1388-2457(03)00006-3

Elble, R. J., Higgins, C., Leffler, K., & Hughes, L. (1994). Factors influencing the amplitude and frequency of essential tremor. *Movement Disorders*, *9*(6), 589–596. https://doi.org/10.1002/mds.870090602

Fahn, S., Tolosa, E., & Marin, C. (1993). Clinical Rating Scale for Tremor. *Parkinson's disease and movement disorders*, *2*, 271–280.

Fan, L., Li, H., Zhuo, J., Zhang, Y., Wang, J., Chen, L., Yang, Z., Chu, C., Xie, S., Laird, A. R., Fox, P. T., Eickhoff, S. B., Yu, C., & Jiang, T. (2016). The Human Brainnetome Atlas: A New Brain Atlas Based on Connectional Architecture. *Cerebral Cortex*, *26*(8), 3508–3526. https://doi.org/10.1093/cercor/bhw157

Fang, W., Chen, H., Wang, H., Zhang, H., Puneet, M., Liu, M., Lv, F., Luo, T., Cheng, O., Wang, X., & Lu, X. (2016). Essential tremor is associated with disruption of functional connectivity in the ventral intermediate Nucleus-Motor Cortex-Cerebellum circuit: ET Is Associated With Disruption of FC in the VIM. *Human Brain Mapping*, *37*(1), 165–178. https://doi.org/10.1002/hbm.23024

Farkas, Z., Szirmai, I., & Kamondi, A. (2006). Impaired rhythm generation in essential tremor. *Movement Disorders*, *21*(8), 1196–1199. https://doi.org/10.1002/mds.20934

Flament, D., Vilis, T., & Hore, J. (1984). Dependence of cerebellar tremor on proprioceptive but not visual feedback. *Experimental Neurology*, *84*(2), 314–325. https://doi.org/10.1016/0014-4886(84)90228-0

Flash, T., & Hogan, N. (1985). The coordination of arm movements: An experimentally confirmed mathematical model. *The Journal of Neuroscience*, *5*(7), 1688–1703. https://doi.org/10.1523/JNEUROSCI.05-07-01688.1985

Franklin, D. W., & Wolpert, D. M. (2011). Computational Mechanisms of Sensorimotor Control. *Neuron*, *72*(3), 425–442. https://doi.org/10.1016/j.neuron.2011.10.006

Fridman, E. (2014). *Introduction to Time-Delay Systems: Analysis and Control*. Springer International Publishing. https://doi.org/10.1007/978-3-319-09393-2

Fung, B. J., Sutlief, E., & Hussain Shuler, M. G. (2021). Dopamine and the interdependency of time perception and reward. *Neuroscience & Biobehavioral Reviews*, *125*, 380–391. https://doi.org/10.1016/j.neubiorev.2021.02.030

Gallea, C., Popa, T., García-Lorenzo, D., Valabregue, R., Legrand, A.-P., Marais, L., Degos, B., Hubsch, C., Fernández-Vidal, S., Bardinet, E., Roze, E., Lehéricy, S., Vidailhet, M., & Meunier, S. (2015). Intrinsic signature of essential tremor in the cerebello-frontal network. *Brain*, *138*(10), 2920–2933. https://doi.org/10.1093/brain/awv171

Gomi, H., & Kawato, M. (1996). Equilibrium-Point Control Hypothesis Examined by Measured Arm Stiffness During Multijoint Movement. *Science*, *272*(5258), 117–120. https://doi.org/10.1126/science.272.5258.117

Gomi, H., & Kawato, M. (1997). Human arm stiffness and equilibrium-point trajectory during multi-joint movement. *Biological Cybernetics*, *76*(3), 163–171. https://doi.org/10.1007/s004220050329

Gordon, N. (1996). Speech, language, and the cerebellum. *International Journal of Language & Communication Disorders*, *31*(4), 359–367. https://doi.org/10.3109/13682829609031327

Gould, D. J., Brueckner, J. K., & Fix, J. D. (2016). *High yield neuroanatomy* (Fifth edition). Wolters Kluwer.

Gréa, H. (2002). A lesion of the posterior parietal cortex disrupts online adjustments during aiming movements. *Neuropsychologia*, *40*(13), 2471–2480. https://doi.org/10.1016/S0028-3932(02)00009-X

Gruol, D. L., Koibuchi, N., Manto, M., Molinari, M., Schmahmann, J. D., & Shen, Y. (Eds.). (2016). *Essentials of Cerebellum and Cerebellar Disorders*. Springer International Publishing. https://doi.org/10.1007/978-3-319-24551-5

Haines, D. E., & Dietrichs, E. (2012). The cerebellum – structure and connections. In *Handbook of Clinical Neurology* (pp. 3–36, Vol. 103). Elsevier. https://doi.org/10.1016/B978-0-444-51892-7.00001-2

Hanajima, R., Tsutsumi, R., Shirota, Y., Shimizu, T., Tanaka, N., & Ugawa, Y. (2016). Cerebellar dysfunction in essential tremor. *Movement Disorders*, *31*(8), 1230–1234. https://doi.org/10.1002/mds.26629

Harris, C. M., & Wolpert, D. M. (1998). Signal-dependent noise determines motor planning. *Nature*, *394*(6695), 780–784. https://doi.org/10.1038/29528

Hellwig, B., Mund, P., Schelter, B., Guschlbauer, B., Timmer, J., & Lücking, C. H. (2009). A longitudinal study of tremor frequencies in Parkinson's disease and essential tremor. *Clinical Neurophysiology*, *120*(2), 431–435. https://doi.org/10.1016/j.clinph.2008.11.002

Helmchen, C., Hagenow, A., Miesner, J., Sprenger, A., Rambold, H., Wenzelburger, R., Heide, W., & Deuschl, G. (2003). Eye movement abnormalities in essential tremor may indicate cerebellar dysfunction. *Brain*, *126*(6), 1319–1332. https://doi.org/10.1093/brain/awg132

Helmich, R. C., Toni, I., Deuschl, G., & Bloem, B. R. (2013). The pathophysiology of essential tremor and parkinson's tremor. *Current Neurology and Neuroscience Reports*, *13*(9). https://doi.org/10.1007/s11910-013-0378-8

Holtbernd, F., & Shah, N. J. (2021). Imaging the Pathophysiology of Essential Tremor—A Systematic Review. *Frontiers in Neurology*, *12*, 680254. https://doi.org/10.3389/fneur.2021.680254

Ibrahim, M. F., Beevis, J. C., & Empson, R. M. (2021). Essential Tremor – A Cerebellar Driven Disorder? *Neuroscience*, *462*(November), 262–273. https://doi.org/10.1016/j.neuroscience.2020.11.002

Iglesias, J. E., Insausti, R., Lerma-Usabiaga, G., Bocchetta, M., Van Leemput, K., Greve, D. N., van der Kouwe, A., Fischl, B., Caballero-Gaudes, C., & Paz-Alonso, P. M. (2018, June). A probabilistic atlas of the human thalamic nuclei combining ex vivo MRI and histology.

Iorio-Morin, C., Fomenko, A., & Kalia, S. K. (2020). Deep-Brain Stimulation for Essential Tremor and Other Tremor Syndromes: A Narrative Review of Current Targets and Clinical Outcomes. *Brain Sciences*, *10*(12), 925. https://doi.org/10.3390/brainsci10120925

Izawa, J., & Shadmehr, R. (2008). On-Line Processing of Uncertain Information in Visuomotor Control. *The Journal of Neuroscience*, *28*(44), 11360–11368. https://doi.org/10.1523/JNEUROSCI.3063-08.2008

Jenkinson, M., & Chappell, M. (2018). *Introduction to neuroimaging analysis* (First edition). Oxford University Press.
OCLC: on1013689383.

Kastner, S., & Arcaro, M. J. (2022, September). The Thalamus in Attention. In M. M. Halassa (Ed.), *The Thalamus* (1st ed., pp. 324–339). Cambridge University Press. https://doi.org/10.1017/9781108674287.018

Kawato, M. (1999). Internal models for motor control and trajectory planning. *Current Opinion in Neurobiology*, *9*(6), 718–727. https://doi.org/10.1016/S0959-4388(99)00028-8

Kilteni, K., & Ehrsson, H. H. (2020). Functional Connectivity between the Cerebellum and Somatosensory Areas Implements the Attenuation of Self-Generated Touch. *The Journal of Neuroscience*, *40*(4), 894–906. https://doi.org/10.1523/JNEUROSCI.1732-19.2019

Kilteni, K., Engeler, P., & Ehrsson, H. H. (2020). Efference Copy Is Necessary for the Attenuation of Self-Generated Touch. *iScience*, *23*(2), 100843. https://doi.org/10.1016/j.isci.2020.100843

Kilteni, K., Houborg, C., & Ehrsson, H. H. (2019). Rapid learning and unlearning of predicted sensory delays in self-generated touch. *eLife*, *8*, e42888. https://doi.org/10.7554/eLife.42888

Klein, J. C., Lorenz, B., Kang, J.-S., Baudrexel, S., Seifried, C., Van De Loo, S., Steinmetz, H., Deichmann, R., & Hilker, R. (2011). Diffusion tensor imaging of white matter involvement in essential tremor. *Human Brain Mapping*, *32*(6), 896–904. https://doi.org/10.1002/hbm.21077

Kronenbuerger, M., Gerwig, M., Brol, B., Block, F., & Timmann, D. (2007). Eyeblink conditioning is impaired in subjects with essential tremor. *Brain*, *130*(6), 1538–1551. https://doi.org/10.1093/brain/awm081

Kumar, V. J., Scheffler, K., & Grodd, W. (2023). The structural connectivity mapping of the intralaminar thalamic nuclei. *Scientific Reports*, *13*(1), 11938. https://doi.org/10.1038/s41598-023-38967-0

Kurtzer, I., Trautman, P., Rasquinha, R. J., Bhanpuri, N. H., Scott, S. H., & Bastian, A. J. (2013). Cerebellar damage diminishes long-latency responses to multijoint perturbations. *Journal of Neurophysiology*, *109*(8), 2228–2241. https://doi.org/10.1152/jn.00145.2012

Lakens, D., Adolfi, F. G., Albers, C. J., Anvari, F., Apps, M. A. J., Argamon, S. E., Baguley, T., Becker, R. B., Benning, S. D., Bradford, D. E., Buchanan, E. M., Caldwell, A. R., Van Calster, B., Carlsson, R., Chen, S.-C., Chung, B., Colling, L. J., Collins, G. S., Crook, Z., … Zwaan, R. A. (2018). Justify your alpha. *Nature Human Behaviour*, *2*(3), 168–171. https://doi.org/10.1038/s41562-018-0311-x

Lefèvre, P., Quaia, C., & Optican, L. M. (1998). Distributed model of control of saccades by superior colliculus and cerebellum. *Neural Networks*, *11*(7-8), 1175–1190. https://doi.org/10.1016/S0893-6080(98)00071-9

Liu, D., & Todorov, E. (2007). Evidence for the Flexible Sensorimotor Strategies Predicted by Optimal Feedback Control. *The Journal of Neuroscience*, *27*(35), 9354–9368. https://doi.org/10.1523/JNEUROSCI.1110-06.2007

Louis, E. D., Faust, P. L., Vonsattel, J.-P. G., Honig, L. S., Rajput, A., Robinson, C. A., Rajput, A., Pahwa, R., Lyons, K. E., Ross, G., Borden, S., Moskowitz, C. B., Lawton, A., & Hernandez, N. (2007). Neuropathological changes in essential tremor: 33 cases

compared with 21 controls. *Brain*, *130*(12), 3297–3307. https://doi.org/10.1093/brain/awm266

Louis, E. D. (2021). The Essential Tremors: Evolving Concepts of a Family of Diseases. *Frontiers in Neurology*, *12*(March), 1–7. https://doi.org/10.3389/fneur.2021.650601

Louis, E. D., & Faust, P. L. (2020a). Essential tremor pathology: Neurodegeneration and reorganization of neuronal connections. *Nature Reviews Neurology*, *16*(2), 69–83. https://doi.org/10.1038/s41582-019-0302-1

Louis, E. D., & Faust, P. L. (2020b). Essential Tremor Within the Broader Context of Other Forms of Cerebellar Degeneration. *The Cerebellum*, *19*(6), 879–896. https://doi.org/10.1007/s12311-020-01160-4

Louis, E. D., & Ferreira, J. J. (2010). How common is the most common adult movement disorder? Update on the worldwide prevalence of essential tremor. *Movement Disorders*, *25*(5), 534–541. https://doi.org/10.1002/mds.22838

Louis, E. D., Joyce, J. L., & Cosentino, S. (2019). Mind the gaps: What we don't know about cognitive impairment in essential tremor. *Parkinsonism and Related Disorders*, *63*(July 2018), 10–19. https://doi.org/10.1016/j.parkreldis.2019.02.038

Lowrey, C. R., Nashed, J. Y., & Scott, S. H. (2017). Rapid and flexible whole body postural responses are evoked from perturbations to the upper limb during goal-directed reaching. *Journal of Neurophysiology*, *117*(3), 1070–1083. https://doi.org/10.1152/jn.01004.2015

Luo, R., Pan, P., Xu, Y., & Chen, L. (2019). No reliable gray matter changes in essential tremor. *Neurological Sciences*, *40*(10), 2051–2063. https://doi.org/10.1007/s10072-019-03933-0

Mai, J. K., & Majtanik, M. (2019). Toward a Common Terminology for the Thalamus. *Frontiers in Neuroanatomy*, *12*, 114. https://doi.org/10.3389/fnana.2018.00114

Martin, T. A., Keating, J. G., Goodkin, H. P., Bastian, A. J., & Thach, W. T. (1996). Throwing while looking through prisms: I. Focal olivocerebellar lesions impair adaptation. *Brain*, *119*(4), 1183–1198. https://doi.org/10.1093/brain/119.4.1183

Mathew, J., & Crevecoeur, F. (2021). Adaptive Feedback Control in Human Reaching Adaptation to Force Fields. *Frontiers in Human Neuroscience*, *15*, 742608. https://doi.org/10.3389/fnhum.2021.742608

Mavroudis, I., Petrides, F., Karantali, E., Chatzikonstantinou, S., McKenna, J., Ciobica, A., Iordache, A.-C., Dobrin, R., Trus, C., & Kazis, D. (2021). A Voxel-Wise Meta-Analysis on the Cerebellum in Essential Tremor. *Medicina*, *57*(3), 264. https://doi.org/10.3390/medicina57030264

Mavroudis, I., Petridis, F., & Kazis, D. (2019). Neuroimaging and neuropathological findings in essential tremor. *Acta Neurologica Scandinavica*, *139*(6), 491–496. https://doi.org/10.1111/ane.13101

Mazzoni, P., Hristova, A., & Krakauer, J. W. (2007). Why Don't We Move Faster? Parkinson's Disease, Movement Vigor, and Implicit Motivation. *The Journal of Neuroscience*, *27*(27), 7105–7116. https://doi.org/10.1523/JNEUROSCI.0264-07.2007

McNamee, D., & Wolpert, D. M. (2019). Internal Models in Biological Control. *Annual Review of Control, Robotics, and Autonomous Systems*, *2*(1), 339–364. https://doi.org/10.1146/annurev-control-060117-105206

McRobbie, D. W., Moore, E. A., Graves, M. J., & Prince, M. R. (2017, April). *MRI from Picture to Proton* (3rd ed.). Cambridge University Press. https://doi.org/10.1017/9781107706958

Meyer-Lohmann, J., Conrad, B., Matsunami, K., & Brooks, V. (1975). Effects of dentate cooling on precentral unit activity following torque pulse injections into elbow movements. *Brain Research*, *94*(2), 237–251. https://doi.org/10.1016/0006-8993(75)90059-1

Miall, R. C., Weir, D. J., Wolpert, D. M., & Stein, J. F. (1993). Is the Cerebellum a Smith Predictor? *Journal of Motor Behavior*, *25*(3), 203–216. https://doi.org/10.1080/00222895.1993.9942050

Miall, R. C., Christensen, L. O., Cain, O., & Stanley, J. (2007). Disruption of state estimation in the human lateral cerebellum. *PLoS Biology*, *5*(11), 2733–2744. https://doi.org/10.1371/journal.pbio.0050316

Mondie, S., & Michiels, W. (2003). Finite spectrum assignment of unstable time-delay systems with a safe implementation. *IEEE Transactions on Automatic Control*, *48*(12), 2207–2212. https://doi.org/10.1109/TAC.2003.820147

Muthuraman, M., Raethjen, J., Koirala, N., Anwar, A. R., Mideksa, K. G., Elble, R., Groppa, S., & Deuschl, G. (2018). Cerebellocortical network fingerprints differ between essential, Parkinson's and mimicked tremors. *Brain*, *141*(6), 1770–1781. https://doi.org/10.1093/brain/awy098

Nashed, J. Y., Crevecoeur, F., & Scott, S. H. (2012). Influence of the behavioral goal and environmental obstacles on rapid feedback responses. *Journal of Neurophysiology*, *108*(4), 999–1009. https://doi.org/10.1152/jn.01089.2011

Nicoletti, V., Cecchi, P., Frosini, D., Pesaresi, I., Fabbri, S., Diciotti, S., Bonuccelli, U., Cosottini, M., & Ceravolo, R. (2015). Morphometric and functional MRI changes in essential tremor with and without resting tremor. *Journal of Neurology*, *262*(3), 719–728. https://doi.org/10.1007/s00415-014-7626-y

Novellino, F., Vasta, R., Saccà, V., Nisticò, R., Morelli, M., Arabia, G., Chiriaco, C., Barbagallo, G., Nicoletti, G., Salsone, M., & Quattrone, A. (2020). Hippocampal impairment in patients with Essential Tremor. *Parkinsonism & Related Disorders*, *72*, 56–61. https://doi.org/10.1016/j.parkreldis.2020.02.006

Ojakangas, C. L., & Ebner, T. J. (1992). Purkinje cell complex and simple spike changes during a voluntary arm movement learning task in the monkey. *Journal of Neurophysiology*, *68*(6), 2222–2236. https://doi.org/10.1152/jn.1992.68.6.2222

Pan, M.-K., & Kuo, S.-H. (2022). Essential tremor: Clinical perspectives and pathophysiology. *Journal of the Neurological Sciences*, *435*, 120198. https://doi.org/10.1016/j.jns.2022.120198

Paris-Robidas, S., Brochu, E., Sintes, M., Emond, V., Bousquet, M., Vandal, M., Pilote, M., Tremblay, C., Di Paolo, T., Rajput, A. H., Rajput, A., & Calon, F. (2012). Defective dentate nucleus GABA receptors in essential tremor. *Brain*, *135*(1), 105–116. https://doi.org/10.1093/brain/awr301

Perry, B. A. L., & Mitchell, A. S. (2019). Considering the Evidence for Anterior and Laterodorsal Thalamic Nuclei as Higher Order Relays to Cortex. *Frontiers in Molecular Neuroscience*, *12*, 167. https://doi.org/10.3389/fnmol.2019.00167

Peyrache, A. (2022, September). The Thalamus in Navigation. In M. M. Halassa (Ed.), *The Thalamus* (1st ed., pp. 340–360). Cambridge University Press. https://doi.org/10.1017/9781108674287.019

Pietracupa, S., Bologna, M., Bharti, K., Pasqua, G., Tommasin, S., Elifani, F., Paparella, G., Petsas, N., Grillea, G., Berardelli, A., & Pantano, P. (2019). White matter rather than gray matter damage characterizes essential tremor. *European Radiology*, *29*(12), 6634–6642. https://doi.org/10.1007/s00330-019-06267-9

Pietracupa, S., Bologna, M., Tommasin, S., Berardelli, A., & Pantano, P. (2021). The Contribution of Neuroimaging to the Understanding of Essential Tremor Pathophysiology: A Systematic Review. *Cerebellum*, (0123456789). https://doi.org/10.1007/s12311-021-01335-7

Pietracupa, S., Bologna, M., Tommasin, S., Elifani, F., Vasselli, F., Paparella, G., Petsas, N., Berardelli, A., & Pantano, P. (2021). No evidence of iron deposition in essential tremor: A susceptibility-weighted imaging study. *Neurological Sciences*, *42*(11), 4667–4672. https://doi.org/10.1007/s10072-021-05173-7

Prasad, S., Shah, A., Bhalsing, K. S., Ingalhalikar, M., Saini, J., & Pal, P. K. (2019). Clinical correlates of abnormal subcortical volumes in Essential Tremor. *Journal of Neural Transmission*, *126*(5), 569–576. https://doi.org/10.1007/s00702-019-02004-0

Pruszynski, J. A., Kurtzer, I., Nashed, J. Y., Omrani, M., Brouwer, B., & Scott, S. H. (2011). Primary motor cortex underlies multi-joint integration for fast feedback control. *Nature*, *478*(7369), 387–390. https://doi.org/10.1038/nature10436

Pruszynski, J. A., Omrani, M., & Scott, S. H. (2014). Goal-Dependent Modulation of Fast Feedback Responses in Primary Motor Cortex. *The Journal of Neuroscience*, *34*(13), 4608–4617. https://doi.org/10.1523/JNEUROSCI.4520-13.2014

Pruszynski, J. A., & Scott, S. H. (2012). Optimal feedback control and the long-latency stretch response. *Experimental Brain Research*, *218*(3), 341–359. https://doi.org/10.1007/s00221-012-3041-8

Qi, S., Cao, H., Wang, R., Jian, Z., Bian, Y., & Yang, J. (2020). Relative increase in cerebellar gray matter in young onset essential tremor: Evidence from voxel-based morphometry analysis. *Journal of Clinical Neuroscience*, *79*, 251–256. https://doi.org/10.1016/j.jocn.2020.07.003

Quaia, C., Lefèvre, P., & Optican, L. M. (1999). Model of the Control of Saccades by Superior Colliculus and Cerebellum. *Journal of Neurophysiology*, *82*(2), 999–1018. https://doi.org/10.1152/jn.1999.82.2.999

Rolls, E. T. (2019). The cingulate cortex and limbic systems for emotion, action, and memory. *Brain Structure & Function*, *224*(9), 3001–3018. https://doi.org/10.1007/s00429-019-01945-2

Romero, J. E., Coupé, P., Giraud, R., Ta, V.-T., Fonov, V., Park, M. T. M., Chakravarty, M. M., Voineskos, A. N., & Manjón, J. V. (2017). CERES: A new cerebellum lobule segmentation method. *NeuroImage*, *147*, 916–924. https://doi.org/10.1016/j.neuroimage.2016.11.003

Rushworth, M. F. S., Nixon, P. D., & Passingham, R. E. (1997). Parietal cortex and movement. *Experimental Brain Research*, *117*(2), 292–310. https://doi.org/10.1007/s002210050224

Schreiber, C., Missal, M., & Lefèvre, P. (2006). Asynchrony Between Position and Motion Signals in the Saccadic System. *Journal of Neurophysiology*, *95*(2), 960–969. https://doi.org/10.1152/jn.00315.2005

Schween, R., McDougle, S. D., Hegele, M., & Taylor, J. A. (2020). Assessing explicit strategies in force field adaptation. *Journal of Neurophysiology*, *123*(4), 1552–1565. https://doi.org/10.1152/jn.00427.2019

Scott, S. H. (2012). The computational and neural basis of voluntary motor control and planning. *Trends in Cognitive Sciences*, *16*(11), 541–549. https://doi.org/10.1016/j.tics.2012.09.008

Scott, S. H. (2016). A Functional Taxonomy of Bottom-Up Sensory Feedback Processing for Motor Actions. *Trends in Neurosciences*, *39*(8), 512–526. https://doi.org/10.1016/j.tins.2016.06.001

Shadmehr, R., & Krakauer, J. W. (2008). A computational neuroanatomy for motor control. *Experimental Brain Research*, *185*(3), 359–381. https://doi.org/10.1007/s00221-008-1280-5

Shanker, V. (2019). Essential tremor: Diagnosis and management. *The BMJ*, *366*. https://doi.org/10.1136/bmj.l4485

Sharma, S., & Pandey, S. (2020). Treatment of essential tremor: Current status. *Postgraduate Medical Journal*, *96*(1132), 84–93. https://doi.org/10.1136/postgradmedj-2019-136647

Shen, X., Finn, E. S., Scheinost, D., Rosenberg, M. D., Chun, M. M., Papademetris, X., & Constable, R. T. (2017). Using connectome-based predictive modeling to predict individual behavior from brain connectivity. *Nature Protocols*, *12*(3), 506–518. https://doi.org/10.1038/nprot.2016.178

Smith, M. A., & Shadmehr, R. (2005). Intact ability to learn internal models of arm dynamics in Huntington's disease but not cerebellar degeneration. *Journal of Neurophysiology*, *93*(5), 2809–2821. https://doi.org/10.1152/jn.00943.2004

Soares, J. M., Magalhães, R., Moreira, P. S., Sousa, A., Ganz, E., Sampaio, A., Alves, V., Marques, P., & Sousa, N. (2016). A Hitchhiker's Guide to Functional Magnetic Resonance Imaging. *Frontiers in Neuroscience*, *10*. https://doi.org/10.3389/fnins.2016.00515

Soares, J. M., Marques, P., Alves, V., & Sousa, N. (2013). A hitchhiker's guide to diffusion tensor imaging. *Frontiers in Neuroscience*, *7*. https://doi.org/10.3389/fnins.2013.00031

Stein, R. B., & Oğuztöreli, M. N. (1976). Tremor and other oscillations in neuromuscular systems. *Biological Cybernetics*, *22*(3), 147–157. https://doi.org/10.1007/BF00365525

Stoodley, C. J., & Schmahmann, J. D. (2010). Evidence for topographic organization in the cerebellum of motor control versus cognitive and affective processing. *Cortex*, *46*(7), 831–844. https://doi.org/10.1016/j.cortex.2009.11.008

Stoodley, C. J., & Schmahmann, J. D. (2018). Functional topography of the human cerebellum. In *Handbook of Clinical Neurology* (pp. 59–70, Vol. 154). Elsevier. https://doi.org/10.1016/B978-0-444-63956-1.00004-7

Strick, L. (1983). The influence of motor preparation on the response of cerebellar neurons to limb displacements. *The Journal of Neuroscience*, *3*(10).

Takei, T., Lomber, S. G., Cook, D. J., & Scott, S. H. (2021). Transient deactivation of dorsal premotor cortex or parietal area 5 impairs

feedback control of the limb in macaques. *Current Biology*, *31*(7), 1476–1487.e5. https://doi.org/10.1016/j.cub.2021.01.049

Tewari, A., Jog, R., & Jog, M. S. (2016). The Striatum and Subthalamic Nucleus as Independent and Collaborative Structures in Motor Control. *Frontiers in Systems Neuroscience*, *10*. https://doi.org/10.3389/fnsys.2016.00017

Therrien, A. S., & Bastian, A. J. (2015). Cerebellar damage impairs internal predictions for sensory and motor function. *Current Opinion in Neurobiology*, *33*, 127–133. https://doi.org/10.1016/j.conb.2015.03.013

Tikoo, S., Pietracupa, S., Tommasin, S., Bologna, M., Petsas, N., Bharti, K., Berardelli, A., & Pantano, P. (2020). Functional disconnection of the dentate nucleus in essential tremor. *Journal of Neurology*, (0123456789). https://doi.org/10.1007/s00415-020-09711-9

Todorov, E., & Jordan, M. I. (2002). Optimal feedback control as a theory of motor coordination. *Nature Neuroscience*, *5*(11), 1226–1235. https://doi.org/10.1038/nn963

Trillenberg, P., Führer, J., Sprenger, A., Hagenow, A., Kömpf, D., Wenzelburger, R., Deuschl, G., Heide, W., & Helmchen, C. (2006). Eye-hand coordination in essential tremor: Eye-Hand Coordination in Essential Tremor. *Movement Disorders*, *21*(3), 373–379. https://doi.org/10.1002/mds.20729

Tseng, Y. W., Diedrichsen, J., Krakauer, J. W., Shadmehr, R., & Bastian, A. J. (2007). Sensory prediction errors drive cerebellum-dependent adaptation of reaching. *Journal of Neurophysiology*, *98*(1), 54–62. https://doi.org/10.1152/jn.00266.2007

Van Der Vliet, R., Frens, M. A., De Vreede, L., Jonker, Z. D., Ribbers, G. M., Selles, R. W., Van Der Geest, J. N., & Donchin, O. (2018). Individual Differences in Motor Noise and Adaptation Rate Are Optimally Related. *eneuro*, *5*(4), ENEURO.0170–18.2018. https://doi.org/10.1523/ENEURO.0170-18.2018

Welzel, J., Güthe, M., Keil, J., Hermann, G., Wolke, R., Maetzler, W., & Becktepe, J. S. (2024). The interplay of sensory feedback, arousal, and action tremor amplitude in essential tremor. *Scientific Reports*, *14*(1), 4301. https://doi.org/10.1038/s41598-024-54528-5

Whitfield-Gabrieli, S., & Nieto-Castanon, A. (2012). *Conn* : A Functional Connectivity Toolbox for Correlated and Anticorrelated Brain Networks. *Brain Connectivity*, *2*(3), 125–141. https://doi.org/10.1089/brain.2012.0073

Wójcik-Pedziwiatr, M., Plinta, K., Krzak-Kubica, A., Zajdel, K., Falkiewicz, M., Dylak, J., Ober, J., Szczudlik, A., & Rudzińska, M. (2016). Eye movement abnormalities in essential tremor. *Journal of Human Kinetics*, *52*(1), 53–64. https://doi.org/10.1515/hukin-2015-0193

Wolpert, D. M., Goodbody, S. J., & Husain, M. (1998). Maintaining internal representations: The role of the human superior parietal lobe. *Nature Neuroscience*, *1*(6), 529–533. https://doi.org/10.1038/2245

Wolpert, D. M., Miall, R. C., & Kawato, M. (1998). Internal models in the cerebellum. *Trends in Cognitive Sciences*, *2*(9), 338–347. https://doi.org/10.1016/S1364-6613(98)01221-2

Xu-Wilson, M., Tian, J., Shadmehr, R., & Zee, D. S. (2011). TMS Perturbs Saccade Trajectories and Unmasks an Internal Feedback Controller for Saccades. *Journal of Neuroscience*, *31*(32), 11537–11546. https://doi.org/10.1523/JNEUROSCI.1584-11.2011

Xu-Wilson, M., Chen-Harris, H., Zee, D. S., & Shadmehr, R. (2009). Cerebellar contributions to adaptive control of saccades in humans. *Journal of Neuroscience*, *29*(41), 12930–12939. https://doi.org/10.1523/JNEUROSCI.3115-09.2009

Yushkevich, P. A., Piven, J., Hazlett, H. C., Smith, R. G., Ho, S., Gee, J. C., & Gerig, G. (2006). User-guided 3D active contour segmentation of anatomical structures: Significantly improved efficiency and reliability. *NeuroImage*, *31*(3), 1116–1128. https://doi.org/10.1016/j.neuroimage.2006.01.015

Zhang, X., & Santaniello, S. (2019). Role of cerebellar GABAergic dysfunctions in the origins of essential tremor. *Proceedings of the National Academy of Sciences*, *116*(27), 13592–13601. https://doi.org/10.1073/pnas.1817689116

Zhang, Y., Huang, P., Wang, X., Xu, Q., Liu, Y., Jin, Z., Li, Y., Cheng, Z., Tang, R., Chen, S., He, N., Yan, F., & Haacke, E. M. (2023). Visualizing the deep cerebellar nuclei using quantitative susceptibility

mapping: An application in healthy controls, Parkinson's disease patients and essential tremor patients. *Human Brain Mapping*, *44*(4), 1810–1824. https://doi.org/10.1002/hbm.26178